Journal Pre-proofs

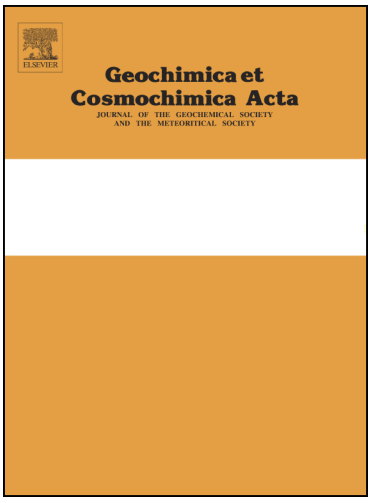

Experimental and theoretical determinations of hydrogen isotopic equilibrium in the system CH_4-H_2-H_2O from 3 to 200°C

Andrew C. Turner, Roman Korol, Daniel L. Eldridge, Markus Bill, Mark E. Conrad, Thomas F. Miller III, Daniel A. Stolper

PII: S0016-7037(21)00249-0
DOI: https://doi.org/10.1016/j.gca.2021.04.026
Reference: GCA 12172

To appear in: *Geochimica et Cosmochimica Acta*

Received Date: 15 June 2020
Revised Date: 20 April 2021
Accepted Date: 21 April 2021

Please cite this article as: Turner, A.C., Korol, R., Eldridge, D.L., Bill, M., Conrad, M.E., Miller, T.F. III, Stolper, D.A., Experimental and theoretical determinations of hydrogen isotopic equilibrium in the system CH_4-H_2-H_2O from 3 to 200°C, *Geochimica et Cosmochimica Acta* (2021), doi: https://doi.org/10.1016/j.gca.2021.04.026

Title: Experimental and theoretical determinations of hydrogen isotopic equilibrium in the system CH_4-H_2-H_2O from 3 to 200°C

Authors: Andrew C. Turner[1*], Roman Korol[2], Daniel L. Eldridge[1,3], Markus Bill[3], Mark E. Conrad[3], Thomas F. Miller III[2], Daniel A. Stolper[1,3]

Affiliations:
[1]Department of Earth and Planetary Science, University of California, Berkeley, CA 94720 USA
[2]Division of Chemistry and Chemical Engineering, California Institute of Technology, Pasadena, CA 91125 USA
[3]Energy Geosciences Division, Lawrence Berkeley National Laboratory, 1 Cyclotron Road, Berkeley, CA 94720 USA

*To whom correspondence should be addressed: acturner@berkeley.edu

Abstract
The stable isotopic composition of methane (CH_4) is commonly used to fingerprint natural gas origins. Over the past 50 years, there have been numerous proposals that both microbial and thermogenic CH_4 can form in or later attain hydrogen isotopic equilibrium with water (H_2O) and carbon isotopic equilibrium with carbon dioxide (CO_2). Evaluation of such proposals requires knowledge of the equilibrium fractionation factors between CH_4 and H_2O or CO_2 at the temperatures where microbial and thermogenic CH_4 form in or are found in the environment, which is generally less than 200°C. Experimental determinations of these fractionation factors are only available above 200°C, requiring extrapolation of these results beyond the calibrated range or the use of theoretical calculations at lower temperatures. Here, we provide a calibration of the equilibrium hydrogen isotopic fractionation factor for CH_4 and hydrogen gas (H_2) ($^{D}\alpha_{CH4(g)\text{-}H2(g)}$) based on experiments using γ-Al_2O_3 and Ni catalysts from 3 to 200°C. Results were regressed as a 2nd order polynomial of $1000\times\ln{}^{D}\alpha_{CH4(g)\text{-}H2(g)}$ vs. 1/T (K^{-1}) yielding:

$$1000 \times \ln{}^{D}\alpha_{CH_4(g)-H_2(g)} = \frac{3.5317 \times 10^7}{T^2} + \frac{2.7749 \times 10^5}{T} - 179.48$$

We combine this calibration with previous experimental determinations of hydrogen isotope equilibrium between H_2, H_2O(g), and H_2O(l) and we provide an interpolatable experimental calibration of $1000\times\ln{}^{D}\alpha_{CH4(g)\text{-}H2O(l)}$ from 3 to 200°C. Our resulting 4th order polynomial is the following equation:

$$1000 \times \ln{}^{D}\alpha_{CH_4(g)-H_2O(l)} = -\frac{7.9443 \times 10^{12}}{T^4} + \frac{8.7772 \times 10^{10}}{T^3} - \frac{3.4973 \times 10^8}{T^2} + \frac{5.4398 \times 10^5}{T} - 382.05$$

At 3°C, the value from our calibration differs by 93‰ relative to what would be calculated based on the extrapolation of the only experimental calibration currently available to temperatures below its calibrated range (lowest temperature of 200°C; Horibe and Craig, 1995). We additionally provide new theoretical estimates of hydrogen isotopic equilibrium between CH_4(g), H_2(g), and H_2O(g) and carbon isotopic equilibrium between CH_4(g) and CO_2(g) using Path Integral Monte Carlo (PIMC) calculations. Our PIMC calculations for hydrogen isotopic equilibrium between CH_4 and H_2 agree 1:1 with our experiments. Finally, we compile carbon and hydrogen isotopic measurements of CH_4, CO_2, and H_2O from various environmental systems and compare observed differences between carbon and hydrogen isotopes to those expected based on isotopic equilibrium. We find that isotopic compositions of some microbial gases from marine sedimentary, coalbed, and shale environments are consistent with those expected for

CH_4-H_2O(l) hydrogen and CH_4-CO_2 carbon isotopic equilibrium. In contrast, microbial terrestrial and pure culture gases are not consistent with both CH_4-H_2O(l) hydrogen and CH_4-CO_2 carbon isotopic equilibrium. These results are explained qualitatively using previously developed conceptual models that link free energy gradients available to microorganisms to the degree that their enzymes can promote isotope-exchange reactions between CH_4, CO_2, and H_2O.

1. Introduction

Stable carbon and hydrogen isotopic compositions are commonly used to trace the sources and sinks of methane (CH_4) in a variety of systems including economic hydrocarbon reservoirs, sediments, lakes, the ocean, hydrothermal systems, and volcanic systems. The basis of this approach is that methane formed by microbial, thermogenic, and abiotic formational processes often (though not always) occupies different fields in plots of D/H (given by δD as defined in footnote 1) vs. $^{13}C/^{12}C$ (given by $\delta^{13}C$; see footnote 1) (e.g., Schoell, 1980; Whiticar et al., 1986; Whiticar, 1999; Etiope and Sherwood Lollar, 2013).

The stable isotopic composition of methane generated by a given process is controlled by (*i*) the source isotopic composition of the carbon and hydrogen (Schoell, 1980; Whiticar et al., 1986; Chung et al., 1988; Waldron et al., 1999) and (*ii*) the isotope effects of the chemical reactions involved in methane formation. The carbon and hydrogen isotopic compositions of thermogenic methane are commonly thought to be controlled by kinetic isotope effects (e.g., Tang et al., 2000; Ni et al., 2011). For microbial gases, both kinetic and equilibrium carbon and hydrogen isotope effects are thought to control methane's isotopic composition (e.g., Whiticar et al., 1986; Whiticar, 1999; Valentine et al., 2004; Okumura et al., 2016). Finally, in high-temperature settings, such as volcanic and hydrothermal systems, equilibrium isotope effects between methane and water (H_2O) or methane and carbon dioxide (CO_2) have been proposed to set methane's isotopic composition (e.g., Horibe and Craig, 1995; Fiebig et al., 2004), though see McCollom (2008) for an alternative interpretation. As such, equilibrium processes are commonly thought to be involved in setting the carbon and hydrogen isotopic composition of methane in nature. Here, we provide both experimental and theoretical calibrations of hydrogen isotopic equilibrium between methane, molecular hydrogen (H_2), and liquid water from 3-200°C. To place this work into context, we first review the history and current thinking on the role of equilibrium processes in setting the carbon and hydrogen isotopic composition of methane. Second, we review previous experimental and theoretical calibrations of the temperature dependence of carbon isotopic equilibrium between methane vs. CO_2 and hydrogen isotopic equilibrium between methane vs. liquid water.

1.1 The role of isotopic equilibrium in setting the isotopic composition of methane

It is commonly assumed that kinetic processes and therefore kinetic isotope effects largely control the carbon and hydrogen isotopic composition of thermogenic and microbial methane. However, over the past 50 years there have been a series of proposals that equilibrium isotope effects also play a role. We begin with a review of previous work on carbon isotopes followed by hydrogen isotopes.

Murata et al. (1969) and Murata et al. (1972) proposed that sedimentary methane and CO_2 can exchange carbon isotopes on geological timescales and come into carbon isotopic equilibrium in both low-temperature sedimentary systems and warmer natural gas reservoirs and hot springs. This proposal was based on the observation that measured differences in the $\delta^{13}C$ of CH_4 vs. CO_2 yield reasonable temperatures based on a sample's collection environment and the assumption that methane and CO_2 are in carbon isotopic equilibrium. Bottinga (1969) made a similar

[1] $\delta D_{sample} = ({}^{D}R_{sample}/{}^{D}R_{VSMOW} - 1) \times 1000$ and $\delta^{13}C_{sample} = ({}^{13}R_{sample}/{}^{13}R_{VPDB} - 1) \times 1000$; ${}^{D}R = [D]/[H]$ and ${}^{13}R = [{}^{13}C]/[{}^{12}C]$. Here VSMOW is the hydrogen isotopic standard and VPDB the carbon isotopic standard. All reported $\delta^{13}C$ and δD values are given relative to these standards.

observation: $\delta^{13}C$ values of sedimentary samples of microbial methane and CO_2 yield reasonable calculated temperatures if one assumes the two are in carbon isotopic equilibrium (also see arguments in Galimov, 1973). Finally, based on similar arguments, Smith et al. (1981) proposed that methane in Australian coal-seam gases also approaches carbon isotopic equilibrium with CO_2. In settings where microorganisms might be expected to be active, Friedman and Murata (1979) proposed that this equilibration could be achieved through isotope-exchange reactions catalyzed by methanogenic microbial organisms.

The hypothesis that methane and CO_2 can achieve carbon isotopic equilibrium in low-temperature sedimentary environments where microorganisms are active was originally rejected largely on the assertion that the rates of carbon isotope exchange in these systems are too sluggish to promote equilibration on geological timescales (Claypool and Kaplan, 1974; Games and Hayes, 1976; Whiticar et al., 1986). This assertion has led to the common assumption that carbon isotope effects for microbial methane generation are controlled by kinetic isotope effects.

Valentine et al. (2004) proposed that both equilibrium and kinetic isotope effects set the carbon isotopic composition of microbial methane. Specifically, they proposed that the free energy available to drive microbial methane generation dictates the overall degree of reversibility of enzymes involved in the reduction of CO_2 to methane. When free energy gradients are low, enzymes catalyze reactions in both the forward and reverse direction (i.e., are reversible) and thus catalyze both the forward reduction of CO_2 to methane and the reverse oxidation of methane back to CO_2. Such reversibility allows for carbon isotopic equilibration to occur between CH_4 and CO_2. In contrast, when free energy gradients are high, enzymes act irreversibly and only catalyze the forward reduction of CO_2 to methane. Under these conditions, only kinetic isotope effects are expressed.

Most recently, using a reaction-diffusion model, Meister et al. (2019) found that fractionation factors required to model the observed differences in the $\delta^{13}C$ of CO_2 and biogenic methane in marine sediments are consistent with what would be expected if the two form in isotopic equilibrium. Based on this, they suggested that methanogens in deep-sea sediments could promote CH_4-CO_2 carbon isotopic equilibration during methane generation. Meister and Reyes (2019) further argued that methanogens can produce methane in carbon isotopic equilibrium with CO_2 because the carbon isotopic composition of methane formed by the reduction of CO_2 from the experiments of Botz et al. (1996) are similar to the values expected for equilibrium at the corresponding growth temperatures (35-85°C). Thus the problem has, over the past 50 years, come full circle, with the initial proposal that methanogens catalyze equilibration of carbon between methane vs. CO_2 in marine sediments, though initially dismissed, receiving renewed support.

Microbially catalyzed carbon isotopic equilibration between methane and CO_2 has also been proposed to occur during anaerobic oxidation of methane at the sulfate-methane transition zone (Yoshinaga et al., 2014). Similar to the ideas of Valentine et al. (2004), Yoshinaga et al. (2014) proposed that the enzymes of anaerobic methanotrophs can operate reversibly and thus catalyze both the forward oxidation of methane to CO_2 and the reduction of CO_2 back to methane, with the degree of exchange a function of free energy available to the system (also see Moran et al., 2005; Holler et al., 2011).

The carbon isotopic composition of thermogenic methane is generally thought to be controlled by kinetic isotope effects (e.g., Tang et al., 2000) However, Smith et al. (1998) showed experimentally that the thermal decomposition of acetic acid yields CO_2 and methane with carbon isotopic compositions consistent with generation in carbon isotopic equilibrium from 290 to 650°C. Most recently, based on observed differences between the $\delta^{13}C$ of CO_2 and thermogenic methane vs. measured methane clumped-isotope based temperatures, Thiagarajan et al. (2020) proposed that thermogenic methane and CO_2 can achieve carbon isotopic equilibrium in the subsurface through reactions that promote methane oxidation and CO_2 reduction.

Equilibrium isotope effects have also been suggested to set the hydrogen isotopic composition of some microbial and thermogenic methane samples. For microbial gases, it has been observed that samples that yield methane clumped-isotope-based temperatures consistent with expected formation temperatures also yield differences between the δD of methane and H_2O that would be predicted if these samples formed in CH_4-H_2O hydrogen isotopic equilibrium (Stolper et al., 2015; Wang et al., 2015; Douglas et al., 2016). Stolper et al. (2015) and Wang et al. (2015) explained this pattern as the result of high degrees of enzymatic reversibility during methanogenesis that catalyzes CH_4-H_2O hydrogen isotope-exchange reactions, equilibrating the two and promoting methane clumped-isotope equilibrium. Based on examinations of biogenic methane and water hydrogen isotope systematics in coal and shale gas systems, Vinson et al. (2017) proposed that microbial methane formed in these systems forms in hydrogen isotopic equilibrium with co-occurring waters. Okumura et al. (2016) proposed that such patterns could also be explained by methanogens generating methane out of hydrogen isotopic equilibrium with water and then that microbes later catalyze hydrogen isotope-exchange reactions between methane and water to equilibrate the two. Finally, it has been proposed that methane clumped-isotopic equilibrium can be promoted during anaerobic methane oxidation (Stolper et al., 2015; Young et al., 2017; Giunta et al., 2019; Ash et al., 2019; Ono et al., 2021). In this explanation, anaerobic methane oxidizing archaea also operate enzymes sufficiently reversibly such that they promote CH_4-H_2O hydrogen isotope-exchange reactions.

It has also been proposed that the hydrogen isotopic composition of thermogenic methane can be influenced by equilibrium processes at elevated temperatures. Specifically, Burruss and Laughrey (2010) proposed, based on relationships between $\delta^{13}C$ and δD values of methane from Paleozoic deposits in the Appalachian Basin, that methane begins exchanging and therefore equilibrating hydrogen isotopes with water at temperatures of 200-300°C. Additionally, Giunta et al. (2019) proposed that thermogenic methane may form in (or achieve) hydrogen isotopic equilibrium with water based on the observed agreement between apparent methane clumped-isotope temperatures (from 118-204°C) and measured differences in the δD of methane and water versus those expected for CH_4-H_2O hydrogen isotopic equilibrium. Most recently, Thiagarajan et al. (2020) proposed that methane equilibrates hydrogen with other gaseous alkanes (e.g., ethane, propane, etc.) in thermogenic gas reservoirs. This proposal is based on the observation that measured methane clumped-isotope-based temperatures are similar to temperatures calculated based on the assumption of hydrogen isotopic equilibrium between methane and other alkanes.

Finally, as noted above, high temperature (>275°C) volcanic and hydrothermal systems are commonly thought to yield methane in isotopic equilibrium with co-occurring water and CO_2 (e.g., Craig, 1953; Bottinga, 1969; Horibe and Craig, 1995; Fiebig et al., 2004; Proskurowski et al., 2006; Wang et al., 2018), although carbon isotopic compositions of methane and CO_2 can also be out of equilibrium (e.g., McCollom, 2008).

Evaluation of whether methane forms in or later achieves isotopic equilibrium with either CO_2 or water requires constraints on the equilibrium fractionation factors between methane and these gases and liquids at relevant environmental temperatures. All microbial and most thermogenic methane is thought to form at temperatures below 200°C (e.g., Hunt, 1995; Takai et al., 2008). In contrast, all experimentally determined equilibrium fractionation factors for $CH_4(g)$-$CO_2(g)$ carbon and $CH_4(g)$-$H_2O(l)$ hydrogen isotopic equilibrium exist only for temperatures greater than 200°C (Horibe and Craig, 1995; Horita, 2001; Kueter et al., 2019). As a result, either experimental determinations of equilibrium fractionation factors must be extrapolated to lower temperatures or theoretical calculations must be used when studying all microbial and most thermogenic samples.

In the following section, we discuss the current knowledge of the equilibrium isotopic composition of methane vs. CO_2 for carbon and methane vs. liquid water for hydrogen based on experimental and theoretical studies.

1.2 Experimental measurements and theoretical calculations of carbon isotopic equilibrium between gaseous CH_4 and CO_2 and hydrogen isotopic equilibrium between gaseous CH_4 and liquid water

Isotopic differences between two phases or species are given using "alpha" notation, where:

$$ {}^{i}\alpha_{A-B} = \frac{R_A}{R_B} = \frac{(1000 + \delta D_A)}{(1000 + \delta D_B)} \quad (1) $$

In eq. (1), R_A is the carbon ($^{13}C/^{12}C$) or hydrogen (D/H) isotopic ratio of phase or species A, and *i* indicates the isotopic system (either D for hydrogen isotopes or 13 for carbon isotopes). α is often termed a fractionation factor. We do not use ${}^{i}\alpha_{A-B}$ exclusively to indicate isotopic equilibrium between phases or species, but instead simply to reflect relative isotopic differences. We give values of α as $1000\times\ln\alpha$ as this form has a theoretically based dependence on temperature for systems at isotopic equilibrium (e.g., Criss, 1999).

The equilibrium carbon isotopic composition of CH_4 vs. CO_2 in the gas phase as a function of temperature has been determined experimentally in two studies: the first from 200-600°C (Horita, 2001) and the second from 300-1200°C (Kueter et al., 2019). These studies yield equilibrium $1000\times\ln{}^{13}\alpha_{CH4(g)\text{-}CO2(g)}$ values in agreement at overlapping experimental temperatures (within 0.01 to 1.01‰ from 300-600°C). Additionally, theoretical and experimental estimates of $1000\times\ln{}^{13}\alpha_{CH4(g)\text{-}CO2(g)}$ for CH_4-CO_2 carbon isotopic equilibrium agree at overlapping temperatures: Horita (2001) notes that theoretical predictions of Richet et al. (1977) are offset by 0.89‰ from experimental data. Kueter et al. (2019) show the combination of their experimental data with those of Horita (2001) are offset from the theoretical calculations of Bottinga (1969) and Richet et al. (1977) by 0.2-0.6‰ and 0.7-1.2‰ respectively.

Both Horita (2001) and Kueter et al. (2019) recommend that their calibrations not be extrapolated to temperatures outside of their calibrated range due to their use of polynomial (Horita, 2001) or power-law (Kueter et al., 2019) fits of $1000\times\ln^{13}\alpha_{CH4(g)\text{-}CO2(g)}$ vs. $1/T$ (K^{-1}). Instead, both studies recommend that if extrapolation is needed, that the temperature dependence of theoretical calculations be fitted to the experimental data and that these fits be used for any extrapolations beyond the experimentally calibrated temperature range. Such a strategy follows the approach outlined in Clayton and Kieffer (1991). In such an approach, it is not the absolute values of $1000\times\ln\alpha$ from the theoretical studies that matter, but rather the predicted change in $1000\times\ln\alpha$ as a function of temperature (i.e., the temperature dependence) as any constant offsets between theoretical and experimental studies will be minimized during fitting of the theoretical calculations to the experimental data.

We are aware of six published theoretical estimates of $1000\times\ln^{13}\alpha_{CH4(g)\text{-}CO2(g)}$ as a function of temperature at isotopic equilibrium that could be used for such an exercise: Craig (1953), Bottinga (1969), Richet et al. (1977), Chen et al. (2019), Thiagarajan et al. (2020), and Gropp et al. (2021). For temperatures lower than those accessed by experiments (i.e. below 200°C), Bottinga (1969), Richet et al. (1977), Chen et al. (2019), Thiagarajan et al. (2020), and Gropp et al. (2021) are in general agreement with maximum differences of 2.3‰ between calculations from 0-200°C. Over this temperature range, these studies yield similar temperature dependencies: calculated differences in $1000\times\ln^{13}\alpha_{CH4(g)\text{-}CO2(g)}$ range from 44.1 to 45.2‰ at 0 vs. 200°C. Values from Craig (1953) from 0-200°C are offset from other theoretical studies by up to 12‰, with predicted change in value over this temperature range of 39.6‰ (indicating a different temperature dependence as well). Horita (2001) attributes this difference between Craig (1953) and later theoretical studies to improvement in the accuracy of spectroscopic data from the 1950s to 1970s. Regardless, the strong agreement between post 1950s theoretical calculations of $1000\times\ln^{13}\alpha_{CH4(g)\text{-}CO2(g)}$ and agreement with experimental determinations at overlapping temperatures provides confidence in using theory as a basis to extrapolate experimental calibrations of $1000\times\ln^{13}\alpha_{CH4(g)\text{-}CO2(g)}$ to temperatures below the experimentally calibrated range (<200°C).

An experimental determination of equilibrium $^{D}\alpha_{CH4(g)\text{-}H2O(l)}$ for temperatures from 200-500°C is given in Horibe and Craig (1995). This is not a direct determination based on co-equilibration of CH_4(g) and H_2O(l); instead, they first equilibrated the hydrogen isotopes of CH_4 and H_2 gas using nickel-thoria catalysts from 200 to 500°C and derived a calibration for $^{D}\alpha_{CH4(g)\text{-}H2(g)}$ vs. temperature. They then combined this expression with other experimentally based estimates of equilibrium $^{D}\alpha_{H2O(l)\text{-}H2(g)}$ values to derive an equation for $^{D}\alpha_{CH4(g)\text{-}H2O(l)}$ vs. temperature. Horibe and Craig (1995) noted that further experiments were needed to constrain the temperature dependence of $^{D}\alpha_{CH4(g)\text{-}H2(g)}$ and $^{D}\alpha_{CH4(g)\text{-}H2O(l)}$ at temperatures below their experimental range (<200°C).

Beyond the typical concerns of extrapolating experimentally derived calibrations of equilibrium α values outside of their calibrated temperature range, the specific extrapolation of the Horibe and Craig (1995) calibration of $^{D}\alpha_{CH4(g)\text{-}H2O(l)}$ to temperatures below 200°C has additional complexity. This is because they provide a fit to their data with $^{D}\alpha_{CH4(g)\text{-}H2(g)}$ linearly dependent

on $1/T^2$. However, such a dependence for $^{D}\alpha_{CH4(g)\text{-}H2(g)}$ is inconsistent with theoretical calculations (e.g., Richet et al., 1977). Instead, it is $\ln^{D}\alpha_{CH4(g)\text{-}H2(g)}$ rather than $^{D}\alpha_{CH4(g)\text{-}H2(g)}$ that has a theoretically based linear or quadratic dependence on 1/T. As such, extrapolation of Horibe and Craig (1995)'s calibration could lead to inaccurate values of $^{D}\alpha_{CH4(g)\text{-}H2(g)}$ at temperatures below 200°C.

One way around this would be to use the approach of Clayton and Kieffer (1991), whereby theoretical estimates of equilibrium $1000\times\ln^{D}\alpha_{CH4(g)\text{-}H2O(l)}$ vs. temperature are fit to experimental data and then used as the basis for the extrapolation — this has not been attempted for this system. The question is whether, as was seen above for the case of carbon isotope equilibrium between CO_2 and methane, current theoretical calculations are in agreement with the experimental results at overlapping temperatures and if there is general agreement in the temperature dependence of $1000\times\ln^{D}\alpha_{CH4(g)\text{-}H2O(l)}$ at temperatures below those calibrated experimentally. Such is needed for a confident extrapolation of the experimental data to temperatures outside of the calibrated range.

We note that, to our knowledge, no theoretical calculations of $1000\times\ln^{D}\alpha_{CH4(g)\text{-}H2O(l)}$ vs. temperature at isotopic equilibrium exist. Instead, theoretical calculations for hydrogen isotopic equilibrium between gaseous methane and water (i.e., $1000\times\ln^{D}\alpha_{CH4(g)\text{-}H2O(g)}$) exist and can be converted to $1000\times\ln^{D}\alpha_{CH4(g)\text{-}H2O(l)}$ using the experimental calibration of $1000\times\ln^{D}\alpha_{H2O(l)\text{-}H2O(g)}$ from Horita and Wesolowski (1994). Horibe and Craig (1995) also used Horita and Wesolowski's (1994) calibration of $^{D}\alpha_{H2O(l)\text{-}H2O(g)}$ to calculate their final equation for $^{D}\alpha_{CH4(g)\text{-}H2O(l)}$ vs. temperature, making comparison of theory to their experimental calibration independent of the choice of calibration for $1000\times\ln^{D}\alpha_{H2O(l)\text{-}H2O(g)}$.

We are aware of seven distinct theoretical estimates from four studies for $1000\times\ln^{D}\alpha_{CH4(g)\text{-}H2O(g)}$ vs. temperature (at isotopic equilibrium): Bottinga (1969), Richet et al. (1977), Liu and Liu (2016), and Gropp et al. (2021). In all studies, calculations were done at a minimum temperature of 0°C and maximum temperatures equal to or greater than 500°C. Bottinga (1969), Richet et al. (1977), and Liu and Liu (2016) provide fractionation factors that include corrections for the anharmonicity of vibrations as well as other higher-order corrections based on either spectroscopic data or theoretical calculations. Gropp et al. (2021) provide calculations of $^{D}\alpha_{CH4(g)\text{-}H2O(g)}$ values without the aforementioned corrections and thus treat the vibrations as harmonic — these follow the classic approaches of Urey (1947) and Bigeleisen and Mayer (1947).

When compared to each other, the theoretical studies disagree significantly from 0-200°C on the value of $1000\times\ln^{D}\alpha_{CH4(g)\text{-}H2O(l)}$ at isotopic equilibrium (Fig. 1). For example, at 0°C there is a maximum disagreement of up to 159‰ between the theoretical studies and up to 164‰ between the theoretical studies and the extrapolation of Horibe and Craig's (1995) calibration. This disagreement is also seen in the calculated temperature dependence over this range (0-200°C), with differences up to 67‰ between theoretical studies and up to 91‰ between theory and the extrapolation of Horibe and Craig's (1995) calibration. Thus, there is significant uncertainty (order 100‰) both on the correct absolute values and temperature dependence of $1000\times\ln^{D}\alpha_{CH4(g)\text{-}H2O(l)}$ from 0 to 200°C. This uncertainty makes it challenging to confidently

extrapolate the calibration of Horibe and Craig (1995) to low (<200°C) temperatures based on theory and is the motivation of the work that we now present.

1.3 This study

Here, we provide an experimentally based calibration of the equilibrium hydrogen isotope fractionation factor for methane and H_2 from 3 to 200°C. Based on previous experimental determinations of hydrogen isotope equilibrium between H_2, H_2O(g), and H_2O(l), we provide an interpolatable calibration of $1000\times\ln{}^{D}\alpha_{CH4(g)\text{-}H2O(l)}$ derived from experimental constraints from 3 to 200°C. We additionally provide new theoretical estimates of hydrogen isotopic equilibrium for $1000\times\ln{}^{D}\alpha_{CH4(g)\text{-}H2(g)}$, $1000\times\ln{}^{D}\alpha_{CH4(g)\text{-}H2O(g)}$, and $1000\times\ln{}^{D}\alpha_{H2O(g)\text{-}H2(g)}$ and of carbon isotopic equilibrium for $1000\times\ln{}^{13}\alpha_{CH4(g)\text{-}CO2(g)}$ based on Path Integral Monte Carlo (PIMC) calculations (Webb and Miller, 2014; Webb et al., 2017; Eldridge et al., 2019). We compare these estimates to our and other experimentally determined calibrations. Finally, we compile measurements of $\delta^{13}C_{CH4}$, $\delta^{13}C_{CO2}$, δD_{CH4}, $\delta D_{H2O(l)}$, and estimated formation temperatures of environmental samples and microbial culture experiments. We compare measured isotopic compositions to those that would be expected for CH_4-H_2O(l) hydrogen and CH_4-CO_2 carbon isotopic equilibrium based on our new estimates in order to evaluate whether samples of methane in nature or microbial cultures appear to form in or attain hydrogen isotopic equilibrium with water and carbon isotopic equilibrium with CO_2.

2. Methods

Here, we describe our procedures to (*i*) experimentally equilibrate the hydrogen isotopic compositions of CH_4 and H_2 using catalysts at temperatures ≤200°C; (*ii*) measure δD values of H_2 and CH_4; (*iii*) calculate ${}^{D}\alpha_{CH4(g)\text{-}H2(g)}$ and $1000\times\ln{}^{D}\alpha_{CH4(g)\text{-}H2(g)}$ values from measured δD values of H_2 and CH_4 and their associated errors; and (*iv*) calculate equilibrium fractionation factors based on theory.

2.1 Catalysts

CH_4 and liquid water do not exchange hydrogen isotopes on laboratory timescales at the temperatures of interest in this study (<200°C) and we are unaware of catalysts that can promote this exchange. Instead, we followed the strategy of Horibe and Craig (1995) and equilibrated the hydrogen isotopic composition of methane and H_2 at known temperatures and then combined the results of these experiments with previous experimental determinations of $1000\times\ln{}^{D}\alpha_{H2O(l)\text{-}H2(g)}$, or $1000\times\ln{}^{D}\alpha_{H2O(g)\text{-}H2(g)}$ combined with $1000\times\ln{}^{D}\alpha_{H2O(l)\text{-}H2O(g)}$.

At the temperatures of interest to this study (<200°C), a catalyst is required to promote C-H and H-H bond activation between methane and H_2. Horibe and Craig (1995) used a nickel-thoria catalyst known to catalyze CH_4 hydrogen isotope exchange. Nickel-based catalysts are generally reactive only at temperatures above ~150-180°C on laboratory timescales (e.g., Morikawa et al., 1936). We instead chose to use γ-Al_2O_3 as the catalyst at all temperatures, while also performing one set of experiments at 200°C using a nickel-based catalyst.

2.1.1 γ-Al_2O_3 catalyst

γ-Al_2O_3 is a phase of alumina that has long been known to catalyze the exchange of hydrogen isotopes between CH_4 and H_2 (Larson and Hall, 1965; Robertson et al., 1975; Wischert et al., 2012; Sattler, 2018) as well as isotopologues of methane (Larson and Hall, 1965; Eldridge et al.,

2019; Wang et al., 2020) on timescales of hours to days at room temperature. The hydrogen isotope-exchange reactions have been proposed to occur at the major (110) termination of γ-Al_2O_3 by the reaction of defect Al_{III}-O Lewis acid-base pairs with CH_4 and H_2 to form Al-CH_3 and Al-H species (as described in Wischert et al., 2012). We purchased commercial pellets of γ-Al_2O_3 (Alfa Aesar no. 43832).

γ-Al_2O_3 requires activation using heat treatment in order to catalyze hydrogen isotope-exchange reactions (e.g., Larson and Hall, 1965; Robertson et al., 1975; John et al., 1979; Wischert et al., 2012). Initial attempts to use unactivated γ-Al_2O_3 to equilibrate the hydrogen isotopic composition of methane with H_2 resulted in no measurable change in δD values of CH_4 and H_2 for experiments held at 100°C for 16 days (data not shown). We activated γ-Al_2O_3 using a procedure modified from Larson and Hall (1965). Specifically, we placed ten 1/8-inch (~3 mm) pellets (~0.23 g) of γ-Al_2O_3 into an ~20 cm long quartz glass tube (ID 4 mm, OD = 6 mm) pre-sealed at one end. Tubes were attached to a glass vacuum manifold in the Department of Earth and Planetary Science at UC Berkeley using Ultra-Torr (Swagelok) fittings and evacuated until baseline vacuum pressure was achieved (<1 mTorr). Pellets were first heated under vacuum using a natural-gas torch to drive off any sorbed gases until baseline pressures were reached. We then heated the catalyst in the presence of ~100 Torr of O_2 using resistance heaters (Ohmite L25J100E, 100 ohm 5% 25W, 1721 MX) set to ~550°C for 5-6 hours. Following this, we evacuated the tubes to baseline pressure (<1 mTorr) and continued heating at ~550°C under vacuum overnight (12-16 hours). Finally, we flame sealed the catalysts under vacuum in the quartz glass tubes and stored until needed. Catalysts were stored under vacuum to avoid potential poisoning from exposure to species in air (e.g., CO_2 and H_2O; Larson and Hall, 1965). We note that a similar protocol was described by us in Eldridge et al. (2019) for the preparation of γ-Al_2O_3 for the equilibration of methane isotopologues and is based on the work presented here.

2.1.2 Nickel catalyst

For one experiment at 200°C, we used a nickel (Ni) catalyst (~66% nickel on silica−alumina; Alfa Aesar, no. 31276). First, the Ni catalyst was added to a 20 mL glass Wheaton vial. The Ni catalyst was not weighed but was instead prepared based on approximate volumes used in previous studies to equilibrate methane isotopologues (Stolper et al., 2014a; Eldridge et al., 2019) with the amount scaled for the volume of gas used. Glass wool was placed above the catalyst powder to hold it in place at the bottom of the vial. The vial was then sealed using a crimped septum (blue chlorobutyl; Bellco Glass) and attached via a syringe needle to a glass vacuum manifold in the Department of Earth and Planetary Science at UC Berkeley using Ultra-Torr fittings as described above. After evacuation to baseline vacuum (<1 mTorr), the base of the vial was heated (while still exposed to vacuum) using a natural-gas torch for ~1 hour to drive off sorbed gases. We then removed the stoppered vial from the vacuum line and stored it until addition of CH_4 and H_2.

2.2 Experimental methodology

2.2.1 Experiment setup and sampling

For the γ-Al_2O_3-catalyzed experiments, we broke open the sealed quartz tubes at the Center for Isotope Geochemistry (Lawrence Berkeley National Laboratory) and immediately placed ~0.45 g (20 pellets) of activated catalyst into 20 mL glass Wheaton vials, sealed these vials using

crimped rubber septa, and evacuated them to baseline (<20 mTorr) on a vacuum manifold using a syringe needle attached to Ultra-Torr fitting, and stored until usage.

After evacuation, we separately injected CH_4 (99.97%, δD = -165‰) and H_2 (99.999%, δD = -235‰) into the vials containing either the γ-Al_2O_3 or Ni catalysts from prefilled Tedlar gas bags (SKC Inc.) at room temperature and pressure. We overpressurized the vials to ~1.5 atm by injecting 10 mL of CH_4 and 20 mL of H_2 into the vials (i.e., 1:1 molar ratio of hydrogen between H_2 and CH_4). The only instances where different stoichiometries were used were a suite of 50°C experiments with H_2:CH_4 ratios of 1:4, 1:2, 1:1 and 2:1. In these experiments, 30 mL of total gas (H_2 + CH_4) was also injected such that the pressure was still ~1.5 atm.

In order to sample gas from an experimental vial, we removed 0.2 mL of gas with a gas-tight syringe (VICI) and injected this gas into a 6 mL glass Wheaton vial pre-sealed with a crimped rubber septum and pre-purged with helium (99.9%). These samples were then stored at room temperature until later mass spectrometric analysis. We note that in subsequent sections, when we refer to a specific "experiment", it indicates the catalyst-containing vials described above that were heated or cooled to experimental temperatures. In contrast, a "sample" refers to an individual sampling of an experiment (stored in a glass vial without catalyst) and is what is used to measure the isotopic composition of an experiment.

2.2.2 Bracketing approach

We used a 'bracketing' approach (O'Neil, 1986) to determine equilibrium $^{D}\alpha_{CH4(g)\text{-}H2(g)}$ values. In a bracketing approach, α values at a given experimental temperature are approached from both higher (top-bracket) and lower (bottom-bracket) initial α values. Demonstration that experiments have achieved isotopic equilibrium between phases or species occurs when both top- and bottom-bracket experiments yield the same (within error) final α values.

In our experiments, the known initial δD of the source CH_4 (δD_{CH4} = -165‰) and H_2 (δD_{H2} = -235‰) result in a starting value of $^{D}\alpha_{CH4(g)\text{-}H2(g)}$ = 1.092. Based on the experimental calibration of Horibe and Craig (1995) equilibrium $^{D}\alpha_{CH4(g)\text{-}H2(g)}$ values at temperatures ≤200°C (i.e., the temperatures of our experiments) are greater than 1.7. Thus, our starting gas composition provides a bottom-bracket for all experiments. We used this starting composition for bottom-bracket experiments at 1, 3, 10, 15, 25, 35, 50, 75, 100, 127, and 156°C. For the 180 and 200°C experiments, we pre-equilibrated experiments at higher temperatures than the final experimental temperature to ensure that these experiments began at $^{D}\alpha_{CH4(g)\text{-}H2(g)}$ values less than 1.7. This was done because these experiments (180 and 200°C) spent sufficient time at room temperature (>1 day) such that, based on our experience, they would have already isotopically equilibrated at room temperature before being heated.

Except for the 1 and 10°C experiments, all other bottom-bracket experiments were immediately placed (<10 seconds) into temperature-controlled environments upon gas addition to minimize isotopic exchange at temperatures other than the desired experimental temperature. The 1 and 10°C experiments required transport from LBNL to UC Berkeley and thus were placed into their final temperature environments hours to days after filling. Although some isotope exchange may have occurred prior to cooling to the desired experimental temperature, transport and storage

temperatures were always above final experimental temperatures and, as such, we assume these represent bottom-bracket experiments as well.

We experimentally created top brackets (i.e., experiments with initial $^{D}\alpha_{CH4(g)\text{-}H2(g)}$ values above the final expected value) by pre-equilibrating experiments at lower temperatures than the final experimental temperature. Such pre-equilibration yields top brackets because, based on theory, equilibrium $^{D}\alpha_{CH4(g)\text{-}H2(g)}$ values increase monotonically with decreasing temperature (Bottinga, 1969; Richet et al., 1977; Gropp et al., 2021). We carried out these pre-equilibrations by either leaving experiments at ~15°C (the room temperature of the laboratory at Lawrence Berkeley National Laboratory) or by placing them in refrigerators at 1 or 3°C or freezers at -9 or -15°C. A sample from all top-bracket pre-equilibrations was taken before heating experiments to final temperatures and the isotopic composition of the gas measured to verify the pre-equilibrations resulted in a successful top-bracket experiment.

2.2.3 Temperatures of experiments

We performed bracketed equilibration experiments at 1, 3, 10, 15, 25, 35, 50, 75, 100, 127, 156, 180, and 200°C. The temperatures quoted here and above are rounded to the nearest degree. More precise temperatures, where applicable, are given in tables and used for all calculations and in all figures. We now describe how temperatures were determined and how samples were held at these temperatures.

The temperatures for the -15 and -9°C freezers and the 1 and 3°C refrigerators were measured with a USB temperature logger (Extech TH10; quoted accuracy of ±1°C) placed directly next to the experiments. The make of each freezer is as follows: -15°C (General Electric Company), -9°C (Maytag), 1°C (Kenmore), 3°C (Maytag). We found that temperature in the -15°C freezer oscillated between -12 and -18°C every 90 minutes. For the -9°C freezer, temperatures were stable between -9 and -8.5°C for 30 hours and then would increase in temperature to -4°C before cooling back to -9 to -8.5°C over a 6-hour period. We decided that the observed temperature variations in the freezers were too large to be used to determine equilibrium $^{D}\alpha_{CH4(g)\text{-}H2(g)}$ at specified temperatures. Therefore, we used freezers for top-bracket pre-equilibrations only. For the 1°C refrigerator, we observed stable temperatures (an average of 0.98°C with variations of ±0.1°C) for 36 hours followed by rapid warming to 8°C, and then cooling back to ~1°C over a 3-hour timespan. Despite this cyclic behavior, we attempted to use this system for equilibration experiments by monitoring the observed cycle and sampling experiments after exposure to 1°C for at least 24 hours. The 3°C refrigerator showed variations of less than ±0.5°C as measured by the Extech temperature monitor.

For 10°C experiments, samples were fully immersed in a recirculating water bath (Neslab RTE-111) with a digital temperature set point. The temperature we report is based on determinations by an external Type K Chromel/Alumel thermocouple. Agreement between internal readout and external thermocouple was within 0.5°C. Temperature varied by at most ±0.2°C over the course of the experiment.

Experiments at room temperature (15°C) were equilibrated on a benchtop at Lawrence Berkeley National Laboratory. The temperature was measured with the same USB temperature logger used in the refrigerators and freezers, placed next to the experiments during two separate ~48

hour periods over the time course of the experiment. The room's temperature varied from 14 to 15°C around a mean of 14.6°C.

For the 25 and 35°C experiments, vials were fully immersed in two non-recirculating water baths (VWR no. 89051 and Cole Parmer no. GH-14576-04) with digital temperature set points. The reported temperatures were measured using the same Type K thermocouple as the 10°C experiment. Agreement between the baths' temperature readouts and the measured external thermocouple temperature was within 0.5°C. The water baths showed variations of less than ±0.5°C over the course of the experiments.

The vials for the 50, 75, 100, 127, and 156°C experiments were placed in dry-block heaters with either analog (127, 156°C; VWR no. 75838-318) or digital (50, 75, 100°C; VWR no. 75838-270) temperature controllers. These heaters were equipped with 8 pre-drilled holes in the aluminum blocks exactly sized for the experimental vials (22 mm diameter). Our reported temperatures for these systems were determined using the same Type K thermocouple as in the 10, 25, and 35°C experiments at a pre-drilled thermocouple hole in each aluminum block. Temperatures varied by <0.5°C spatially between the 8 pre-drilled holes for experiment vials (measured at the base of the hole) vs. the thermocouple hole, and also varied by <0.5°C over the course of the experiment. Digital readout temperatures were typically 1 to 2°C lower than the external thermocouple readout.

The 180 and 200°C experiments were placed in a stirred oil-bath system with accompanying digital temperature control (Ace Glass no. 9601-335). Reported temperatures were determined using the same thermocouple used to measure the temperatures in the heating block, water bath, and water chiller experiments. Disagreement between the system's temperature readout and external thermocouple temperature was less than 0.5°C. Temperatures varied by <0.2°C over the course of experiment.

We assume that equilibration occurred at the above experimental temperatures based on the following rationale. Experimental vials used in the water baths, refrigerators, water chillers, and freezers were entirely at a uniform temperature throughout the course of each experiment. Thus the measured temperatures directly reflect the temperature of the whole experiment. For the dry-block and oil-bath experiments only, the experimental vials were not at a uniform temperature. This is because the 20 mL vials used are taller than the aluminum block such that the top of a vial (top 30 mm of the total 75 mm height) where the septum is located is exposed to room-temperature air for the duration of the experiment. In the oil bath experiments, the need to grip and stabilize the vials in the oil only allowed for the bottom 40 mm of the vial to be submerged. We do not believe this is an issue as the catalyst pellets, which are where the hydrogen isotope-exchange reactions take place, are only ~3 mm tall and were dispersed on their sides in direct contact with the bottom of the vials (which were at the measured temperature) for the entirety of the experiments.

For the oil-bath and dry-block experiments, sampling of experiments was done while the vials were at the experimental temperature. In order to sample experiments in the water baths, refrigerators, water chillers, and freezers, vials had to be removed from their temperature-controlled environments and briefly exposed to room temperature during sampling. The effects

of this exposure were minimized by sampling experiments within ~10 seconds of their removal from the temperature-controlled environment. We demonstrate in Section 3.2.1 that this brief exposure to room temperature is unlikely to be an issue.

2.3 Isotopic measurements: mass spectrometry and standardization

The hydrogen isotopic composition (δD values; see footnote 1) of H_2 and CH_4 were analyzed at the Center for Isotope Geochemistry at the Lawrence Berkeley National Laboratory using a gas-chromatograph isotope-ratio mass spectrometer (GC-IRMS) system (Thermo Scientific GC TraceGas Ultra system connected to a Thermo Scientific Delta V Plus isotope-ratio mass spectrometer). The gases were sampled using a gas-tight syringe and injected into a stainless-steel loop (10 µL to 250 µL calibrated volumes) attached on a 6-port valve (VICI-Valco). The H_2 and CH_4 were separated chromatographically on a HP-mole sieve fused silica capillary column (30 m x 0.32 mm) using helium as carrier gas. Following chromatographic separation, both H_2 and CH_4 were passed through a ceramic tube at 1450°C, where CH_4 was pyrolyzed and converted to H_2. In this method, the δD values of H_2 (δD_{H2}) and CH_4 (δD_{CH4}) are determined from the same sample gas injection. Ceramic tubes were pre-conditioned by injecting 250 µL of pure CH_4 three times the day before the measurement session.

Measured δD values were first corrected for instrument linearity as described in the appendix (Section A1). Application of these linearity corrections modify our final calculated experimental $1000\times\ln{}^{D}\alpha_{CH4(g)\text{-}H2(g)}$ by an average of 0.33 ± 2.5 ‰ (1 standard deviation, 1σ) and thus do not influence any interpretations.

Following linearity corrections, we corrected measured δD_{CH4} and δD_{H2} values to external H_2 standards purchased from Oztech Trading Corp. with δD_{H2} = -762.61, -364.06, and -124.80‰. These standards were calibrated based on measurements relative to the SMOW, GISP, and SLAP international water standards. The value for the lowest δD standard (-762.61‰) is outside of the range of values for which international reference standards exist (the lowest of which is SLAP with δD_{H2} = -428‰) and, as verified by Oztech Trading Corp., is based on the extrapolation of the calibration curve determined using these water standards to lower values.

δD_{CH4} measurements were further standardized using three CH_4 samples calibrated at the UC Davis Stable Isotope Facility with δD_{CH4} = -159.3‰, -83.2‰, and +20.0‰ based on the methodology given in Yarnes (2013). These determinations are anchored to internationally recognized standards (NGS-1 and NGS-2; see Yarnes, 2013).

Data reported were measured during four separate analytical sessions: February 2019, June 2019, August 2019, and November 2019. In the February 2019 session only, we measured only one methane standard (δD_{CH4} = -159.3‰) and only two of the three Oztech standards (δD_{H2} = -364.06, and -124.80‰). Data were corrected based on measured standard values, but due to this limited standardization, we only report measured δD values of H_2 and methane for initial experiments from this session (i.e., either samples taken immediately upon gas addition to the experimental vials for selected bottom-brackets or after pre-equilibration for top-brackets [six top brackets total]). The δD_{H2} and δD_{CH4} values for the initially injected values of the bottom-bracket experiments are intermediate in value for the H_2 standards and thus allow for interpolation of standards for correction. This is not true for the top-bracket experiments.

However, potential inaccuracies for top-bracket values are considered unimportant. This is because for the pre-equilibrated top-bracket samples, all initial $1000\times\ln{}^{D}\alpha_{CH4(g)\text{-}H2(g)}$ values in the February 2019 session are >80‰ above final values. Average $1000\times\ln{}^{D}\alpha_{CH4(g)\text{-}H2(g)}$ of samples equilibrated at the same temperatures (3 and 15°C) in this session vs. other sessions with full standardization agree within 16.5‰. As such, these can be used to demonstrate top brackets started above final values given differences of >80‰.

2.4 Calculation of $^{D}\alpha_{CH4(g)\text{-}H2(g)}$ and $1000\times ln^{D}\alpha_{CH4(g)\text{-}H2(g)}$ values

Our goal is to determine the value of $1000\times\ln{}^{D}\alpha_{CH4(g)\text{-}H2(g)}$ at a given experimental temperature both for starting and final values. We now describe the process by which we went from a single injection of a sample derived from an experiment into the GC-IRMS system to our final averaged $1000\times\ln{}^{D}\alpha_{CH4(g)\text{-}H2(g)}$ values.

We calculated $^{D}\alpha_{CH4(g)\text{-}H2(g)}$ values from a given experiment (except for some of the 50°C stoichiometry experiments as described below) as follows: we injected gas from a sample into the GC-IRMS and measured both δD_{CH4} and δD_{H2} from the same injection. δD_{CH4} and δD_{H2} values were measured for two to six injections of a single sample for final experimental temperatures and one to two injections for pre-equilibrations. We calculated the $^{D}\alpha_{CH4(g)\text{-}H2(g)}$ value from δD_{CH4} and δD_{H2} values of a given injection and then averaged the $^{D}\alpha_{CH4(g)\text{-}H2(g)}$ values of all replicate injections. $1000\times\ln{}^{D}\alpha_{CH4(g)\text{-}H2(g)}$ values were calculated directly from this average. We note that calculating the final average $1000\times\ln{}^{D}\alpha_{CH4(g)\text{-}H2(g)}$ value of a given experiment by using the average δD_{CH4} and the average δD_{H2} values of replicate gas injections instead of the average $^{D}\alpha_{CH4(g)\text{-}H2(g)}$ changes final $1000\times\ln{}^{D}\alpha_{CH4(g)\text{-}H2(g)}$ by less than 0.24‰ in all cases.

For the 50°C bottom-bracket experiments with 1:4 and 1:2 H_2:CH_4 stoichiometries only, a single measurement injection could not yield sample injection peak areas that allowed for the simultaneous determination of δD_{CH4} and of δD_{H2} values. For these two experiments only, we calculated the final average $^{D}\alpha_{CH4(g)\text{-}H2(g)}$ value for a given experiment by using the average δD_{CH4} and δD_{H2} values from different injections in which gas volumes introduced to the mass spectrometer were altered to yield measurable H_2 or CH_4 peak areas.

To determine the bracketed $1000\times\ln{}^{D}\alpha_{CH4(g)\text{-}H2(g)}$ at a given experimental temperature, we averaged the top- and bottom-bracket $^{D}\alpha_{CH4(g)\text{-}H2(g)}$ values. Final $1000\times\ln{}^{D}\alpha_{CH4(g)\text{-}H2(g)}$ were then calculated from this average. When only one bottom and one top bracket were measured, we took the average of both $^{D}\alpha_{CH4(g)\text{-}H2(g)}$ values. In cases where multiple distinct bottom- or top-bracket experiments were performed at the same temperature (e.g., there are five different bottom-bracket experiments at 50°C), all bottom- or top-bracket $^{D}\alpha_{CH4(g)\text{-}H2(g)}$ values from the different experiments were first averaged, and then averaged with the already averaged top and/or bottom-bracket $^{D}\alpha_{CH4(g)\text{-}H2(g)}$ values.

2.5 Theoretical calculations

Here, we describe how fractionation factors (α) were calculated theoretically for carbon or hydrogen isotopic equilibrium between molecules. Theoretical calculations for isotopic equilibrium were based on calculations of partition function ratios for isotopologues with one rare isotope (i.e., $^{12}CH_3D$ or $^{13}CH_4$) vs. the unsubstituted molecule ($^{12}CH_4$). We report so-called reduced partition function ratios (RPFRs) in which the ratio of isotopic masses and symmetry

numbers are factored out (e.g., Urey, 1947; Bigeleisen and Mayer, 1947; Richet et al., 1977; O'Neil, 1986; Blanchard et al., 2017).

We calculated RPFRs using two distinct approaches: (*i*) We calculated RPFRs using the approaches first outlined by Bigeleisen and Mayer (1947) and Urey (1947), which we term 'harmonic' calculations. In this approach, the total partition function is assumed to factorize into vibrational, rotational and translational components; then the vibrations are approximated as harmonic, rotations as rigid, and both rotations and translations are assumed to be classical. (*ii*) We calculated RPFRs using the Path-Integral Monte Carlo (PIMC) approach (e.g., Cheng and Ceriotti, 2014; Webb et al., 2017). This approach includes a fully anharmonic and quantum mechanical description of the RPFRs (Webb and Miller, 2014; Webb et al., 2017; Eldridge et al., 2019) and thus it is a less approximate method as compared to harmonic calculations. Indeed, PIMC calculations have been used to identify sources of error in harmonic calculations of RPFRs (Webb and Miller, 2014; Webb et al., 2017; Eldridge et al., 2019).

When computing RPFRs we neglected the effects of: (*i*) intermolecular interactions, since the gases are dilute; (*ii*) electronic excitations, since the excited states are well-separated for all the molecules considered here; (*iii*) internal structure of the nuclei; and (*iv*) relativistic effects, since the molecules only contain light atoms (Lutz and Hutson, 2016).

2.5.1 Potential energy surfaces and harmonic frequencies

In order to calculate an RPFR using either the harmonic or PIMC approach, the potential energy surface of the molecule must first be specified. For the PIMC calculations, we used published potentials for CH_4, CO_2, and H_2O, and we calculated the surface for H_2. We refer to these potential energy surfaces as 'reference' potentials. The potential for methane was taken from Lee et al. (1995) and was calculated in that study at the coupled-cluster level with single and double excitations where triple excitations are included perturbatively (i.e., CCSD(T)) using correlation-consistent polarized triple zeta (cc-pVTZ) and quadruple zeta (cc-pVQZ) basis sets. The potential energy surface for H_2O(g) was taken from Partridge and Schwenke (1997) who computed it at internally contracted multireference configuration interaction (icMRCI) and CCSD(T) levels of theory with augmented correlation-consistent polarized quintuple-zeta (aug-cc-pV5Z) and correlation-consistent polarized sextuple zeta (cc-pV6Z) basis sets and three-body terms fitted to reproduce the experimental line positions in rovibrational spectra of water. The carbon dioxide reference potential was taken from Huang et al. (2012). In that study, the CCSD(T)/aug-cc-pVTZ surface was refined based on extrapolation to the one-particle basis set limit, corrections for scalar relativity, higher-order electron correlations, and spectroscopic data from the HITRAN2008 database. We calculated the potential energy surface for H_2 using the Molpro software package (version 2019.2) with CCSD (exact for the two-electron problem) and cc-pVQZ basis set — details of the calculation are given in appendix Section A3.1.

Harmonic calculations of RPFRs solely require determination of the harmonic frequencies at an energy-minimized geometry. We calculated harmonic frequencies (see Table EA1), obtained from the same reference potentials as used for the PIMC calculations (details in Section A3.2). As such, these RPFRs can be compared directly to PIMC results and used to quantify the importance of anharmonic and quantum effects that are absent in the harmonic treatment; we later refer to these harmonic RPFRs as 'reference harmonic' lines.

We also computed the harmonic frequencies from a variety of molecular structures optimized using a hierarchy of levels of theory; these included the restricted Hartree-Fock (RHF) method (a mean-field theory that does not take into account the electron-electron correlations) along with three successively better approximations for the correlation energy: second order Møller-Plesset perturbation theory (MP2) and coupled-cluster with single and double excitations (CCSD), as well as CCSD(T), where triple excitations are included perturbatively (Blinder, 2019; Townsend et al., 2019; Ulusoy and Wilson, 2019). These levels of theory were paired with basis sets of various sizes (cc-pVXZ and aug-cc-pVXZ as defined above, where X=D [double], T [triple], or Q [quadruple]) (Dunning, 1989) using the Molpro software package as described in Section A3. These calculations were done in order to determine the sensitivity of our theoretical calculations of RPFRs to electronic correlations and basis set completeness.

2.5.2 Harmonic RPFR calculations

The RPFR of an isotopologue pair calculated using the harmonic approach (Urey, 1947; Bigeleisen and Mayer, 1947; Richet et al., 1977; O'Neil, 1986; Blanchard et al., 2017) is given by:

$$\mathrm{RPFR}_{\mathrm{harmonic}} = e^{-(E_0^* - E_0)/k_B T} \prod_{j=1}^{a} \frac{\omega_j^*}{\omega_j} \times \frac{1 - e^{-hc\omega_j/k_B T}}{1 - e^{-hc\omega_j^*/k_B T}} \quad (2)$$

In eq. (2), E_0 is the zero-point energy, ω_j is the harmonic frequency (given as wavenumber, cm^{-1}) of the j^{th} normal mode, a is the total number of vibrational modes ($a = 3N - 5$ for linear molecules, $a = 3N - 6$ for non-linear molecules), and * indicates the molecule with a heavy isotopic substitution.

2.5.3 PIMC calculations

PIMC calculations employ the imaginary-time path integral formalism (Feynman and Hibbs, 1965) to map the quantum mechanical partition function onto the classical partition function (Schweizer et al., 1981):

$$Q(N,\beta) = \lim_{P\to\infty} \frac{1}{\sigma} \prod_{i=1}^{N} \left(\frac{m_i P}{2\pi\beta\hbar^2}\right)^{\frac{3P}{2}} \int \prod_{j=1}^{N} \prod_{k=1}^{P} d\boldsymbol{r}_j^{(k)} e^{-\beta_P U_P\left(\{\boldsymbol{r}_j^{(k)}\}\right)} \quad (3)$$

Quantum Boltzmann statistics of the N-particle system are obtained from the classical statistics of an extended classical system, where each of N quantum particles is replaced with a ring-polymer with P beads at inverse temperature $\beta_P = \beta/P$. The beads interact via an effective potential:

$$U_P\left(\{\boldsymbol{r}_j^{(k)}\}\right) = \sum_{j=1}^{N} \sum_{k=1}^{P} \frac{m_j \omega_P^2}{2} \left(\boldsymbol{r}_j^{(k)} - \boldsymbol{r}_j^{(k-1)}\right)^2 + \sum_{k=1}^{P} U\left(\boldsymbol{r}_1^{(k)}, \ldots, \boldsymbol{r}_N^{(k)}\right) \quad (4)$$

In eq. (4), $\boldsymbol{r}_j^{(k)}$ indicates the position of the j^{th} atom in the k^{th} ring-polymer bead, $\omega_P = 1/(\beta_P \hbar)$ is the intra-bead vibrational frequency, $\boldsymbol{r}_j^{(0)} = \boldsymbol{r}_j^{(P)}$, and $U(\boldsymbol{r}_1, \ldots, \boldsymbol{r}_N)$ is the Born–Oppenheimer potential energy surface for the molecular system or the molecular potential. Note that the indistinguishability of identical nuclei in the path integral calculations in eq. (3) is treated using the classical, rotational symmetry number, σ. This is a valid assumption since quantum statistics of identical nuclei can be ignored for temperatures above 100K based on the estimate of the free ring-polymer radius of gyration (Ceperley, 1995).

The methodology for computing the partition function ratios with PIMC in this study follows that employed by Webb and Miller (2014), Webb et al. (2017), and Eldridge et al. (2019), except they reported partition function ratios whereas we report reduced partition function ratios (RPFRs), for which the masses of heavy and light isotopes (m_i and m_i^*) and symmetry numbers (σ, σ^*) are factored out of the computed ratio. The direct scaled-coordinate estimator (Cheng and Ceriotti, 2014) was used to calculate the ratio of partition functions (eq. 3) for heavy vs. light isotopologues. Heavy isotopologue configurations were sampled with PIMC in Cartesian coordinates with an explicit staging transformation (Tuckerman et al., 1993). The staging length, *j*, was set such that 38−42% of all proposed staging moves are accepted. Prior to any data collection, each sampling trajectory was equilibrated for 10^5 Monte Carlo steps, with *P*/*j* staging moves (rounded up to the nearest integer) attempted per Monte Carlo step. Thereafter, ring-polymer configurations were sampled every 10 Monte Carlo steps. The total number of Monte Carlo moves for each partition function ratio calculation was 2×10^8.

Aside from neglecting nuclear exchange, PIMC calculations give an exact answer for RPFRs for a specified potential energy surface in the limit of infinite sampling and infinite number of beads *P*. In practice, a finite number of beads can be chosen to achieve target accuracy, while the number of samples controls statistical uncertainty. The number of beads employed in the PIMC calculations was determined based on explicit convergence tests for the individual RPFRs over the range of temperatures studied. We ensured that the accuracy was within the standard error (s.e.) of the mean. This error is reported for every PIMC calculation as a measure of statistical uncertainty.

2.5.4 Diagonal Born-Oppenheimer corrections

Non-Born-Oppenheimer effects (i.e., inaccuracies associated with the use of the Born-Oppenheimer approximation) are usually negligible compared to the those inherent to the potential energy surface. However, diagonal Born-Oppenheimer corrections (DBO corrections) can become important in high-accuracy electronic structure calculations for small molecules (Valeev and Sherrill, 2003; Feller et al., 2006). DBO corrections are first-order perturbation-theory corrections to the Born-Oppenheimer approximation that correct for the dependence of the electronic wave function on the nuclear coordinates when calculating the nuclear kinetic energy contribution.

We used DBO corrections (Zhang and Liu, 2018) calculated at the CCSD level (Gauss et al., 2006) with the augmented core-valence Dunning basis set (i.e., aug-cc-pCVTZ; Woon and Dunning, 1995; Peterson and Dunning, 2002) for molecules in optimized geometries. DBO corrections were assumed to be locally independent of the nuclear coordinates based on weak (<5 cm^{-1}) dependence for hydrogen around equilibrium (Kolos and Wolniewicz, 1964; Wolniewicz, 1983). With this assumption, the calculated energy shifts associated with this correction (ΔC; see table A1) affect the RPFRs via a free energy shift according to the following equation:

$$\mathrm{RPFR}_{\mathrm{PIMC}}^{\mathrm{DBOC}} = \mathrm{RPFR}_{\mathrm{PIMC}} \exp\left(-\frac{\Delta C}{k_B T}\right) \quad (5)$$

While DBO corrections can become important for fractionation of isotopes of hydrogen between different chemical species, they vanish in importance for self-exchange reactions (where all reactants and products are isotopologues) due to cancellation of errors (Bardo and Wolfsberg, 1975) and can be safely neglected in these cases (such as in work presented by Zimmermann and Vaníček, 2009; Webb and Miller, 2014; Webb et al., 2017; Eldridge et al., 2019). Moreover, they can be neglected for heavy-atom fractionation processes, since they decrease rapidly with increasing mass. More discussion of these effects is given in Section 4.5.3.

3. Results

3.1 Precision and accuracy of measurements

3.1.1 External precision of δD measurements

We estimated the analytical reproducibility (i.e., external precision) for our δD measurements via replicate analyses of H_2 and CH_4 in-house standards. External reproducibility (1σ) of the H_2 and CH_4 standards across all sessions is ±2.0‰ (n = 52) and ±2.3‰ (n = 73) respectively.

3.1.2 Precision of $1000\times ln^{D}\alpha_{CH4(g)\text{-}H2(g)}$ determinations for individual experiments

The average value for $1000\times\ln^{D}\alpha_{CH4(g)\text{-}H2(g)}$ for each top and bottom-bracket experiment is given in Table 1. All individual mass spectrometric measurements for each sample are given in Table EA2 and averages of all top or bottom experiments for a given temperature in Table EA3. Given our typical external 1σ reproducibility of δD_{H2} and δD_{CH4} measurements (±2.0‰ and ±2.3‰ respectively; see above), we estimated (using a Monte Carlo error propagation scheme assuming Gaussian error distribution) that the expected external precision of measured $1000\times\ln\alpha_{CH4(g)\text{-}H2(g)}$ from a given experiment should be between ±4-7‰ (1σ) depending on the value of $^{D}\alpha_{CH4(g)\text{-}H2(g)}$. For our data set, 34 of the 36 final values of $1000\times\ln^{D}\alpha_{CH4(g)\text{-}H2(g)}$ for individual top- or bottom-bracket brackets yield standard deviations within or better than the expected range of 4-7‰. The two experiments that yielded lower precisions were replicated a sufficient number of times such that the final standard error was less than 6‰.

3.1.3 Accuracy of measured $^{D}\alpha_{CH4(g)\text{-}H2(g)}$ values

Accuracy of measured δD values requires standardization to internationally recognized standards. Two sources of inaccuracy can arise in such an approach — accuracy of the standards used and accuracy as a function of sample δD.

For our measurements, H_2 standards are traceable to international water standards (VSMOW, VSLAP, and GISP). Systematic inaccuracies (i.e., constant offsets) will cancel when alpha values are calculated as they will be the same for both CH_4 and H_2. We additionally corrected the CH_4 measurements to CH_4 standards measured at the UC Davis Stable Isotope Facility to account for potential fractionations associated with pyrolysis of CH_4 to H_2. These standards are ultimately anchored to multiple international standards including those from NIST (NGS-1 and NGS-2; Yarnes, 2013).

Beyond the standards used, our measured sample δD_{H2} and δD_{CH4} values differ by hundreds of per mil and were often outside of the calibration range of standards creating potential inaccuracies associated with extrapolations beyond the standard calibration curves. All experimental δD_{H2} values were within the interpolatable δD range of the Oztech H_2 standards (-762.61 to -124.80‰). In contrast, only 8 of 36 experimental CH_4 samples had δD values within

the interpolatable δD range of the CH_4 standards (–159.3‰ to +20.0‰), and only 1 CH_4 sample (from the nickel catalyst experiment) was within the range of the Oztech H_2 standards. Specifically, the other 28 of 36 experiments yielded methane δD values between +20.0‰ and +270‰. Additionally, although measured δD values of H_2 from the experiments were within the range of the Oztech H_2 standards, all but two experiments (both at 200°C) yielded H_2 with δD values less than the that of the SLAP standard (δD_{VSMOW} = -428‰), which is the international standard with the lowest accepted δD value available. This is an issue as it is known that δD_{H2} measurements of samples require standardization to external standards with both lower and higher δD values in order to achieve interlaboratory agreement (Brand and Coplen, 2001). As a result, the lack of international standards with δD_{H2} values less than -428‰ creates the potential for inaccuracies in our measured values at these low δD values.

In order to evaluate the accuracy of our δD determinations independent of our standardization scheme, we equilibrated samples of H_2 and CH_4 with varying stoichiometries of H_2 vs. CH_4 (1:4, 1:2, 1:1 and 2:1) at 50°C. By altering the stoichiometries used for the equilibration, we were able to modify the final equilibrated δD values of the CH_4 and H_2 such that we created a 106‰ range in δD_{H2} (-676 to -570‰) and a 297‰ range in δD_{CH4} (-112 to 185‰). The idea of this test is as follows: if our measured δD values are indeed not only precise, but accurate, then measured $1000\times\ln{}^{D}\alpha_{CH4(g)\text{-}H2(g)}$ values for samples isotopically equilibrated at the same temperature should be identical within error despite the >100‰ ranges in δD_{CH4} and δD_{H2} values. For these experiments, all measured δD_{H2} values were within the δD range of the Oztech standards. The δD_{CH4} values for two of the experiments (H_2:CH_4 stoichiometries of 1:4 and 1:2) were within the range of the CH_4 standards calibrated at UC Davis, and the other two (1:1 and 2:1) were elevated. Thus, this set of experiments allows us to examine samples that both do and do not require extrapolation of corrections beyond the standardized δD_{CH4} range.

The average $1000\times\ln{}^{D}\alpha_{CH4(g)\text{-}H2(g)}$ values of these experiments vs. δD_{H2} and δD_{CH4} are given in Table A2 and shown in Figure 2A and 2B respectively. Based on a linear regression, the slopes for $1000\times\ln{}^{D}\alpha_{CH4(g)\text{-}H2(g)}$ vs. δD_{H2} and $1000\times\ln{}^{D}\alpha_{CH4(g)\text{-}H2(g)}$ vs. δD_{CH4} are 0.002 ± 0.044 and 0.002 ± 0.016 (±1 s.e.) respectively. The slopes are within ±1 s.e. of (and thus statistically indistinguishable from) a value of zero. Based on this, we proceed with the assumption that our CH_4 and H_2 δD measurements are accurate or, if inaccurate, the inaccuracies are systematic such that they will cancel in calculations of ${}^{D}\alpha_{CH4(g)\text{-}H2(g)}$

3.2 $1000\times ln^{D}\alpha_{CH4(g)\text{-}H2(g)}$ values for experiments from 1-200°C

3.2.1 Initial values of top and bottom brackets

Initial and final top- and bottom-bracket $1000\times\ln{}^{D}\alpha_{CH4(g)\text{-}H2(g)}$ values are given in Table 1. As discussed in Section 2.2.2, for most experiments (1, 3, 10, 15, 25, 35, 50, 75, 100, 127, and 156°C) bottom brackets were performed using the initial isotopic composition of the CH_4 and H_2 added to the vials at the start of the experiments. This created an initial ${}^{D}\alpha_{CH4(g)\text{-}H2(g)}$ = 1.092 ($1000\times\ln{}^{D}\alpha_{CH4(g)\text{-}H2(g)}$ = 88‰). We verified that adding gases to the vials did not fractionate the gases (and thus resulted in bottom bracket experiments) through a series of spot checks. Specifically, we sampled some of these experiments (3, 15, 50, 75, 127, and 156°C) within 10 seconds of gas addition before placing them at desired experimental temperature (see Section 2.2.2). The average $1000\times\ln{}^{D}\alpha_{CH4(g)\text{-}H2(g)}$ of these six initial samples is 85.8 ± 2.6‰ (1 s.e.),

within 1 s.e. of the known starting gas composition of 88‰. This demonstrates two important aspects of our experiments: First, the initial starting point for bottom bracket experiments that were not pre-equilibrated was the $^{D}\alpha_{CH4(g)\text{-}H2(g)}$ of the starting gas composition (within ±1 s.e.). Second, the time it took to sample these experiments after gas addition (10 seconds) did not measurably alter the initial δD values. Based on this, we conclude that removal of samples from water baths, refrigerators, or freezers and exposure to ambient air for 10 seconds during sampling is unlikely to have disturbed measured δD values beyond analytical precision.

For all other bottom brackets where the starting composition was the initial gas composition (1, 10, 25, 35, and 100°C), we did not sample the initial bottom bracket composition. For these experiments, we assumed the initial gas composition to be the starting composition as discussed above — we consider this justified based on the above spot checks. For the 180 and 200°C experiments, the bottom brackets were created by pre-heating the experiments to 200 and 230°C respectively and a sub-sample taken before lowering the temperature of the vials to the final experimental temperature. In both cases, $1000\times\ln^{D}\alpha_{CH4(g)\text{-}H2(g)}$ values from the pre-equilibrations are less than the final measured $1000\times\ln^{D}\alpha_{CH4(g)\text{-}H2(g)}$.

At every experimental temperature, a top-bracket experiment was also performed, and a sample taken to check that the initial $1000\times\ln^{D}\alpha_{CH4(g)\text{-}H2(g)}$ was larger than the final $1000\times\ln^{D}\alpha_{CH4(g)\text{-}H2(g)}$ value. In all cases except for the 25°C experiment (where sampling of the pre-equilibrated top bracket failed; see below), these values were above the final $1000\times\ln^{D}\alpha_{CH4(g)\text{-}H2(g)}$ of a given experiment.

Sampling of the top bracket for the 25°C experiment at the pre-equilibration temperature of 3°C failed. This was only found after heating the experiment to the final temperature of 25°C. Nonetheless, we believe that the final $1000\times\ln^{D}\alpha_{CH4(g)\text{-}H2(g)}$ of this top-bracket experiment was approached from an initially higher value. This is because isotopic equilibrium at 3°C is reached within 1 day (see equilibration time in Table 1) in other experiments performed here. The top bracket for the 25°C experiment was pre-equilibrated at 3°C for 8 days prior to heating to 25°C and thus should have reached hydrogen isotopic equilibrium at 3°C. Additionally, the final $1000\times\ln^{D}\alpha_{CH4(g)\text{-}H2(g)}$ values for the top and bottom brackets, which were both held at 25°C for 25.4 hours each, yield values within 6‰ of each other and thus agree within typical experimental reproducibilities (see below). This indicates that the catalysts were active during the experiments following the pre-equilibrations. Based on this, we use this top-bracket experiment in our calibration of the equilibrium temperature dependence of $^{D}\alpha_{CH4(g)\text{-}H2(g)}$.

3.2.2 Evaluation of the bracketed experiments.

In a successfully bracketed set of experiments, the initial values of$1000\times\ln^{D}\alpha_{CH4(g)\text{-}H2(g)}$ are larger or smaller than the final value (depending on the bracketing direction). This requirement was discussed in the above section and is shown visually in Figure 3A and 3B.

Another requirement for a successfully bracketed experiment is that the final top- and bottom-brackets yield the same (within error) value of $^{D}\alpha_{CH4(g)\text{-}H2(g)}$. Such agreement is taken as demonstration that isotopic equilibrium was achieved in the experiments (O'Neil, 1986). Thus, in order to know whether $^{D}\alpha_{CH4(g)\text{-}H2(g)}$ values of brackets agree within error, we need a constraint on our typical experimental reproducibility for determinations of $1000\times\ln^{D}\alpha_{CH4(g)\text{-}H2(g)}$. We

estimated our experimental reproducibility using the 50°C experiments where five bottom-bracket experiments and one top-bracket experiment were performed. These six experiments yield ±1σ reproducibility of 4.2‰. As a first pass, we consider any pairs of final top- and bottom-bracket $1000\times\ln^{D}\alpha_{CH4(g)\text{-}H2(g)}$ values that yield standard deviations of less than 4.2‰ as being successfully bracketed. The 3, 10, 25, 50, 75, 100, and 127°C experiments pass this test. Of the remaining experiments with standard deviations higher than 4.2‰, the 15, 35, 157, and 180°C experiments yield final top-bracket $1000\times\ln^{D}\alpha_{CH4(g)\text{-}H2(g)}$ values that are lower than the final bottom bracket values. Final top-bracket values that are less than bottom-bracket values are not expected assuming a unidirectional approach to equilibrium and thus we propose these also were successfully bracketed. These experiments yield standard deviations of up to 9.6‰, and we expect that this is a more conservative estimate of our true external experimental reproducibility.

The 1°C and 200°C experiments both show elevated standard deviations for top- and bottom-bracket experiments and yield top-bracket experiments with $1000\times\ln^{D}\alpha_{CH4(g)\text{-}H2(g)}$ larger than the bottom-bracket experiments — such a difference can indicate that equilibrium was not reached at the end of the experiment. The standard deviation of the top and bottom brackets for the 1 and 200°C experiments are 26.3 and 23.1‰, respectively. For comparison, as stated above, the next highest standard deviation is 9.6‰. The high standard deviation for the 200°C experiments is driven by one of the two 200°C top-bracket experiments (note that for the 200°C experiment, the top and bottom brackets were replicated twice each). This top bracket value for $1000\times\ln^{D}\alpha_{CH4(g)\text{-}H2(g)}$ differs by more than 35‰ from all other 200°C experiments, indicating poor experimental reproducibility. Removal of this experiment results in a standard deviation between the remaining top and bottom brackets of 10.5‰, similar to the other experiments we consider successful (i.e., 9.6‰). We are unsure why this single 200°C experiment disagreed with the other experiments. Regardless, we assume it failed for unknown reasons and exclude it for the final calculation of $1000\times\ln^{D}\alpha_{CH4(g)\text{-}H2(g)}$ for the 200°C experiment. We use the other experiments at 200°C for our final calculation of $1000\times\ln^{D}\alpha_{CH4(g)\text{-}H2(g)}$ and include these in our calibration.

For the 1°C experiment, only one top and one bottom bracket were performed. As discussed in the methods section, the refrigerator used for this experiment exhibited a duty cycle in which temperatures would change every 36 hours by 7°C before returning to 1°C. Although we attempted to sample only when temperatures were 1°C for 24 hours, we suspect this temperature oscillation has impacted the final $1000\times\ln^{D}\alpha_{CH4(g)\text{-}H2(g)}$ values. Regardless, due to the large measured difference in the $1000\times\ln^{D}\alpha_{CH4(g)\text{-}H2(g)}$ values of top and bottom brackets at 1°C (1σ of 26.3‰) and the higher value for the top vs. bottom bracket, we consider this experiment to be unsuccessful and we do not include it in our calibration of $1000\times\ln^{D}\alpha_{CH4(g)\text{-}H2(g)}$ vs. temperature.

3.2.3 Calculation of the equilibrium $^{D}a_{CH4(g)\text{-}H2(g)}$ values as a function of temperature for our experiments

We present final averaged values of $1000\times\ln^{D}\alpha_{CH4(g)\text{-}H2(g)}$ for experiments (average of the top and bottom brackets) that we consider to have reached hydrogen isotopic equilibrium in Figure 3C and D as well as Table 2.

We obtained an interpolatable expression for $1000\times\ln^{D}\alpha_{CH4(g)\text{-}H2(g)}$ as a function of temperature by regressing $1000\times\ln^{D}\alpha_{CH4(g)\text{-}H2(g)}$ vs. $1/T$ (K^{-1}) over 3-200°C using a 2nd order polynomial (Fig. 3C):

$$1000 \times \ln {}^{D}\alpha_{CH_4(g)-H_2(g)} = \frac{3.5317 \times 10^7}{T^2} + \frac{2.7749 \times 10^5}{T} - 179.48 \quad (6)$$

A quadratic fit was employed as, based on ANOVA, only terms up to 2nd order were statistically significant ($p < 0.05$). Residuals to the fit have a 1σ of 5.9‰. The polynomial terms and associated errors for this equation as well as others derived below are given in Table EA4, and in an Excel spreadsheet calculator in Table EA5.

3.3 Theoretical equilibrium calculations

The results of PIMC calculations for hydrogen-isotope RPFRs vs. temperature for CH_4, H_2, and H_2O are given in Table 3 and the carbon-isotope RPFRs vs. temperature for CH_4 and CO_2 in Table 4. In these tables, all given PIMC values include DBO corrections unless otherwise noted; uncorrected PIMC values and differences between DBO-corrected and uncorrected values are given in Tables A3 and A4. For hydrogen-isotope calculations from 0 to 500°C, DBO corrections are between -34 to -12‰ for $1000\times\ln{}^{D}\alpha_{H2O(g)\text{-}H2(g)}$, +12 to +34‰ for $1000\times\ln{}^{D}\alpha_{CH4(g)\text{-}H2O(g)}$, and +0.1 to +0.3‰ for $1000\times\ln{}^{D}\alpha_{CH4(g)\text{-}H2(g)}$ from 0 to 500°C. For carbon $1000\times\ln{}^{13}\alpha_{CH4(g)\text{-}CO2(g)}$ calculations, DBO corrections are between -0.3 and -0.05‰ from 0 to 1300°C. For consistency, we use the DBO-corrected PIMC values in all cases, even when the correction is minor (<1‰).

Values of $1000\times\ln{}^{D}\alpha_{CH4(g)\text{-}H2(g)}$, $1000\times\ln{}^{D}\alpha_{CH4(g)\text{-}H2O(g)}$, $1000\times\ln{}^{D}\alpha_{H2O(g)\text{-}H2(g)}$, and $1000\times\ln{}^{13}\alpha_{CH4(g)\text{-}CO2(g)}$ for DBO-corrected PIMC calculations were fit as a function of 1/T using a 4th order polynomial (Fig. A1; see Table EA6 for the coefficients). Although ANOVA indicates higher order terms are statistically significant ($p < 0.05$) in some cases, their inclusion changed values of 1000×lnα by less than 0.5‰ for hydrogen isotopes and less than 0.05‰ for carbon isotopes in all cases across the calculated range in temperatures. We consider this insignificant and limit the fits to 4th order terms for simplicity.

3.4 Determination of ${}^{D}\alpha_{H2O(l)\text{-}H2(g)}$ vs. temperature at isotopic equilibrium

In order to calculate the equilibrium fractionation factor between CH_4(g) and liquid water (${}^{D}\alpha_{CH4(g)\text{-}H2O(l)}$) using our experimental calibration for ${}^{D}\alpha_{CH4(g)\text{-}H2(g)}$, it is necessary to know ${}^{D}\alpha_{H2O(l)\text{-}H2(g)}$ as a function of temperature for an isotopically equilibrated system. The hydrogen-isotope fractionation factor between gaseous H_2 and liquid water has been determined experimentally by Rolston et al. (1976) from 6 to 95°C. Additionally, equilibrium hydrogen isotope fractionation factors between gaseous H_2 and water vapor (${}^{D}\alpha_{H2O(g)\text{-}H2(g)}$) have been determined experimentally by Suess (1949) from 80 to 200°C and by Cerrai et al. (1954) from 51 to 742°C. We use these experiments to construct a calibration of ${}^{D}\alpha_{H2O(l)\text{-}H2(g)}$ as a function of temperature. To do this, we convert experimentally determined values of ${}^{D}\alpha_{H2O(g)\text{-}H2(g)}$ to ${}^{D}\alpha_{H2O(l)\text{-}H2(g)}$ using the experimentally based calibration for hydrogen isotopic equilibrium between water vapor and liquid water (${}^{D}\alpha_{H2O(l)\text{-}H2O(g)}$) given by Horita and Wesolowski (1994). This calibration is based on experiments (Merlivat et al., 1963; Bottinga, 1968; Rennow, 1970; Majoube, 1971; Stewart and Friedman, 1975; Kakiuchi and Matsuo, 1979; Horita and Wesolowski, 1994) that span a temperature range of 0.75 to 350°C. Horita and Wesolowski (1994) state that the calibration can be extrapolated from 0°C to the critical point of water (374°C).

In order to calculate a fit to the experimental data vs. temperature, we first average published experimental values of $1000\times\ln^{D}\alpha_{H2O(g)\text{-}H2(g)}$ or $1000\times\ln^{D}\alpha_{H2O(l)\text{-}H2(g)}$ performed within 1°C of each other from a given study (i.e., values from different studies at similar temperatures are not averaged). We take these averages to prevent experiments replicated at the same temperature from having undue weight in our fits. Following this, we convert $1000\times\ln^{D}\alpha_{H2O(g)\text{-}H2(g)}$ to $1000\times\ln^{D}\alpha_{H2O(l)\text{-}H2(g)}$ using the polynomial fit from Horita and Wesolowski (1994) (the first equation in their abstract). Note that we only used data from Cerrai et al. (1954) for experiments performed below the critical point of water (374°C). The compiled experimental data is displayed in Figure 4A and given in Table EA7.

Generally, when experiments from different studies were performed over a similar temperature range (~50 to 200°C), there is agreement between all three studies. As previously noted in Rolston et al. (1976) and Bardo and Wolfsberg (1976), two data points from Cerrai et al. (1954) at 59 and 64°C differ both from other data in that calibration as well as those from Rolston et al. (1976) over the same temperature range. These points are noted in the figure and are omitted from our calibration due to the apparent anomalous behavior (see discussion in Rolston et al., 1976). We discuss how their inclusion would change the fits below.

We initially calculated the temperature dependence of $1000\times\ln^{D}\alpha_{H2O(l)\text{-}H2(g)}$ vs. $1/T$ (K^{-1}) using a 4th order polynomial fit to the experimental data given in Figure 4A. However, the best-fit line had multiple changes in concavity. In contrast, theory predicts a smooth, concave up temperature dependence (Bardo and Wolfsberg, 1976; Horita and Wesolowski, 1994; Gropp et al., 2021; this study). We believe this difference is due to the polynomial fit being influenced by the scatter of the experimental data, which is approximately ±25‰ from 0 to 374°C.

In order to use the experimental data as a constraint on the temperature dependence of $1000\times\ln^{D}\alpha_{H2O(l)\text{-}H2(g)}$, but at the same time avoid fitting the experimental noise, we do not directly regress these experimentally determined equilibrium $1000\times\ln\alpha$ values vs. $1/T$; instead, we perform a least squares fit of the theoretical DBO-corrected PIMC calculations to the experimental data, where only a constant (temperature-independent) term is allowed to vary. This is done to ensure the theoretically expected shape of the temperature dependence for $1000\times\ln^{D}\alpha_{H2O(l)\text{-}H2(g)}$ is preserved in the fit to the experimental data. To do this we combined our DBO-corrected PIMC calculations of $1000\times\ln^{D}\alpha_{H2O(g)\text{-}H2(g)}$ at the experimental temperatures with those of $1000\times\ln^{D}\alpha_{H2O(l)\text{-}H2(g)}$ using the calibration of Horita and Wesolowski (1994). A constant offset is then added to the theoretical values based on the least squares fit to the experiment. Alternative fits with multiplicative terms are discussed in the appendix and yield maximum differences of 10‰ at 0°C. We then found the final equation for $1000\times\ln^{D}\alpha_{H2O(l)\text{-}H2(g)}$ as a function of temperature as follows: we calculated $1000\times\ln^{D}\alpha_{H2O(g)\text{-}H2(g)}$ based on our DBO-corrected PIMC calculations from 0 to 374°C at 0.1°C intervals, added the offset term found above, and then added the $1000\times\ln^{D}\alpha_{H2O(l)\text{-}H2O(g)}$ value calculated at that temperature based on the calibration of Horita and Wesolowski (1994). We then fit a 4th order polynomial to these points. This yielded the following equation, which is explicitly valid from 6.7 to 357°C (i.e., the experimental temperature range):

$$1000 \times \ln^{D}\alpha_{H_2O(l)-H_2(g)} = \frac{7.9443\times10^{12}}{T^4} - \frac{8.7772\times10^{10}}{T^3} + \frac{3.8504\times10^{8}}{T^2} - \frac{2.6650\times10^{5}}{T} + 202.57 \quad (7)$$

The PIMC calculations were offset by 0.49‰ (±1.91‰, 1 s.e.) to fit the experimental data (Fig. 4C). Although the offset required for the DBO-corrected PIMC fit is within 1 s.e. of 0, we still apply this offset (0.49‰) in eq. (7) for consistency. For this fit, the standard deviation of the residual from all experiments is 12.3‰. The mean and ±1σ of residuals vs. eq. (7) for each individual published data set are: 1.3 ± 5.2‰ for Suess (1949), -2.6 ± 15.4‰ for Cerrai et al. (1954), and 2.3 ± 10.1‰ for Rolston et al. (1976) (Fig. 4B). Finally, we note that inclusion of the two omitted data points from Cerrai et al. (1954) discussed above changes the constant term added to our PIMC calculations by -2.7‰ (-2.16‰ vs. 0.49‰).

The residuals of fits show no obvious pattern either as a function of temperature or study, scattering about a value of 0‰ for all studies (Fig. 4B and C). This indicates that the experiments and theory agree in terms of the expected temperature dependence and justifies our approach to using the theoretical temperature dependence as a basis for our fit to the experiments. Additionally, it shows that experiments from different studies are in agreement when they overlap in temperature. We note that this is in contrast with the conclusions of Horibe and Craig (1995) and Wang et al. (2015). They considered these experimental calibrations to be in disagreement at high temperatures (>300°C) (Horibe and Craig, 1995) and low temperatures (<100°C) (Wang et al., 2015).

In Figure 4A, B, and C, we also include other theoretical calculations and experimental values of $1000\times\ln{}^{D}\alpha_{H2O(l)\text{-}H2(g)}$ (Bottinga, 1969; Bron et al., 1973; Bardo and Wolfsberg, 1976; Richet et al., 1977; Gropp et al., 2021). We discuss these below in Section 4.4.

3.5 Determination of ${}^{D}a_{CH4(g)\text{-}H2O(l)}$ and of ${}^{D}a_{CH4(aq)\text{-}H2O(l)}$ as a function of temperature at isotopic equilibrium

We derived an equation for $1000\times\ln{}^{D}\alpha_{CH4(g)\text{-}H2O(l)}$ vs. 1/T (K^{-1}) at isotopic equilibrium by subtracting our equation for $1000\times\ln{}^{D}\alpha_{H2O(l)\text{-}H2(g)}$ (eq. 7) from our equation for $1000\times\ln{}^{D}\alpha_{CH4(g)\text{-}H2(g)}$ (eq. 6). This equation can be interpolated from 3 to 200°C (Fig. 5).

$$1000\times\ln{}^{D}\alpha_{CH_4(g)-H_2O(l)} = -\frac{7.9443\times10^{12}}{T^4}+\frac{8.7772\times10^{10}}{T^3}-\frac{3.4973\times10^{8}}{T^2}+\frac{5.4398\times10^{5}}{T}-382.05 \quad (8)$$

We use 3°C as our lower limit as this is the lowest temperature at which we equilibrated the hydrogen isotopes of CH_4 and H_2 experimentally. We note that the lowest temperature available for $H_2O(l)$-$H_2(g)$ hydrogen isotope equilibrium is 6.7°C. However, as our calibration of $1000\times\ln{}^{D}\alpha_{H2O(l)\text{-}H2(g)}$ is based on a theoretical fit to the experimental data, we consider it acceptable to use eq. (8) for to calculate equilibrium $1000\times\ln{}^{D}\alpha_{CH4(g)\text{-}H2O(l)}$ values from 3 to 200°C.

Finally, CH_4 is found in the environment both as a gas and dissolved in water. To account for this, we use the experimentally measured values of $1000\times\ln(CD_4/CH_4)$ in gas vs. liquid given in Gomes and Grolier (2001) from 12-51°C. We convert these to values of $1000\times\ln{}^{D}\alpha_{CH4(aq)\text{-}CH4(g)}$ by assuming the isotopes are randomly distributed amongst all isotopologues. As such, the 4th root of gaseous or dissolved CD_4/CH_4 ratios allows for the calculation of equilibrium $1000\times\ln{}^{D}\alpha_{CH4(aq)\text{-}CH4(g)}$ values. These solubility isotope effects show no apparent temperature dependence from 12-

51°C — linear regression of $1000\times\ln^{D}\alpha_{CH4(aq)\text{-}CH4(g)}$ vs. 1000/T (K^{-1}) yields a slope of -1.3 ± 2.6 (1 s.e.). Based on this, we assume the value of $1000\times\ln^{D}\alpha_{CH4(aq)\text{-}CH4(g)}$ from 12 to 51°C is constant and equal to 4.2 ± 0.4‰ (1 s.e.). This is the average of the experimental determinations of $1000\times\ln^{D}\alpha_{CH4(aq)\text{-}CH4(g)}$ at all temperatures.

Incorporating this isotope effect into eq. (8) yields the following equation for $1000\times\ln^{D}\alpha_{CH4(aq)\text{-}H2O(l)}$ vs. 1/T (K^{-1}) at isotopic equilibrium:

$$1000 \times \ln^{D}\alpha_{CH_4(aq)-H_2O(l)} = -\frac{7.9443\times10^{12}}{T^4}+\frac{8.7772\times10^{10}}{T^3}-\frac{3.4973\times10^{8}}{T^2}+\frac{5.4398\times10^{5}}{T}-386.25 \quad (9)$$

This equation can be interpolated from 12-51°C (Fig. 5).

3.6 Determination of $^{13}a_{CH4(g)\text{-}CO2(g)}$ and $^{13}a_{CH4(aq)\text{-}CO2(aq)}$ at isotopic equilibrium as a function of temperature

Here we present equations for carbon isotopic equilibrium between CH_4(g) and CO_2(g) and between CH_4(aq) and CO_2(aq) vs. temperature. We use these in Section 5 in order to compare the carbon isotopic composition of CH_4 and CO_2 from environmental samples relative to what is expected for isotopic equilibrium between the two.

As discussed in the introduction (Section 1.2), we are aware of two studies that experimentally determined the equilibrium fractionation factors between CH_4(g) and CO_2(g) ($^{13}\alpha_{CH4(g)\text{-}CO2(g)}$): Horita (2001) and Kueter et al. (2019). Between these two studies, experimentally determined values of $^{13}\alpha_{CH4(g)\text{-}CO2(g)}$ for isotopic equilibrium are available from 200 to 1200°C and are in agreement (within 0.01 to 1.01‰) where experiments overlap in temperature (300 to 600°C).

We are interested here in values for $^{13}\alpha_{CH4(g)\text{-}CO2(g)}$ at isotopic equilibrium at temperatures <200°C, i.e., overlapping the temperature range of the CH_4-H_2 equilibration experiments performed in this study. As no experimental calibrations are available at these temperatures, we estimate these values using the approach based on that of Clayton and Kieffer (1991) discussed above in which a theoretical calibration is offset to fit the experimental data and used as the basis for extrapolations to lower temperatures. A similar approach was taken in both Horita (2001) and Kueter et al. (2019). Specifically, we use the fourth order polynomial fit of $1000\times\ln^{13}\alpha_{CH4(g)\text{-}CO2(g)}$ vs. 1/T (K^{-1}) to our theoretically calculated points (the DBO-corrected PIMC values; see Section 3.3), and then fit these curves to the experimental data using a constant offset to minimize the sum of square residuals as above (see Section 3.5). This results in the following equation (Fig. A2):

$$1000 \times \ln^{13}\alpha_{CH_4(g)-CO_2(g)} = -\frac{2.6636\times10^{11}}{T^4}+\frac{2.8883\times10^{9}}{T^3}-\frac{1.3292\times10^{7}}{T^2}+\frac{1.7783\times10^{3}}{T}-0.70 \quad (10)$$

In our DBO-corrected PIMC calculations, the theoretical curve is decreased by 0.56‰ (±0.12‰, 1 s.e.) to fit the experimental data. For comparison, PIMC calculations without the DBO correction yield an offset of 0.94‰ (±0.08‰, 1 s.e.) to fit the experimental data. Alternative fits with multiplicative terms are discussed in the appendix and yield maximum differences at 0°C of 3‰.

We account for isotope effects associated with the dissolution of CO_2 and methane in water using the experimental data from Vogel et al. (1970) in which CO_2(g) and CO_2(aq) were equilibrated from 0 to 60°C. We refit the data in terms of $1000\times\ln{}^{13}\alpha_{CO2(aq)\text{-}CO2(g)}$ vs. 1/T (K^{-1}) (the fit was originally given as $1000\times({}^{13}\alpha_{CO2(aq)\text{-}CO2(g)}-1)$ vs. T(°C)) to allow for the interconversion of lnα calibrations of various species via addition (or subtraction) of polynomial terms. This refit results in the following equation:

$$1000 \times \ln{}^{13}\alpha_{CO_2(aq)-CO_2(g)} = -\frac{378.46}{T}+0.2016 \quad (11)$$

For methane, Bacsik et al. (2002) provides values for experimental determinations of $1000\times\ln{}^{13}\alpha_{CH4(aq)\text{-}CH4(g)}$ at isotopic equilibrium at 20, 50, and 80°C that were originally presented in Harting et al. (1976). We used this data to find the following equation:

$$1000 \times \ln{}^{13}\alpha_{CH_4(aq)-CH_4(g)} = \frac{485.54}{T}-1.0453 \quad (12)$$

Combination of eqs. (10), (11), and (12) yields the following equation for carbon isotopic equilibrium between aqueous CH_4 and CO_2:

$$1000 \times \ln{}^{13}\alpha_{CH_4(aq)-CO_2(aq)} = -\frac{2.6636\times10^{11}}{T^4}+\frac{2.8883\times10^{9}}{T^3}-\frac{1.3292\times10^{7}}{T^2}+\frac{2.6423\times10^{3}}{T}-1.95 \quad (13)$$

This resulting equation is interpolatable from 20-60°C.

Again, the terms for these fits and their associated errors are given in Table EA4, and an Excel-based calculator in Table EA5.

4. Discussion

4.1 Comparison of our calibration of $1000\times\ln{}^{D}\alpha_{CH4(g)\text{-}H2(g)}$ vs. that of Horibe and Craig (1995)

We compare our calibration of $1000\times\ln{}^{D}\alpha_{CH4(g)\text{-}H2(g)}$ (3-200°C) at isotopic equilibrium to the published experimental calibration from Horibe and Craig (1995) (200-500°C) in Figure 6A and B. Extrapolation of their best-fit line to the temperatures covered by our experiments yields maximum differences in calculated vs. measured $1000\times\ln{}^{D}\alpha_{CH4(g)\text{-}H2(g)}$ of 92.6‰ (at 3°C).

These differences are due to at least two factors. First, the equation that Horibe and Craig (1995) provide for the temperature dependence of ${}^{D}\alpha_{CH4(g)\text{-}H2(g)}$ is based on a fit of ${}^{D}\alpha_{CH4(g)\text{-}H2(g)}$ vs. $1/T^2$. They regressed α vs. $1/T^2$ instead of lnα vs. $1/T^2$ because, as they state, polynomial fits of α vs. $1/T^2$ yield fits with uniform precision as a function of the value of α. Regardless of the merit of their argument, based on theoretical studies, ${}^{D}\alpha_{CH4(g)\text{-}H2(g)}$ is not expected to vary linearly with $1/T^2$ from 3 to 500°C. For example, from 3 to 500°C, theoretically calculated RPFRs from Richet et al. (1977) and our PIMC calculations indicate that $1000\times\ln{}^{D}\alpha_{CH4(g)\text{-}H2(g)}$ vs. 1/T follows a 2nd order polynomial relationship. If instead we fit the data from Horibe and Craig (1995) using a 2nd order polynomial relationship for $1000\times\ln{}^{D}\alpha_{CH4(g)\text{-}H2(g)}$ vs. 1/T and extrapolate to 3°C, our measured $1000\times\ln{}^{D}\alpha_{CH4(g)\text{-}H2(g)}$ at 3°C is within 3‰ of the predicted extrapolated value (1291.8‰ vs. 1288.4‰). Thus, some degree of the difference observed between our study vs. extrapolated values from the equation given in Horibe and Craig (1995) at low temperatures (<200°C) is likely due to their decision to fit ${}^{D}\alpha_{CH4(g)\text{-}H2(g)}$ vs. $1/T^2$.

The second factor appears to be true disagreement between the two studies at overlapping experimental temperatures. Specifically, both studies equilibrated CH_4 and H_2 near 200°C (200.2°C here and 203.4°C in Horibe and Craig, 1995). $1000\times\ln{}^{D}\alpha_{CH4(g)\text{-}H2(g)}$ values at 200°C based on the best-fit lines of the two studies are offset by 22.9‰. This is not simply an issue of differences at a single experimental temperature. Rather, as can be seen in Figure 6B, our data from 157-200°C lie consistently above values that would be expected based on the projection of the Horibe and Craig (1995) calibration to lower temperatures. We are unsure of the origin of this offset. Both studies demonstrate that measured ${}^{D}\alpha_{CH4(g)\text{-}H2(g)}$ values do not depend on the bulk isotopic composition of the gases. Further evaluation of comparability of the isotopic compositions from Horibe and Craig (1995) to ours is difficult as they do not provide measurements of external standards.

The question is which, if any, of the two determinations of $1000\times\ln{}^{D}\alpha_{CH4(g)\text{-}H2(g)}$ vs. temperature is accurate? To examine this, we used natural samples commonly thought to form in or achieve isotopic equilibrium at known temperatures. Specifically, we examined measured values of ${}^{D}\alpha_{CH4(g)\text{-}H2O(l)}$ from black-smoker hydrothermal systems with known venting temperatures. Previous studies have assumed that in such high temperature (>200°C) systems, the methane emitted is in hydrogen isotopic equilibrium with the vented fluids at the venting temperature (e.g., Horibe and Craig, 1995; Proskurowski et al., 2006). Such an assumption is independently supported by studies of methane clumped-isotopic compositions from black smokers that indicate that methane in these systems yields apparent clumped-isotope temperatures above 270°C (Wang et al., 2015; Douglas et al., 2017; Wang et al., 2018). We compare CH_4 to liquid water as the H_2 re-equilibrates to lower temperatures following venting (e.g. Proskurowski et al., 2006). We discuss our ability to assign observed differences to issues in calibrations of ${}^{D}\alpha_{CH4(g)\text{-}H2(g)}$ vs. ${}^{D}\alpha_{H2(g)\text{-}H2O(l)}$ below.

We compiled measurements of ${}^{D}\alpha_{CH4(g)\text{-}H2O(l)}$ from vents with fluid temperatures between 200 and 374°C and compared the ${}^{D}\alpha_{CH4(g)\text{-}H2O(l)}$ values measured vs. those that would be predicted by Horibe and Craig (1995) based on hydrogen isotopic equilibrium at the vent temperature (Fig. A3). Using the equation for ${}^{D}\alpha_{CH4(g)\text{-}H2O(l)}$ given by Horibe and Craig (1995) (see unnumbered equation given in their final paragraph) results in an average under prediction of $1000\times\ln{}^{D}\alpha_{CH4(g)\text{-}H2O(l)}$ of 12.3‰ (±2.0‰ 1 s.e.).

The equation for ${}^{D}\alpha_{CH4(g)\text{-}H2O(l)}$ given by Horibe and Craig (1995) is based on the combination of their calibration for ${}^{D}\alpha_{CH4(g)\text{-}H2(g)}$ with calibrations of ${}^{D}\alpha_{H2O(g)\text{-}H2(g)}$ from Suess (1949) and $\alpha_{H2O(l)\text{-}H2O(g)}$ from Horita and Wesolowski (1994), both of which are used in our calibration as well. These calibrations of ${}^{D}\alpha_{CH4(g)\text{-}H2(g)}$ and ${}^{D}\alpha_{H2O(l)\text{-}H2O(g)}$ can be interpolated from 200-374.1°C. However, the maximum temperature used in the experiments of Suess (1949) to constrain ${}^{D}\alpha_{H2O(g)\text{-}H2(g)}$ is 200°C. Horibe and Craig (1995) fit the experiments from Suess (1949) such that ${}^{D}\alpha_{H2O(g)\text{-}H2(g)}$ depends linearly on $1/T^2$ and extrapolated this fit to higher temperatures. For reasons discussed above, there is not a theoretical basis to assume ${}^{D}\alpha_{H2O(g)\text{-}H2(g)}$ depends linearly on $1/T^2$. To examine potential issues associated with this extrapolation, we combined our calibration of ${}^{D}\alpha_{H2O(l)\text{-}H2(g)}$ (eq. 7, this study) with that of ${}^{D}\alpha_{CH4(g)\text{-}H2(g)}$ from Horibe and Craig (1995) to calculate ${}^{D}\alpha_{CH4(g)\text{-}H2O(l)}$ values. This combination allows for interpolation from 3 to

374°C based on experimental calibrations. Using this equation, the Horibe and Craig (1995) calibration under predicts hydrothermal $^{D}\alpha_{CH4(g)-H2O(l)}$ values by an average of 29.8‰ (±1.7‰; 1 s.e.). This difference is similar in magnitude (22.9‰) and of the same sign that we observe between our calibration of $^{D}\alpha_{CH4(g)-H2(g)}$ at 200°C vs. the data given in Horibe and Craig (1995).

Consequently, our experiments and hydrothermal samples suggest that experimentally determined values of $^{D}\alpha_{CH4(g)-H2(g)}$ given in Horibe and Craig (1995) may be too low by 20‰ to 30‰ for unknown reasons. As we are uncertain of the cause of this discrepancy and because we could not use our experimental setup to bracket temperatures above 200°C, we do not attempt to provide a single calibration of $^{D}\alpha_{CH4(g)-H2(g)}$ from 3-500°C through combination of the two studies.

4.2 Comparison of our experimentally determined $^{D}\alpha_{CH4(g)-H2O(l)}$ calibration to theoretical calculations and to the experimental calibration of Horibe and Craig (1995)

In Figure 5, we compare our experimentally based calibration of $^{D}\alpha_{CH4(g)-H2O(l)}$ for isotopic equilibrium to the experimentally based calibration of Horibe and Craig (1995) for temperatures from 0 to 200°C. Over this temperature range, the two calibrations show disagreement, the magnitude of which increases with decreasing temperature (Fig. 5). For example, at 3°C (our lowest temperature experiment), the two calibrations disagree by 76‰. As discussed above in Section 4.1, some of this disagreement is likely due to offsets in the calibrations and some due to extrapolations of α with an assumed linear dependence on $1/T^2$. Our calibration indicates that methane formed in the near-surface (for example, 0-50°C) should be between ~200‰ and ~175‰ lower in δD compared to the source waters vs. ~275‰ to ~220‰ based on the calibration of Horibe and Craig (1995). As will be discussed below, a difference of ~200‰ between δD_{CH4} and $\delta D_{H2O(l)}$ is commonly observed in deep-sea sediments (as reviewed in Whiticar et al., 1986 and Whiticar, 1999).

4.3 Comparison of our experimentally determined $1000\times ln^{D}\alpha_{CH4(g)-H2(g)}$ fractionation factor to theoretical calculations

As introduced above (Section 1.2), there are several published theoretical calculations of equilibrium $1000\times ln^{D}\alpha_{CH4(g)-H2(g)}$ values as a function of temperature (Bottinga, 1969; Richet et al., 1977; Gropp et al., 2021). In Figure 6C, we compare the differences between $1000\times ln^{D}\alpha_{CH4(g)-H2(g)}$ predicted based on the best-fit line to our experimental data (eq. 6) vs. those from previous theoretical studies, our PIMC calculations, and the extrapolation of the calibration given by Horibe and Craig (1995).

Visually, our theoretical PIMC calculations for isotopic equilibrium best match our experimental data. For example, the largest disagreement between the fit to the PIMC calculations and the fit to the experimental data is 7‰, at 3°C (disagreement between individually calculated and measured points is up to 16.5‰). We show this agreement quantitatively with a plot of $1000\times ln^{D}\alpha_{CH4(g)-H2(g)}$ of PIMC calculations vs. our experiments performed at same temperature (Fig. 7). The slope of the best-fit line is 0.986 ± 0.009 (1 s.e.) with an intercept of 10.99 ± 8.81 (1 s.e.). Thus, these determinations of $1000\times ln^{D}\alpha_{CH4(g)-H2(g)}$ agree within 2 s.e. of the 1:1 line both in slope and intercept. Put another way, satisfyingly, our experimental results agree 1:1 with our theoretical calculations at the highest levels of theory (PIMC with DBO corrections) as yet employed for these calculations.

Other theoretical calculations of $^{D}\alpha_{CH4(g)-H2(g)}$ also visually agree with our experimental data, although not as closely as the calculations presented in this work. These include one set of calculations from Richet et al. (1977) in which $X(CH_4)$, their so-called 'excess factor', is calculated using a harmonic approximation (labeled as R77 (1) in Fig. 6C), which shows a maximum difference of 18‰ vs. the fit to our experimental data. Additionally, recent calculations from Gropp et al. (2021) differ from the fit to our experimental data by at most +34‰ (referred to by them as M06-L) or -26‰ (referred to by them as HCTH). The other theoretical calibrations show larger differences: the curve for the Bottinga (1969) calculations is up to 95‰ greater than the fit to our experimental data, while the curve from Richet et al. (1977) in which $X(CH_4)$ is calculated with anharmonic corrections (labeled as R77 (2) in Fig. 6C) is up to 87‰ lower.

Finally, in Figure A4 we compare $1000\times\ln^{D}\alpha_{CH4(g)-H2(g)}$ from Horibe and Craig (1995) vs. our DBO-corrected PIMC results. Data from Horibe and Craig (1995) are offset to lower values than those based on theory from 18 to 37‰. In addition to the offset itself, the degree of offset is a function of temperature (increasing with increasing temperature) indicating that there is a difference in the temperature dependence between PIMC calculations from this study and the data from Horibe and Craig (1995).

4.4 Comparison of experimental vs. theoretically based calculations of $1000\times ln^{D}\alpha_{H2O(l)-H2(g)}$ for isotopic equilibrium

In Figure 4, various theoretically based calculations of equilibrium $1000\times\ln^{D}\alpha_{H2O(l)-H2(g)}$ values are compared to experimental data as a function of temperature. We note that in all cases, theoretical calculations are for $1000\times\ln^{D}\alpha_{H2O(g)-H2(g)}$ and are converted to $1000\times\ln^{D}\alpha_{H2O(l)-H2(g)}$ using the experimental calibration of equilibrium $^{D}\alpha_{H2O(l)-H2O(g)}$ values from Horita and Wesolowski (1994). Our theoretical calculations of equilibrium $1000\times\ln^{D}\alpha_{H2O(l)-H2(g)}$ values based on the PIMC methodology with the DBO correction are in close agreement with the experimental data. For example, using the same minimization scheme as described in Section 3.4 (Fig. 4), the DBO-corrected PIMC theoretical calculations are offset by -0.49‰ from the experimental data. In contrast, we observe a +24.5‰ offset between PIMC theoretical calculations without the DBO correction and experimental data. Additionally, the harmonic RPFR calculated here using the same reference potentials ('reference harmonic' line) as used for PIMC calculations is offset by +54.4‰ from the experimental data. Offsets between experiments and other theoretical calculations which include anharmonic corrections to harmonic RPFRs are as follows: +2.7‰ from Bottinga (1969); +21.1‰ for Bron et al. (1973), -16.3‰ for Richet et al. (1977), and +6.1‰ from Bardo and Wolfsberg (1976). Calculations presented in Gropp et al. (2021), which do not include anharmonic corrections, are offset by +32.9‰ (M06-L) and +21.0‰ (HCTH) from the experimental data. We note that the theoretical calculations presented in Bardo and Wolfsberg (1976) also include an adiabatic correction to the Born-Oppenheimer (B-O) approximation (Kleinman and Wolfsberg, 1973; Bardo and Wolfsberg, 1978), which is the same sort of correction as the DBO correction presented in this work. Here, we base our correction off of values calculated by Zhang and Liu (2018) which used more rigorous levels of theory and larger basis sets.

4.5 Accuracy of theoretical calculations

The observed differences between the various theoretical calculations vs. experimentally measured values of equilibrium fractionation factors may be due to inaccuracies in theoretical calculations or aspects of the experiments. We note that as the theoretical calculations do not all agree for a given set of molecules, at a minimum, they cannot all be accurate. The following subsections examine the sensitivity of calculated RPFRs to a range of factors, including: (*i*) level of electronic structure theory; (*ii*) vibrational anharmonicity; and (*iii*) DBO corrections.

4.5.1 Accuracy of the electronic structure method

Accurate theoretical calculations of RPFRs necessarily require the use of accurate potential energy surfaces. However, obtaining accurate potential energy surfaces remains challenging even for the small molecules we are investigating. For the PIMC calculations, we used high quality reference potentials as described in Section 2.5.1. However, these potentials are not exact, and small inaccuracies in electronic energy could result in inaccurate RPFRs. There are two issues that need to be addressed to validate the accuracy of these potentials: electronic correlation effects and basis set completeness (i.e., achieving the Hartree-Fock limit).

We explored the magnitude of the error resulting from the inaccuracies in reference potentials at equilibrium geometry as follows. Harmonic RPFRs were computed using eq. (2) based on the normal mode frequencies obtained with either increasingly refined treatment of electronic correlation using the same basis set or using the same electron-correlation treatment with increasing basis set size (see Section A3 for more information). These calculations were then compared to the harmonic result, obtained using the reference potentials. We interpret convergence of harmonic RPFRs with respect to the level of theory or basis set size to indicate sufficient accuracy of the electronic structure methods. Finally, the level of agreement between the converged result and that obtained from the reference harmonic potentials is used as an estimate of the possible size of inaccuracies that result from the reference potentials used in this study (Section 2.5.1).

We computed the harmonic frequencies using the RHF, MP2, CCSD, CCSD(T) levels of theory (abbreviations defined in Section 2.5.1; H_2 was not calculated at CCSD(T) level, as it is exact as CCSD). For these calculations, we used the same high-quality basis set (aug-cc-pVQZ) throughout. For the basis set convergence test, harmonic frequencies were computed at the CCSD(T) level of theory using the following standard and augmented correlation-consistent polarized valence basis sets: cc-pV*X*Z and aug-cc-pV*X*Z. Here *X* denotes the progression of the basis set size: D for double-, T for triple- and Q for quadruple-ζ (Dunning, 1989; Woon and Dunning, 1995). The electron-electron correlation test results are given in Figure 8 and the basis set size test results in Figure 9. We plot δRPFR on the y-axis, where $\delta\text{RPFR} = 1000\times\ln(\text{RPFR}_X/\text{RPFR}_{\text{reference}})$ and is reported in ‰. X denotes the value of the variable tested and the reference is the RPFR calculated using harmonic frequencies from the same potential energy surface as used in the PIMC calculations (the so-called reference harmonic lines; Section 2.5.1). This choice of reference is not meant to indicate that the reference results are necessarily the most accurate but is used simply for the purpose of comparison. The RHF results in Figure 9 are scaled down by a factor of 10 in order to fit on the same axis.

Focusing first on carbon isotopes (panels D and E of Figs. 8 and 9), RPFR values converge to ±3‰ at low (25°C) temperatures and to less than 1‰ above 300°C once the MP2 level and

triple-ζ basis set size are reached. These differences are similar in magnitude to the disagreement between the DBO-corrected PIMC calculations and experimental values (~0.56‰), suggesting that disagreements of this size could be due to inaccuracies in the reference potential energy surfaces.

Turning to hydrogen isotopes, RPFR calculations for H_2 converge to ±3‰ at triple-ζ (recall that CCSD treatment is exact for H_2). In contrast, for H_2O and CH_4 we observe changes of up to 35‰ for H_2O and 20‰ for CH_4 at 0°C in calculated RPFRs from CCSD to CSSD(T) (panels 8B, 8C). There is better (<4‰ difference) agreement between the CCSD(T) and reference calculations for H_2O and CH_4. However, the reference calculations for both molecules are also done at the CCSD(T) level, though for the case of water, icMRCI and experimental data are used as well — regardless these similarities may result in some of the agreement seen between at the CCSD(T) level and reference results. Basis set size does not influence CH_4 results (panel 9C) by more than 3‰ at triple-ζ or above. In contrast, for water (panel 9B), increasing from cc-pVQZ to aug-cc-pVQZ results in changes of up to 12‰ at 0°C. These results indicate that for CH_4 and H_2O, the theoretical calculations at the CCSD(T) level and cc-pVQZ have not converged to insignificant (sub per mil) levels. However, without still higher level electronic structure calculations, precise estimates of errors are difficult to make for CH_4 and H_2O.

4.5.2 Influence of anharmonicity and other quantum effects on RPFRs

Here we discuss the importance of the inclusion of anharmonic and quantum effects (e.g., non-rigid rotations and non-classical approximations) included in RPFRs calculated with PIMC. Figure 10 compares calculations of $1000\times\ln{}^{D}\alpha_{CH4(g)\text{-}H2(g)}$, $1000\times\ln{}^{D}\alpha_{CH4(g)\text{-}H2O(g)}$, $1000\times\ln{}^{D}\alpha_{H2O(g)\text{-}H2(g)}$ (panel A), and $1000\times\ln{}^{13}\alpha_{CH4(g)\text{-}CO2(g)}$ (panel B) based on RPFRs calculated using the PIMC method to the harmonic calculations based on the same potential energy surfaces (reference harmonic line). Differences between $1000\times\ln{}^{D}\alpha_{CH4(g)\text{-}H2(g)}$, $1000\times\ln{}^{D}\alpha_{CH4(g)\text{-}H2O(g)}$, and $1000\times\ln{}^{D}\alpha_{H2O(g)\text{-}H2(g)}$ calculated using PIMC vs. harmonic calculations are up to +10, -40, and -30‰ at 0°C (where the largest difference occurs). The same patterns (but smaller magnitude differences) are observed for carbon isotopic equilibrium, i.e. errors in RPFRs of different species do not cancel out (Fig. 10B). The difference in $1000\times\ln{}^{13}\alpha_{CH4(g)\text{-}CO2(g)}$ for PIMC vs. harmonic calculations is up to -2.5‰ at 0˚C.

Webb and Miller (2014) and Eldridge et al. (2019) demonstrated that the equilibrium methane clumped-isotope compositions of $^{13}CH_3D$ do not change by more than 0.06‰ from 27 to 327°C when PIMC or harmonic partition function ratios are used in their calculations. This is due to almost perfect cancellation of nearly identical errors in harmonic partition function ratios of clumped methane isotopologues. However, when calculating fractionation factors between different species, the error of the harmonic partition function ratios only cancels partially (i.e., Fig. 10A).

This shows that unlike the case for clumped-isotope studies, the cancellation of errors in harmonic partition function ratios or PIMC approaches cannot be assumed when dealing with equilibrium isotope-exchange reactions between different species. For example, neglecting anharmonic and quantum effects accounted for in PIMC calculations leads to significant (up to ~40‰) errors in calculated theoretical $1000\times\ln{}^{D}\alpha$ values for hydrogen isotopes and ~2.5‰

errors in theoretical $1000\times\ln^{13}\alpha$ values for carbon isotopes for environmentally relevant conditions on Earth's surface (i.e., at or above 0°C) for the species examined here.

4.5.3 Diagonal Born-Oppenheimer correction

The effect of the DBO correction on the calculated magnitudes of isotopic fractionations of D/H between small molecules has been explored in previous theoretical calculations (Kleinman and Wolfsberg, 1973; Bardo and Wolfsberg, 1975; Bardo and Wolfsberg, 1978; Zhang and Liu, 2018) and compared to experiments for HD-H_2O (Bardo and Wolfsberg, 1976) and D_2-HCl (Postma et al., 1988). To assess whether or not a DBO correction is of importance to an exchange reaction involving some atom *A*, the difference in electron density on *A* in two different molecules must be considered in addition to the mass of *A*. The DBO correction will increase in magnitude as (*i*) *A* decreases in mass (i.e., a bigger correction for hydrogen vs. carbon); (*ii*) *A* is substituted by a heavier isotope (i.e., a bigger correction for T/H vs. D/H, where T is tritium); and (*iii*) *A* is bonded to electron-withdrawing atoms or groups in one molecule and electron-donating in the other (e.g., the correction for H_2O/H_2 is greater than for CH_4/H_2). These empirical rules follow from the expression for DBO energy correction (see eq. (3) of Valeev and Sherrill, 2003).

Our results follow these guidelines. For example, as described in Section 3.3, we find that DBO corrections have magnitudes of up to 34‰ on calculated hydrogen fractions for H_2O-H_2 and CH_4-H_2O but are negligible (<0.5‰) for calculations for hydrogen isotope fractionations for CH_4-H_2 and carbon isotope equilibrium for CH_4-CO_2 (see Table A3 and A4; Fig. 10A and B). Richet et al. (1977) did not employ DBO corrections as they considered them minor for systems exchanging atoms other than hydrogen; for exchange of hydrogen isotopes, they argue, the corrections computed by Kleinman and Wolfsberg (1973) are poorly constrained such that the error on the correction approached the size of the correction. Using modern electronic structure theory methods, DBO corrections have been recomputed (Zhang and Liu, 2018) with better accuracy (see Table A2). Importantly, the application of these more accurate DBO corrections reduces the difference of theoretically derived $1000\times\ln^{D}\alpha_{H2O(l)\text{-}H2(g)}$ values from 24.5‰ to 0.49‰ relative to experimental determinations, and from 0.66‰ to 0.56‰ for $1000\times\ln^{13}\alpha_{CH4(g)\text{-}CO2(g)}$ values. This agreement suggests that their inclusion does yield more accurate theoretical calculations, especially for hydrogen isotopes.

We note that to our knowledge, this work presents the first case in which DBO corrections have been included in a path-integral statistical mechanical calculation. Non-Born-Oppenheimer effects are typically discussed in the context of non-adiabatic dynamics. The necessity to correct the path-integral result for such a small energy difference highlights two important aspects of the equilibrium isotope effect: (*i*) some gas mixtures have DBO corrections up to 6-8 cm^{-1}, large enough to confirm the role of these non-Born-Oppenheimer effects on the equilibrium distribution experimentally; (*ii*) path-integral calculations using the best available potential energy surfaces are accurate enough to reveal such small energy differences between the electronic ground states of small molecules.

4.5.4 Differences in theoretical vs. experimental determinations of equilibrium fractionation factors

The sensitivity tests and comparisons described in the previous sections indicate the following: (*i*) inclusion of anharmonic and quantum effects via use of the PIMC approach has a significant (up to 40‰) effect on equilibrium $1000\times\ln{}^{D}\alpha$ values for $1000\times\ln{}^{D}\alpha_{CH4(g)\text{-}H2(g)}$, $1000\times\ln{}^{D}\alpha_{CH4(g)\text{-}H2O(g)}$, and $1000\times\ln{}^{D}\alpha_{H2O(g)\text{-}H2(g)}$ from 0 to 500°C. (*ii*) DBO corrections further change the computed RPFRs by up to 34‰ for $1000\times\ln{}^{D}\alpha_{CH4(g)\text{-}H2O(g)}$ and up to -34‰ for $1000\times\ln{}^{D}\alpha_{H2O(g)\text{-}H2(g)}$. (*iii*) RPFRs computed with PIMC for ^{13}C are likely accurate to at least ±3‰; the inaccuracy appears to be predominantly due to the electronic structure calculations (i.e., the quality of the potential energy surface). (*iv*) The accuracy bounds for the RPFRs involving hydrogen isotopes are more difficult to estimate but are likely <10‰ based on calculations presented in Figures 8 and 9 and are likewise related to the approximations employed when calculating the potential energy surfaces. Higher-level theoretical calculations will be needed to resolve this.

We observe that when RPFRs for hydrogen isotopes are calculated using PIMC and the DBO corrections, we achieve close agreement with experimental observations of ${}^{D}\alpha_{H2O(l)\text{-}H2(g)}$ (Fig. 4) and ${}^{D}\alpha_{CH4(g)\text{-}H2(g)}$ (Fig. 7). In contrast, not including these terms in the computation of ${}^{D}\alpha_{H2O(l)\text{-}H2(g)}$ results in offsets in theoretical calculations relative to experimental observations of ~25‰. This indicates that these corrections, which are not always included in theoretical calculations of RPFRs, can be important for hydrogen isotope equilibrium calculations. We note that in making this comparison between theory and experiment we assume that the experiments are of sufficient quality both in precision and accuracy to reflect the true equilibrium isotopic compositions. We believe that our equilibrations of CH_4 and H_2 given the bracketing approach are sufficiently accurate and precise for this purpose. This is because the residual of the data to our best-fit line is ±5.9‰ (1σ), whereas differences between theoretical treatments can be greater (up to 30‰ for harmonic calculations with our reference potential). In contrast, for water-H_2 hydrogen-isotope equilibrations, experimental results show scatter of >25‰ at given temperatures. This scatter makes exact comparisons between experiment and theory more challenging and indicates that future experimental equilibrations of H_2(g) and H_2O(l) using modern techniques will be useful for the comparison of experiments and theory.

5. Comparison to environmental data and microbial culture experiments

The purpose of the above calibrations was to establish what equilibrium values for ${}^{D}\alpha_{CH4(g)\text{-}H2O(l)}$ are at low (<200°C) temperatures in order to examine whether or not methane is found in nature in hydrogen isotopic equilibrium with co-occurring waters. As discussed in the introduction, both the hydrogen isotopic composition of methane vs. water and carbon isotopic composition of methane vs. CO_2 have been used previously to infer whether or not methane forms in or out of isotopic equilibrium with these other species. For hydrogen isotopes, at temperatures below 200°C, this has been done in a variety of ways. For example, Stolper et al. (2015) averaged the two different theoretical calculations of Richet et al. (1977) for ${}^{D}\alpha_{CH4(g)\text{-}H2O(g)}$, which disagree by 92‰ at 0°C, and combined this average with the calibration of ${}^{D}\alpha_{H2O(g)\text{-}H2O(l)}$ from Horita and Wesolowski (1994). Wang et al. (2015) extrapolated the calibration of ${}^{D}\alpha_{CH4(g)\text{-}H2(g)}$ from Horibe and Craig (1995) to lower (<200°C) temperatures and combined this with various experimental calibrations of ${}^{D}\alpha_{H2(g)\text{-}H2O(l)}$. Okumura et al. (2016) extrapolated the equation for ${}^{D}\alpha_{CH4(g)\text{-}H2O(l)}$ from Horibe and Craig (1995) to lower temperatures. Finally, Gropp et al. (2021) presented new theoretical calculations of ${}^{D}\alpha_{CH4(g)\text{-}H2O(g)}$ and combined these with ${}^{D}\alpha_{H2O(g)\text{-}H2O(l)}$ from Horita and Wesolowski (1994) to find ${}^{D}\alpha_{CH4(g)\text{-}H2O(l)}$. These various approaches result in differences of up to

~85‰ in the equilibrium value of $^{D}\alpha_{CH4(g)\text{-}H2O(l)}$ at 0°C. We consider this a conservative estimate of the uncertainty of this value prior to the experiments presented above.

Regardless of this large prior uncertainty in the equilibrium value of $^{D}\alpha_{CH4(g)\text{-}H2O(l)}$ at low temperatures, Stolper et al. (2015), Wang et al. (2015), and Okumura et al. (2016) all found that terrestrial and pure-culture systems generally exhibit values farther from methane-water hydrogen isotopic equilibrium as compared to marine sedimentary systems. Stolper et al. (2015), Wang et al. (2015), Okumura et al. (2016), and Vinson et al. (2017) interpreted these differences as being caused by the degree of reversibility in methanogenic pathways as tied to the energy available in the environment. However, quantitative descriptions of the degree of disequilibrium in these systems and whether or not samples were in fact in equilibrium or simply close was not possible given the uncertainties discussed above.

Additionally, as discussed in the introduction, carbon isotope compositions between methane and CO_2 in marine sediments are commonly similar to values calculated based on theoretical estimates of equilibrium and, on this basis, it has been proposed that methane may form in or reach isotopic equilibrium with CO_2 in marine sediments (Bottinga, 1969; Yoshinaga et al., 2014; Meister et al., 2019; Meister and Reyes, 2019; Gropp et al., 2021).

In the following section we revisit these proposals through a comparison of measured values for $^{D}\alpha_{CH4(g)\text{-}H2O(l)}$ and $^{13}\alpha_{CH4(g)\text{-}CO2(g)}$ from environmental or microbial cultures vs. those predicted for isotopic equilibrium based on our experimental calibrations for $^{D}\alpha_{CH4(g)\text{-}H2O(l)}$ (eq. 8) and theoretical calibration of $^{13}\alpha_{CH4(g)\text{-}CO2(g)}$ as offset to fit experimental data above 200°C (eq. 10). Recall that we use α as a measure of isotopic differences and it does not imply a sample is or is not in equilibrium (see Section 1.2) unless otherwise noted.

For the environmental data, we compiled measurements of samples with measured $\delta^{13}C$ values of both CO_2 and CH_4, δD values of both liquid water and CH_4, and an estimate for the gas's formation temperature. A similar compilation but only for samples from marine settings was recently given in Gropp et al. (2021) while comparison of $^{D}\alpha_{CH4(g)\text{-}H2O(l)}$ vs. $^{13}\alpha_{CH4(g)\text{-}CO2(g)}$ with values at equilibrium is provided in Okumura et al. (2016) on a more limited dataset. Our compilation updates these previous studies expanding on sample sets and explicitly compares them to expected values for isotopic equilibrium as a function of temperature.

For hydrogen isotopes, we only examine systems at temperatures less than 200°C (i.e., those that have temperatures that overlap our calibration). For carbon, we include systems above 200°C. For samples from low temperature sedimentary or lake settings, the temperature we use is the sample collection temperature. For samples from laboratory methanogen cultures, we use the experimental temperature. We avoid environmental systems with significant gradients in water isotopic compositions (e.g., estuaries or brackish systems). For thermogenic gases, the sampling temperature is unlikely to be the gas formation temperature given that thermogenic gases typically migrate in the subsurface. Instead, we only include gases with measured clumped-isotope-based temperatures and we use this as a stand-in for the formation temperature as was done in the studies from which these samples were taken — see discussions in Stolper et al., (2014b), Stolper et al. (2018) and Thiagarajan et al. (2020) on the validity and basis of this assumption.

We divide samples into six separate categories: marine sediments, terrestrial, coalbed/shale/gas field, laboratory cultures grown at high pH_2, laboratory cultures grown at low pH_2, and thermogenic. These divisions are based on previous isotopic classification schemes (e.g., Whiticar et al., 1986; Burke, 1993; Stolper et al., 2015; Wang et al., 2015; Okumura et al., 2016; Stolper et al., 2018). We note that Okumura et al. (2016) classified environmental samples as being either "aged" (i.e., samples from geologic reservoirs) or "young" (i.e., samples from culture experiments or natural environments). The marine sediment, terrestrial, and coalbed/shale/gas field samples are collected from sediments, bogs, swamps, permafrost, lakes, aquifers, and shallow economic reservoirs in which the gas source is thought to be dominantly microbial. Both aerobic and anaerobic consumption of methane can occur in these settings which can modify the isotopic compositions of the methane and CO_2. In order to avoid the effects of methane consumption, we exclude samples from terrestrial systems from the top 10 cm of sediments or from oxygenated lake waters where aerobic methanotrophy occurs. We also exclude samples from marine systems at or above the sulfate-methane transition zone where methane oxidation commonly occurs.

Data from laboratory cultures are from pure or enrichment cultures of methanogens grown under defined conditions. For these experiments, we only compiled data for hydrogenotrophic methanogens (i.e., H_2 consuming methanogens). We did not compile data from methylotrophic methanogens as the isotopic composition of their produced methane is a function of both the source water and source methyl group for hydrogen isotopes and the methyl carbon isotopic composition for carbon isotopes. For hydrogenotrophic cultures, we avoid samples in which H_2 with a deuterium label was introduced as such labeling can have a time-dependent effect on the δD of the resultant methane until the H_2 is isotopically equilibrated with the fluid medium (Kawagucci et al., 2014; Okumura et al., 2016). When samples from such systems (those that used deuterium enriched H_2) are used, they are from the final time point of the experiment following H_2 hydrogen-isotope equilibration with the source water. As discussed above, laboratory cultures are divided into two broad categories: high pH_2 and low pH_2. High pH_2 samples are those grown with head spaces comprised dominantly of H_2 and CO_2 pressurized at over one atmosphere – this is the more common growth technique. Low pH_2 cultures are those either purposely grown with low pH_2 headspaces or grown in co-cultures with fermenting organisms that keep pH_2 values within a controlled range. This separation is done as it has been observed that pH_2 levels affect both measured ${}^{13}\alpha_{CH4(g)\text{-}CO2(g)}$ and ${}^{D}\alpha_{CH4(g)\text{-}H2O(l)}$ values (Burke, 1993; Valentine et al., 2004; Penning et al., 2005; Okumura et al., 2016).

For thermogenic gases, we dominantly relied on the recent compilation of Thiagarajan et al. (2020) for samples with measured $\delta^{13}C_{CH4}$, $\delta^{13}C_{CO2}$, and methane clumped-isotope temperatures and do not recompile them here. We filter their data such that samples with methane/(ethane+propane) ratios greater than 50 are excluded to avoid samples with potential biogenic methane contributions (Bernard et al., 1976), except for unconventional shale gas systems where samples are known to be thermogenic. We are aware of only a few samples of thermogenic methane with measured clumped-isotope temperatures, measured δD_{CH4} values, and measured or estimated δD_{H2O} values, and this handful ($n = 8$) of samples is included here (Wang et al., 2015; Giunta et al., 2019). We are not aware of any thermogenic samples where δD_{CH4}, δD_{H2O}, $\delta^{13}C_{CO2}$, and $\delta^{13}C_{CH4}$ were all measured.

In doing these comparisons, many samples have measurements of only some of the parameters of interest, i.e., they do not all have measurements of δD_{CH4}, δD_{H2O}, $\delta^{13}C_{CO2}$, $\delta^{13}C_{CH4}$ values, and environmental/clumped-isotope temperatures. Thus not all samples are comparable in all examined spaces. Compiled environmental data is given in Table EA8 and culture data in Table EA9. Data references are given in those tables and in the list in Appendix A4.

Before examining the data, we raise and discuss a series of caveats associated with interpreting the meaning of observed isotopic differences between CH_4 and CO_2 or CH_4 and H_2O from environmental samples. First, the CO_2, CH_4, and H_2O in a sample may not be cogenetic. For example, the methane may have diffused through sediments and mixed with waters and/or CO_2 unrelated to its formation pathway. In this case, the environmental temperature is also unrelated to the gas's formational temperature. Alternatively, the CO_2 may have been added after methane generation largely ceased through, for example, dissimilatory or fermentative metabolisms.

Second, methane formed in isotopic equilibrium with CO_2 by methanogens will not necessarily exhibit the expected equilibrium isotopic difference between the accumulated methane and the remaining CO_2. For example, if methane forms in equilibrium within a methanogenic cell and is then emitted (but does not equilibrate further), a Rayleigh-like distillation process (Criss, 1999) will occur — this is commonly observed in sediments where the $\delta^{13}C$ of residual CO_2 rises due to methanogenesis (e.g., Claypool and Kaplan, 1974). During such a process, the carbon isotopic difference between methane, which is the accumulated product, and CO_2, the residual reactant, will not be the value for equilibrium except at the start of the reaction. Furthermore, during methanogenesis, fermentation of organic matter, assuming a stoichiometry of CH_2O, results in the net addition of one mole CO_2 for every one mole of CH_4 generated, further complicating the interpretation of sedimentary $\delta^{13}C_{CH4}$ and $\delta^{13}C_{CO2}$ values (e.g., Meister et al., 2019). For hydrogen isotopes, this is not an issue as there is sufficient water that its isotopic composition does not change due to methanogenesis.

Third, in making these comparisons we must assume that isotopic measurements of different studies are comparable. Interlaboratory agreement for carbon isotopes of CO_2 and hydrogen isotopes of water can be achieved via anchoring to internationally available standards. However, such standards have not always existed for methane. Exploration of this issue based on interlaboratory comparisons (Dai et al., 2012) show that differences for δD_{CH4} of up to 15‰ and for $\delta^{13}C_{CH4}$ of up to 0.2‰ are routine for the same samples measured in different laboratories.

5.1 Comparison of environmental data to equilibrium isotopic calibrations

We begin with a comparison of hydrogen isotopes by plotting measured $1000\times\ln{}^{D}\alpha_{CH4(g/aq)\text{-}H2O(l)}$ values vs. temperature (°C) for environmental samples and cultures (n = 877) and our calibrations for isotopic equilibrium (Fig. 11). Here 'g/aq' indicates calculations for methane either in the gas or aqueous phase. We include both as we do not know if the environmental methane was originally dissolved (aq) or gaseous (g), we compare samples to equilibrium curves for methane in both states — these differ by ~4‰ and do not influence any interpretations. A few first-order observations can be made from this comparison: (*i*) All laboratory cultures yield methane out of CH_4(g/aq)-H_2O(l) hydrogen isotopic equilibrium by about 100-400‰ and commonly yield values that do not overlap with those from environmental samples — low and

high pH_2 cultures overlap in values of $1000\times\ln^{D}\alpha_{CH4(g/aq)-H2O(l)}$, but cultures grown at low pH_2 conditions yield values that are generally elevated (i.e., less negative) than in high pH_2 experiments. (*ii*) Terrestrial microbial methane samples are typically out of CH_4(g/aq)-H_2O(l) hydrogen isotopic equilibrium by 50 to 200‰. (*iii*) Microbial marine sedimentary and coalbed/shale/gas field gases yield values that overlap with those expected for equilibrium. Median deviations from equilibrium are -15‰ and -14‰ for marine sedimentary and coalbed/shale/gas field gases respectively. However, the distributions are asymmetric, with more values being lower than expected for equilibrium in both cases. (*iv*) The small number of thermogenic gases yield clumped-isotope-based temperatures that are within ~140‰ of the value expected for isotopic equilibrium between CH_4(g/aq)-H_2O(l) with a median difference of -50‰.

We note that for marine sedimentary samples above 50°C, $1000\times\ln^{D}\alpha_{CH4(g/aq)-H2O(l)}$ are consistently lower than expected for equilibrium. These samples are from deeply buried in marine sediments and have warm environmental temperature due to geothermal gradients. If the methane was made at shallower depths and lower temperatures and then buried, it would appear out of equilibrium at the current temperature in the direction observed (lower value of $1000\times\ln^{D}\alpha_{CH4(g/aq)-H2O(l)}$). This shows one way in which using collection temperatures as a stand-in for formation temperatures for this exercise can introduce some uncertainty.

Next, we compare $1000\times\ln^{13}\alpha_{CH4(g/aq)-CO2(g/aq)}$ values vs. temperature for our calibrations vs. environmental data and laboratory culture experiments (n = 959) in Figure 12A with a zoom-in figure from 0 to 60°C in Figure 12B. Again, as we do not know if the environmental samples of methane and CO_2 were originally gaseous or dissolved, we provide calibrations for both in the gas phase and both aqueous — these calibrations differ by <2‰ over the temperature range plotted (0-300°C) and so the distinction is unimportant for our purposes. First order observations are as follows: (*i*) laboratory cultures yield methane out of CH_4(g/aq)-CO_2(g/aq) carbon isotopic equilibrium with $1000\times\ln^{13}\alpha_{CH4(g/aq)-CO2(g/aq)}$ both above and below the expected value for equilibrium. These deviations show no obvious relationship to growth temperature. High pH_2 cultures typically have $1000\times\ln^{13}\alpha_{CH4(g/aq)-CO2(g/aq)}$ greater than what is expected for isotopic equilibrium (but not always), while the handful of cultures grown under low pH_2 conditions generally (but again not always) exhibit $1000\times\ln^{13}\alpha_{CH4(g/aq)-CO2(g/aq)}$ less than expected for isotopic equilibrium. We note that it has long been observed that $1000\times\ln^{13}\alpha_{CH4(g/aq)-CO2(g/aq)}$ values of pure- culture experiments correlate with pH_2 levels, with lower values observed for low pH_2 conditions and higher values for high pH_2 conditions (Valentine et al., 2004; Penning et al., 2005; Okumura et al., 2016; Rhim, 2020). Okumura et al. (2016) previously observed that high pH_2 conditions yield $1000\times\ln^{13}\alpha_{CH4(g/aq)-CO2(g/aq)}$ generally greater than isotopic equilibrium and low pH_2 conditions less than equilibrium. Below we propose an explanation for this. (*ii*) Terrestrial gases largely yield $1000\times\ln^{13}\alpha_{CH4(g/aq)-CO2(g/aq)}$ values higher than expected for CH_4(g/aq)-CO_2(g/aq) carbon isotopic equilibrium (though some are lower). (*iii*) Microbial coalbed/shale/gas field gases yield $1000\times\ln^{13}\alpha_{CH4(g/aq)-CO2(g/aq)}$ values that overlap with the those expected for formation or attainment of CH_4(g/aq)-CO_2(g/aq) carbon isotopic equilibrium, but show differences from -20 to +46‰ vs. equilibrium. The median difference is 3‰. (*iv*) Marine sedimentary gases yield values of $1000\times\ln^{13}\alpha_{CH4(g/aq)-CO2(g/aq)}$ that also overlap with those expected for equilibrium but extend up to 34‰ above or -20‰ below those expected for equilibrium with a median difference of 8‰. (*v*) Thermogenic gases scatter around the expected equilibrium curve (±25‰) in which the temperatures used are measured clumped-isotope

temperatures. Thiagarajan et al. (2020) interpreted this as indicating that methane and CO_2 commonly reach isotopic equilibrium in thermogenic systems; we refer the reader to that study for further interpretation.

We note that both the marine sedimentary and coalbed/shale/gas field microbial samples yield some values of $1000\times\ln{}^{13}\alpha_{CH4(g/aq)\text{-}CO2(g/aq)}$ that are in what we consider to be fairly close agreement (given various uncertainties inherent in this approach) with values expected for carbon isotopic equilibrium (within ±10‰) between methane and CO_2, but some also show a deviation from equilibrium to values higher and lower values than expected. Such deviations may indicate formation out of carbon isotopic equilibrium. However, it must be kept in mind that this could also result from effects associated with addition of CO_2 to sedimentary pore fluids with low (-25‰) $\delta^{13}C$ values following methane generation (which would generally raise $1000\times\ln{}^{13}\alpha_{CH4(g/aq)\text{-}CO2(g/aq)}$ values) and semi-closed system behavior in which residual CO_2 is enriched in $\delta^{13}C$ due to methanogenesis creating lower $1000\times\ln{}^{13}\alpha_{CH4(g/aq)\text{-}CO2(g/aq)}$ than expected for equilibrium. Precise determinations of $^{13}\alpha_{CH4(g/aq)\text{-}CO2(g/aq)}$ in these systems generally necessitate modeling reactions and transport in the sedimentary column at every site (e.g., Meister et al., 2019), which is beyond the scope of this work.

Finally, we directly compare measured values of $1000\times\ln{}^{13}\alpha_{CH4(g/aq)\text{-}CO2(g/aq)}$ vs. $1000\times\ln{}^{D}\alpha_{CH4(g/aq)\text{-}H2O(l)}$ from environmental and laboratory culture samples (n = 755) as well as the curves expected for isotopic equilibrium (Fig. 13). A similar comparison on a more limited environmental data set (using the extrapolation of the equation of Horibe and Craig (1995) for $1000\times\ln{}^{D}\alpha_{CH4(g)\text{-}H2O(l)}$) is given in Okumura et al. (2016). This space has the advantage that it does not require us to assume a gas formation temperature. No thermogenic gases are included as we are not aware of any that have measurements of all four isotopic properties. First order observations are: (*i*) Methane from laboratory cultures and terrestrial environments yield methane out of combined CH_4(g/aq)-CO_2(g/aq) carbon and CH_4(g/aq)-H_2O(l) hydrogen isotopic equilibrium and do not appear to plot in the same spaces as other environmental methane samples. Additionally, high and low pH_2 cultures generally occupy different areas in this field mostly due to differences in values of $1000\times\ln{}^{13}\alpha_{CH4(g/aq)\text{-}CO2(g/aq)}$. For the terrestrial gases there appears to be a negative correlation between measured $1000\times\ln{}^{13}\alpha_{CH4(g/aq)\text{-}CO2(g/aq)}$ and $1000\times\ln{}^{D}\alpha_{CH4(g/aq)\text{-}H2O(l)}$. This trend is likely caused by methane being generated in terrestrial settings from both acetoclastic and hydrogenotrophic methanogens (e.g., Thauer, 1998). It has previously been observed in laboratory cultures that acetoclastic methanogens generally generate methane with lower δD_{CH4} values and higher $\delta^{13}C_{CH4}$ values compared to methane formed by hydrogenotrophic methanogens (as reviewed in Chanton et al., 2004) As such, we expect the observed relationship is related in part to relative contributions of methane from various methanogenic metabolisms, but with formation occurring out of combined CH_4(g/aq)-CO_2(g/aq) carbon and CH_4(g/aq)-H_2O(l) hydrogen isotopic equilibrium in either case. (*ii*) The co-equilibrium line appears to represent an upper bound for microbial marine sedimentary and coalbed/shale/gas field samples. Some samples cluster on the line and many fall below the line; few samples are above it.

5.2 Interpretation of the environmental data.

As has been observed before (Stolper et al., 2015; Wang et al., 2015; Okumura et al., 2016), the above examination shows that biogenic terrestrial and microbial culture samples generally

appear to be out of carbon and hydrogen isotopic equilibrium with co-occurring CO_2 and water. Biogenic methane from marine sedimentary and coalbed/shale/gas field systems can also be out of isotopic equilibrium with co-occurring CO_2 and water, but approach and often have isotopic compositions consistent with those expected for equilibrium. Thus the new calibrations employed here support previous inferences that methane can form in or attain hydrogen and carbon isotopic equilibrium with water and CO_2 in the environment in some systems but not in others (Stolper et al., 2015; Wang et al., 2015; Okumura et al., 2016). We now outline a conceptual model to describe these patterns in the context of the observed deviations from equilibrium.

As proposed in Stolper et al. (2015), Wang et al. (2015), and Gropp et al. (2021), the data above can be understood using the conceptual model of Valentine et al. (2004) where the free energy available to methanogens dictates the degree of reversibility of enzymes and, as a result, the amount of isotope exchange and thus equilibration that occurs between methane and water or CO_2. Isotopic equilibrium is approached at low free energy gradients when enzymes are fully reversible and exchange hydrogen between methane and H_2O and carbon between methane and CO_2 occurs. Isotopic compositions at intermediate and high free energies are controlled a combination of equilibrium and kinetic isotope effects in which some steps are wholly or partially reversible and others are not — this is indicated schematically at the bottom of Figure 14 (see also schematic Figure 7 of Valentine et al., 2004, and Figure 6 in Okumura et al., 2016).

We begin with the microbial cultures. Cultures grown under high pH_2 conditions exhibit $1000\times\ln{}^{D}\alpha_{CH4(g/aq)\text{-}H2O(l)}$ values that are generally lower than expected for isotopic equilibrium and $1000\times\ln{}^{13}\alpha_{CH4(g/aq)\text{-}CO2(g/aq)}$ values greater than expected for isotopic equilibrium (Figs. 13 and 14). In contrast, cultures grown under low pH_2 conditions generally exhibit lower values for $1000\times\ln{}^{13}\alpha_{CH4(g/aq)\text{-}CO2(g/aq)}$ that are less than expected for isotopic equilibrium and $1000\times\ln{}^{D}\alpha_{CH4(g/aq)\text{-}H2O(l)}$ values that, though also lower than expected for equilibrium, are less out of equilibrium in general than high pH_2 culture conditions (Figs. 13 and 14). These differences emerge as data clusters in Figure 13 for the microbial culture experiments. We propose these clusters reflect experimental conditions where specific and different rate-limiting enzymatic steps in the methane formational pathway are commonly reached. Based on the framework of Valentine et al. (2004), this would indicate that for conditions used in previous experiments, methanogens in pure culture exhibit a range of how reversible their enzymes are, but never approach full reversibility and thus isotopic equilibrium (Fig. 14). We note that there is a set of high pH_2 data that also show $1000\times\ln{}^{13}\alpha_{CH4(g/aq)\text{-}CO2(g/aq)}$ values and $1000\times\ln{}^{D}\alpha_{CH4(g/aq)\text{-}H2O(l)}$ values similar to those of the low pH_2 data (from Miller et al., 2018). These samples were grown at elevated pH_2 but alkaline conditions (pH up to 11.3) such that CO_2 concentrations were low in the experiments (as compared to typical high pH_2 experiments with ~4:1 H_2:CO_2 headspaces). Thus these samples may actually be more comparable to the low pH_2 samples in a thermodynamic sense where lower free energy gradients are available due to low pCO_2 instead of low pH_2. This is supported by the fact that when methanogens were grown at lower pH (<8), they plot in the same area as other more typical high pH_2 experiments. Exploration of how $1000\times\ln{}^{D}\alpha_{CH4(g/aq)\text{-}H2O(l)}$ and $1000\times\ln{}^{13}\alpha_{CH4(g/aq)\text{-}CO2(g/aq)}$ values vary as either pH_2 or pCO_2 are varied could help constrain if and how enzymatic reversibility relates to the free energy available to methanogens and how these map on to observed isotope effects.

As discussed above, in microbial culture experiments, $1000\times\ln^{13}\alpha_{CH4(g/aq)\text{-}CO2(g/aq)}$ go from being too high compared to equilibrium in high pH_2 cultures to too low compared to equilibrium in the experiments as pH_2 decreases (Figs. 13 and 14) (also noted but not explained by Okumura et al., 2016), while $1000\times\ln^{D}\alpha_{CH4(g/aq)\text{-}H2O(l)}$ are always lower than expected for equilibrium. We propose this indicates that during methanogenesis, changes in the rate-limiting steps and degree of reversibility as free energy gradients decrease results in a switch of the kinetic carbon isotope effects from one that results in methane that is higher in $\delta^{13}C$ value relative to CO_2 to one that is lower as compared to the value expected for isotopic equilibrium. However, this does not occur for hydrogen isotopes, which continue to approach equilibrium values from lower $1000\times\ln^{D}\alpha_{CH4(g/aq)\text{-}H2O(l)}$ values as reversibility increases. Reversible enzymatic carbon and hydrogen isotope exchange following this step would then increase both $1000\times\ln^{13}\alpha_{CH4(g/aq)\text{-}CO2(g/aq)}$ and $1000\times\ln^{D}\alpha_{CH4(g/aq)\text{-}H2O(l)}$ values to their expected equilibrium values. In this explanation, $1000\times\ln^{D}\alpha_{CH4(g/aq)\text{-}H2O(l)}$ values monotonically increase in their approach to equilibrium as reversibility increases while $1000\times\ln^{13}\alpha_{CH4(g/aq)\text{-}CO2(g/aq)}$ values jump from above to below equilibrium and then approach equilibrium as reversibility increases. Quantitative modeling of such steps in a metabolic pathway requires knowledge or estimates of equilibrium and kinetic isotope effects for all reactions (both forward and reverse) and intermediates involved in methanogenesis as a function of temperature and is beyond the scope of this work — models that attempt this have been presented by Wang et al. (2015), Cao et al. (2019), and Gropp et al. (2021).

Although terrestrial samples also are generally out of CH_4-H_2O hydrogen isotopic and CH_4-CO_2 carbon isotopic equilibrium, they do not typically display the same range of fractionation factors as culture experiments. Instead, their $1000\times\ln^{13}\alpha_{CH4(g/aq)\text{-}CO2(g/aq)}$ values are typically -40 to -85‰ and $1000\times\ln^{D}\alpha_{CH4(g/aq)\text{-}H2O(l)}$ values are typically -400 to -250‰ (Fig. 14). As also observed by Okumura et al. (2016), these ranges are more similar to those observed in low pH_2 experiments, though the precise zones occupied in the comparison of $1000\times\ln^{13}\alpha_{CH4(g/aq)\text{-}CO2(g/aq)}$ vs. $1000\times\ln^{D}\alpha_{CH4(g/aq)\text{-}H2O(l)}$ values for terrestrial vs. laboratory cultures differ. As discussed in Section 5.1, this difference is likely due in part to terrestrial samples including contributions of methane from a mixture of acetoclastic and hydrogenotrophic methanogens, which express different isotope effects when grown in the laboratory. Regardless, these samples, though out of isotopic equilibrium with CO_2 and water, appear generally closer to isotopic equilibrium with CO_2 and H_2O than high pH_2 pure-culture experiments. We take this to indicate that these samples show a larger degree of isotopic reversibility than high pH_2 pure-culture experiments and are thus more similar to low pH_2 pure culture conditions (Fig. 14).

In contrast to the terrestrial and pure-culture samples, microbial marine sedimentary and coalbed/shale/gas field methane appear to be found, not uncommonly, with isotopic compositions consistent with those expected for hydrogen and carbon isotopic equilibrium with co-occurring water and CO_2. Previous studies have also argued for this (Stolper et al., 2015; Wang et al., 2015; Okumura et al., 2016; Meister et al., 2019; Meister and Reyes, 2019). The newly presented calibration for equilibrium $1000\times\ln^{D}\alpha_{CH4(g/aq)\text{-}H2O(l)}$ indicates this is correct to within ~15‰ (i.e., interlaboratory agreement) as opposed to ~85‰ uncertainties due to previous lack of knowledge of what $1000\times\ln^{D}\alpha_{CH4(g/aq)\text{-}H2O(l)}$ was at low temperatures discussed above. Additionally, the apparent co-equilibrium for carbon and hydrogen isotopes between methane and water and methane and CO_2 for some gases supports this observation as well (Fig. 14). The

presence of isotopic equilibrium in these settings and disequilibrium in others can be understood as follows: in marine sedimentary and coalbed/shale/gas field systems it has been argued (e.g., Stolper et al., 2015; Wang et al., 2015; Okumura et al., 2016; Meister et al., 2019; Meister and Reyes, 2019) that available organic carbon is less reactive (i.e., less labile) given its transport through the water column and sediments where prior consumption by aerobic and dissimilatory anaerobic metabolisms has occurred (in the case of marine sedimentary systems) or subsequent burial and thermal transformations (in the case of coalbed/shale/gas field systems). Such refractory reactants would result in low free energy gradients for methanogens and in turn promote enzymatic reversibility and thus isotope-exchange reactions. As discussed in Stolper et al. (2018), this contrasts with terrestrial environments where organic matter is more labile and thus provides a higher substrate availability to consortia of microbial organisms. This would promote higher free energy gradients to methanogens, less reversible enzymes, and thus expression of kinetic isotope effects. A similar situation would occur in pure-culture experiments with relatively high pH_2 levels and use of growth media specifically designed to support the rapid growth of organisms and promotion of high free energy gradients for methanogens and limited enzymatic reversibility (e.g., Valentine et al., 2004).

An alternative mechanism by which methane could be in hydrogen isotopic equilibrium with water and carbon isotopic equilibrium with CO_2 is through enzymatic re-equilibration after being generated. Specifically, Okumura et al. (2016) argued that methane could be produced out of hydrogen isotopic equilibrium by methanogens and then, after formation, later be equilibrated by methanogens in sediments. Alternatively, equilibration could occur via the action of anaerobic methanotrophs, which are known to catalyze exchange of carbon and hydrogen isotopes between methane and water during methane consumption (Holler et al., 2011; Yoshinaga et al., 2014; Marlow et al., 2017). It has been proposed that under low free energy conditions, anaerobic methanotrophic enzymes (which are thought to be the same as those for methanogens, just operating in reverse; Hallam et al., 2004) operate reversibly and can partially equilibrate both the carbon isotopes of methane and CO_2 (Holler et al., 2011; Yoshinaga et al., 2014) and potentially the hydrogen isotopes of methane and water (Stolper et al., 2015). Again, this hypothesis requires that low free energy gradients promote isotope-exchange reactions between CH_4 and CO_2 and CH_4 and H_2O, leading to equilibrium. Young et al. (2017), Giunta et al. (2019), and Ash et al. (2019) have all interpreted equilibrium methane clumped-isotope compositions in microbial systems as being caused by anaerobic methanotrophs through promotion of hydrogen isotope-exchange reactions. As such, isotopic re-equilibration of methane by anaerobic methane oxidation could also explain both the bulk and clumped-isotope data in marine sedimentary and coalbed/shale/gas field data (also see recent experimental data from Ono et al., 2021).

Whether methane forms in or later attains carbon and hydrogen isotopic equilibrium during methanogenesis or later via re-equilibration by other methanogens or methanotrophs (or during other processes that may be occurring) cannot be determined from the above comparisons (Figs. 11, 12, and 13). This is because these comparisons can only identify whether the methane is currently in equilibrium, not how it reached that equilibrium. Regardless, new calibrations for $1000\times\ln{}^{D}\alpha_{CH4(g/aq)\text{-}H2O(l)}$ from this study strongly support previous suggestions that marine sedimentary and coalbed/shale/gas field microbial methane can be in hydrogen isotopic equilibrium with co-occurring waters while terrestrial and laboratory cultures are not. This same pattern emerges for carbon isotopes.

Finally, it is important to note that near CH_4-H_2O and CH_4-CO_2 hydrogen and carbon isotopic equilibrium in biogenic gases from marine sedimentary and coalbed/shale/gas field systems is not universal. Numerous samples are found out of isotopic equilibrium. In the context of the model presented above, this requires that there is sufficient free energy available that methanogens form methane that is close to but not in isotopic equilibrium with co-occurring CO_2 and H_2O and, as such, show some degree of irreversibility in one or more steps. This is not surprising and would indicate that gradients in carbon lability in marine sediments and coalbed/shale/gas field systems exist. As such, comparing hydrogen and carbon isotopes of methane vs. what is expected for equilibrium could be used as a probe into the free energy available in such systems.

6. Summary and Conclusions

Experimentally interpolatable calibrations of hydrogen isotopic equilibrium between methane and liquid water as a function of temperature prior to this work were only available for temperatures above 200°C (Horibe and Craig, 1995). Additionally, theoretical calculations of CH_4-H_2O hydrogen isotopic equilibrium from 0-200°C differ in value by ~160‰ between each other and the extrapolation of the experimental calibration of Horibe and Craig (1995) to low temperatures. Here we presented an experimental calibration of hydrogen isotopic equilibrium for the CH_4-H_2O(l) system that is interpolatable from 3 to 200°C. This was done by equilibrating the hydrogen isotopes of CH_4 and H_2 using γ-Al_2O_3 as a catalyst based on a bracketing approach and combining this calibration with previous experimental determinations of hydrogen isotopic equilibrium between molecular hydrogen and water. We then compared this work both to new theoretical calculations of equilibrium hydrogen isotopic fractionation factors in the CH_4-H_2-H_2O system using Path Integral Monte Carlo (PIMC) calculations and to environmental data.

We found that our experimental calibration of $1000\times\ln{}^{D}\alpha_{CH4(g)\text{-}H2(g)}$ agrees 1:1 with theoretical calculations performed using the PIMC approach (with or without the DBO correction). Additionally, comparison of previous experimental determinations of $1000\times\ln{}^{D}\alpha_{H2O(l)\text{-}H2(g)}$ agree 1:1 within 1 s.e. with our theoretical DBO-corrected PIMC calculations. We investigated potential sources of error for the theoretical calculations. It appears that deviations of at least ~10‰ for theoretical calculations of hydrogen isotope equilibrium between species are plausible given changes in both the theoretical level and basis set sizes used to calculate the potential energy surface for H_2O and CH_4, which are then used for the PIMC calculations; these errors are challenging to exactly quantify due to a lack of convergence with increasing level of theoretical treatment. We note that anharmonicity, quantum effects, and DBO corrections can each individually have large effects (up to 34‰ for hydrogen isotopes) on final calculated RPFRs and α values, and their inclusion was needed here to yield agreement between theory and experiment. Finally, we additionally provided a theoretical calibration of $1000\times\ln{}^{13}\alpha_{CH4(g)\text{-}CO2(g)}$ based on the PIMC method. It agrees with experimental data from 200-1300°C with an average offset of 0.56‰.

We compared our experimental calibrations for $1000\times\ln{}^{D}\alpha_{CH4(g/aq)\text{-}H2O(l)}$ to samples from microbial cultures, microbial marine sedimentary, coalbed/shale/natural gas, terrestrial samples, and thermogenic gases. We find that microbial culture and terrestrial gases are generally out of CH_4-H_2O(l) hydrogen isotopic equilibrium while microbial marine sedimentary and

coalbed/shale gas systems can be found near isotopic equilibrium. Limited thermogenic data also indicates thermogenic gases may form in hydrogen isotopic equilibrium with co-occurring waters. A similar set of observations was also made for carbon isotopes between methane and CO_2.

For microbial systems, we used prior frameworks to interpret these results to be the product of the control of free energy availability to microorganisms on whether kinetic or equilibrium isotope effects are expressed during methane generation. Specifically, in energy replete conditions such as microbial cultures and terrestrial systems, enzymes of methanogenesis operate wholly or partially irreversibly and kinetic isotope effects are expressed. In settings where free energy gradients are low, the enzymes of either methanogens or anaerobic methanotrophs operate reversibly, equilibrating the hydrogen and carbon isotopes of methane with CO_2 and water either during methane generation or afterwards in the sediments. This indicates that both the hydrogen and carbon isotopes of methane are tracers of environmental energy conditions under which methane is generated or stored.

Acknowledgements
DAS acknowledges support from the National Science Foundation under Grant No. EAR-1911296 and the Donors of the American Chemical Society Petroleum Research Fund. Work at Lawrence Berkeley National Laboratory was supported by the U.S. Department of Energy, Office of Science, Office of Basic Energy Sciences, Chemical Sciences, Geosciences, and Biosciences Division, under Award Number DE-AC02-05CH11231. TFM acknowledges support from the National Science Foundation under Grant No. CHE-1611581. RK acknowledges Michael Webb (Princeton) and Xuecheng Tao (Caltech) for valuable discussions, and Ryan DiRisio (U. Washington) for sharing his code that obtains harmonic frequencies from a potential energy surface. We thank Margarida Costa Gomes (ENS Lyon) for clarification on the CD_4/CH_4 gas-liquid partitional experiments. We also thank Edward Hornibrook for handling this paper and David T. Wang and an anonymous reviewer for constructive reviews.

Supplementary Information
In the associated Electronic Annex file, we provide reference harmonic frequencies used to compute reference harmonic RPFRs (Table EA1), individual mass spectrometric measurements of all experiments (Table EA2), average values from top- or bottom-bracket experiments (Table EA3), coefficients of 4th order polynomial fits to experimental data (Table EA4), an Excel-based $1000\times\ln\alpha$ value calculator (Table EA5), coefficients and associated errors of 4th order polynomial fits to DBO-corrected PIMC calculations (Table EA6), compiled experimental estimates of $^{D}\alpha_{H2O(g)\text{-}H2(g)}$ and $^{D}\alpha_{H2O(l)\text{-}H2(g)}$ (Table EA7), compiled natural data (Table EA8), and compiled culture data (Table EA9).

References

Ash J. L., Egger M., Treude T., Kohl I., Cragg B., Parkes R. J., Slomp C. P., Sherwood Lollar B. and Young E. D. (2019) Exchange catalysis during anaerobic methanotrophy revealed by 12CH2D2 and 13CH3D in methane. *Geochem. Perspect. Lett.*, 26–30.

Bacsik Z., Lopes J. N. C., Gomes M. F. C., Jancsó G., Mink J. and Pádua A. A. H. (2002) Solubility isotope effects in aqueous solutions of methane. *J. Chem. Phys.* **116**, 10816–10824.

Bardo R. D. and Wolfsberg M. (1975) The nuclear mass dependence of the adiabatic correction to the Born–Oppenheimer approximation. *J. Chem. Phys.* **62**, 4555–4558.

Bardo R. D. and Wolfsberg M. (1976) A theoretical calculation of the equilibrium constant for the isotopic exchange reaction between water and hydrogen deuteride. *J. Phys. Chem.* **80**, 1068–1071.

Bardo R. D. and Wolfsberg M. (1978) The adiabatic correction for nonlinear triatomic molecules: Techniques and calculations. *J. Chem. Phys.* **68**, 2686–2695.

Bernard B. B., Brooks J. M. and Sackett W. M. (1976) Natural gas seepage in the Gulf of Mexico. *Earth Planet. Sci. Lett.* **31**, 48–54.

Bigeleisen J. and Mayer M. G. (1947) Calculation of Equilibrium Constants for Isotopic Exchange Reactions. *J. Chem. Phys.* **15**, 261–267.

Blanchard M., Balan E. and Schauble E. A. (2017) Equilibrium Fractionation of Non-traditional Isotopes: a Molecular Modeling Perspective. *Rev. Mineral. Geochem.* **82**, 27–63.

Blinder S. M. (2019) Chapter 1 - Introduction to the Hartree-Fock method. In *Mathematical Physics in Theoretical Chemistry* (eds. S. M. Blinder and J. E. House). Developments in Physical & Theoretical Chemistry. Elsevier. pp. 1–30.

Bottinga Y. (1969) Calculated fractionation factors for carbon and hydrogen isotope exchange in the system calcite-carbon dioxide-graphite-methane-hydrogen-water vapor. *Geochim. Cosmochim. Acta* **33**, 49–64.

Bottinga Y. (1968) Hydrogen isotope equilibriums in the system hydrogen-water. *J. Phys. Chem.* **72**, 4338–4340.

Botz R., Pokojski H.-D., Schmitt M. and Thomm M. (1996) Carbon isotope fractionation during bacterial methanogenesis by CO2 reduction. *Org. Geochem.* **25**, 255–262.

Brand W. A. and Coplen T. B. (2001) An interlaboratory study to test instrument performance of hydrogen dual-inlet isotope-ratio mass spectrometers. *Fresenius J. Anal. Chem.* **370**, 358–362.

Bron J., Chang C. F. and Wolfsberg M. (1973) Isotopic Partition Function Ratios Involving H2, H2O, H2S, H2Se, and NH3. *Z. Für Naturforschung A* **28**, 129–136.

Burke R. A. (1993) Possible influence of hydrogen concentration on microbial methane stable hydrogen isotopic composition. *Chemosphere* **26**, 55–67.

Burruss R. C. and Laughrey C. D. (2010) Carbon and hydrogen isotopic reversals in deep basin gas: Evidence for limits to the stability of hydrocarbons. *Org. Geochem.* **41**, 1285–1296.

Cao X., Bao H. and Peng Y. (2019) A kinetic model for isotopologue signatures of methane generated by biotic and abiotic CO2 methanation. *Geochim. Cosmochim. Acta* **249**, 59–75.

Ceperley D. M. (1995) Path integrals in the theory of condensed helium. *Rev. Mod. Phys.* **67**, 279–355.

Cerrai E., Marchetti C., Renzoni R., Roseo L., Silvestri M. and Villani S. (1954) A THERMAL METHOD FOR CONCENTRATING HEAVY WATER. NUCLEAR ENGINEERING, PART I. *Chem Eng Progr Symp. Ser. No. 11* **50**, 271–280.

Chanton J., Chaser L., Glasser P. and Siegel D. (2004) Carbon and hydrogen isotopic effects in microbial methane from terrestrial environments. In *Stable isotopes and biosphere-atmosphere interactions, physiological ecology series* pp. 85–105.

Chen X., Tao M., Zhou Z. and Li D. (2019) A new theoretical calculation of the equilibrium constant and temperature for the carbon isotope exchange reaction between CH4 and CO2. *Geothermics* **79**, 140–144.

Cheng B. and Ceriotti M. (2014) Direct path integral estimators for isotope fractionation ratios. *J. Chem. Phys.* **141**, 244112.

Chung H. M., Gormly J. R. and Squires R. M. (1988) Origin of gaseous hydrocarbons in subsurface environments: Theoretical considerations of carbon isotope distribution. *Chem. Geol.* **71**, 97–104.

Claypool G. E. and Kaplan I. R. (1974) The Origin and Distribution of Methane in Marine Sediments. In *Natural Gases in Marine Sediments* (ed. Isaac R. Kaplan). Marine Science. Springer US, Boston, MA. pp. 99–139.

Clayton R. N. and Kieffer S. W. (1991) Oxygen isotopic thermometer calibrations. In Stable isotope geochemistry : A tribute to samuel Epstein. pp. 3–10.

Craig H. (1953) The geochemistry of the stable carbon isotopes. *Geochim. Cosmochim. Acta* **3**, 53–92.

Criss R. E. (1999) *Principles of Stable Isotope Distribution*., Oxford University Press, USA.

Dai J., Xia X., Li Z., Coleman D. D., Dias R. F., Gao L., Li Jian, Deev A., Li Jin, Dessort D., Duclerc D., Li L., Liu J., Schloemer S., Zhang W., Ni Y., Hu G., Wang X. and Tang Y. (2012) Inter-laboratory calibration of natural gas round robins for δ2H and δ13C using off-line and on-line techniques. *Chem. Geol.* **310–311**, 49–55.

Douglas P. M. J., Stolper D. A., Eiler J. M., Sessions A. L., Lawson M., Shuai Y., Bishop A., Podlaha O. G., Ferreira A. A., Santos Neto E. V., Niemann M., Steen A. S., Huang L., Chimiak L., Valentine D. L., Fiebig J., Luhmann A. J., Seyfried W. E., Etiope G., Schoell M., Inskeep W. P., Moran J. J. and Kitchen N. (2017) Methane clumped isotopes: Progress and potential for a new isotopic tracer. *Org. Geochem.* **113**, 262–282.

Douglas P. M. J., Stolper D. A., Smith D. A., Walter Anthony K. M., Paull C. K., Dallimore S., Wik M., Crill P. M., Winterdahl M., Eiler J. M. and Sessions A. L. (2016) Diverse origins of Arctic and Subarctic methane point source emissions identified with multiply-substituted isotopologues. *Geochim. Cosmochim. Acta* **188**, 163–188.

Dunning T. H. (1989) Gaussian basis sets for use in correlated molecular calculations. I. The atoms boron through neon and hydrogen. *J. Chem. Phys.* **90**, 1007–1023.

Eldridge D. L., Korol R., Lloyd M. K., Turner A. C., Webb M. A., Miller T. F. and Stolper D. A. (2019) Comparison of Experimental vs Theoretical Abundances of 13CH3D and 12CH2D2 for Isotopically Equilibrated Systems from 1 to 500 °C. *ACS Earth Space Chem.* **3**, 2747–2764.

Etiope G. and Sherwood Lollar B. (2013) ABIOTIC METHANE ON EARTH. *Rev. Geophys.* **51**, 276–299.

Feller D., Peterson K. A. and Crawford T. D. (2006) Sources of error in electronic structure calculations on small chemical systems. *J. Chem. Phys.* **124**, 054107.

Fiebig J., Chiodini G., Caliro S., Rizzo A., Spangenberg J. and Hunziker J. C. (2004) Chemical and isotopic equilibrium between CO2 and CH4 in fumarolic gas discharges: Generation of CH4 in arc magmatic-hydrothermal systems. *Geochim. Cosmochim. Acta* **68**, 2321–2334.

Friedman I. and Murata K. J. (1979) Origin of dolomite in Miocene Monterey Shale and related formations in the Temblor Range, California. *Geochim. Cosmochim. Acta* **43**, 1357–1365.

Galimov E. M. (1973) *Izotopy ugleroda v neftegazovoj geologii*. Nedra Press, Moscow. Translated and reprinted in English as TT F-682, *Carbon Isotopes in Oil-Gas Geology*, National Aeronautics and Space Administration, Washington, 1974.

Games L. M. and Hayes J. M. (1976) Isotopic and quantitative analysis of the major carbon fractions in natural water samples. *Anal. Chem.* **48**, 130–135.

Gauss J., Tajti A., Kállay M., Stanton J. F. and Szalay P. G. (2006) Analytic calculation of the diagonal Born-Oppenheimer correction within configuration-interaction and coupled-cluster theory. *J. Chem. Phys.* **125**, 144111.

Giunta T., Young E. D., Warr O., Kohl I., Ash J. L., Martini A., Mundle S. O. C., Rumble D., Pérez-Rodríguez I., Wasley M., LaRowe D. E., Gilbert A. and Sherwood Lollar B. (2019) Methane sources and sinks in continental sedimentary systems: New insights from paired

clumped isotopologues 13CH3D and 12CH2D2. *Geochim. Cosmochim. Acta* **245**, 327–351.

Gomes M. F. C. and Grolier J.-P. (2001) Determination of Henry's law constants for aqueous solutions of tetradeuteriomethane between 285 and 325 K and calculation of the H/D isotope effect. *Phys. Chem. Chem. Phys.* **3**, 1047–1052.

Gropp J., Iron M. A. and Halevy I. (2021) Theoretical estimates of equilibrium carbon and hydrogen isotope effects in microbial methane production and anaerobic oxidation of methane. *Geochim. Cosmochim. Acta* **295**, 237–264.

Hallam S. J., Putnam N., Preston C. M., Detter J. C., Rokhsar D., Richardson P. M. and DeLong E. F. (2004) Reverse Methanogenesis: Testing the Hypothesis with Environmental Genomics. *Science* **305**, 1457–1462.

Harting P., Schütze H. and Christoph G. (1976) Der thermodynamische Kohlenstoffisotopieeffekt im System CH4–H2O. *Isot. Isot. Environ. Health Stud.* **12**, 232–234.

Holler T., Wegener G., Niemann H., Deusner C., Ferdelman T. G., Boetius A., Brunner B. and Widdel F. (2011) Carbon and sulfur back flux during anaerobic microbial oxidation of methane and coupled sulfate reduction. *Proc. Natl. Acad. Sci.* **108**, E1484–E1490.

Horibe Y. and Craig H. (1995) DH fractionation in the system methane-hydrogen-water. *Geochim. Cosmochim. Acta* **59**, 5209–5217.

Horita J. (2001) Carbon isotope exchange in the system CO2-CH4 at elevated temperatures. *Geochim. Cosmochim. Acta* **65**, 1907–1919.

Horita J. and Wesolowski D. J. (1994) Liquid-vapor fractionation of oxygen and hydrogen isotopes of water from the freezing to the critical temperature. *Geochim. Cosmochim. Acta* **58**, 3425–3437.

Huang X. (黄新川), Schwenke D. W., Tashkun S. A. and Lee T. J. (2012) An isotopic-independent highly accurate potential energy surface for CO2 isotopologues and an initial 12C16O2 infrared line list. *J. Chem. Phys.* **136**, 124311.

Hunt J. M. (1995) Petroleum geochemistry and geology. **743**.

John C. S., Kemball C., Pearce E. A. and Pearman A. J. (1979) Exchange of alkanes with deuterium over γ-alumina. *J. Chem. Res. Synop.*, 400–401.

Kakiuchi M. and Matsuo S. (1979) Direct measurements of D/H and $^{18}O/^{16}O$ fractionation factors between vapor and liquid water in the temperature range from 10 to 40°C. *Geochem. J.* **13**, 307–311.

Kawagucci S., Kobayashi M., Hattori S., Yamada K., Ueno Y., Takai K. and Yoshida N. (2014) Hydrogen isotope systematics among H2–H2O–CH4 during the growth of the

hydrogenotrophic methanogen Methanothermobacter thermautotrophicus strain ΔH. *Geochim. Cosmochim. Acta* **142**, 601–614.

Kleinman L. I. and Wolfsberg M. (1973) Corrections to the Born-Oppenheimer approximation and electronic effects on isotopic exchange equilibria. *J. Chem. Phys.* **59**, 2043–2053.

Kolos W. and Wolniewicz L. (1964) Accurate Adiabatic Treatment of the Ground State of the Hydrogen Molecule. *J. Chem. Phys.* **41**, 3663–3673.

Kueter N., Schmidt M. W., Lilley M. D. and Bernasconi S. M. (2019) Experimental determination of equilibrium CH4–CO2–CO carbon isotope fractionation factors (300–1200°C). *Earth Planet. Sci. Lett.* **506**, 64–75.

Larson J. G. and Hall W. K. (1965) Studies of the Hydrogen Held by Solids. VII. The Exchange of the Hydroxyl Groups of Alumina and Silica-Alumina Catalysts with Deuterated Methane. *J. Phys. Chem.* **69**, 3080–3089.

Lee T. J., Martin J. M. L. and Taylor P. R. (1995) An accurate ab initio quartic force field and vibrational frequencies for CH4 and isotopomers. *J. Chem. Phys.* **102**, 254–261.

Liu Q. and Liu Y. (2016) Clumped-isotope signatures at equilibrium of CH4, NH3, H2O, H2S and SO2. *Geochim. Cosmochim. Acta* **175**, 252–270.

Lutz J. J. and Hutson J. M. (2016) Deviations from Born-Oppenheimer mass scaling in spectroscopy and ultracold molecular physics. *J. Mol. Spectrosc.* **330**, 43–56.

Majoube M. (1971) Fractionnement en oxygène 18 et en deutérium entre l'eau et sa vapeur. *J. Chim. Phys.* **68**, 1423–1436.

Marlow J. J., Steele J. A., Ziebis W., Scheller S., Case D., Reynard L. M. and Orphan V. J. (2017) Monodeuterated Methane, an Isotopic Tool To Assess Biological Methane Metabolism Rates. *mSphere* **2**.

McCollom T. M. (2008) Observational, Experimental, and Theoretical Constraints on Carbon Cycling in Mid-Ocean Ridge Hydrothermal Systems. In *Magma to Microbe* American Geophysical Union (AGU). pp. 193–213.

Meister P., Liu B., Khalili A., Böttcher M. E. and Jørgensen B. B. (2019) Factors controlling the carbon isotope composition of dissolved inorganic carbon and methane in marine porewater: An evaluation by reaction-transport modelling. *J. Mar. Syst.* **200**, 103227.

Meister P. and Reyes C. (2019) The Carbon-Isotope Record of the Sub-Seafloor Biosphere. *Geosciences* **9**, 507.

Merlivat L., Botter R. and Nief G. (1963) ISOTOPIC FRACTIONATION DURING DISTILLATION OF WATER. *J. Chim. Phys. Fr. Merged Rev Gen Colloides Form J Chim Phys Rev Gen Colloides* **Vol: 60**.

Miller H. M., Chaudhry N., Conrad M. E., Bill M., Kopf S. H. and Templeton A. S. (2018) Large carbon isotope variability during methanogenesis under alkaline conditions. *Geochim. Cosmochim. Acta* **237**, 18–31.

Moran J. J., House C. H., Freeman K. H. and Ferry J. G. (2005) Trace methane oxidation studied in several Euryarchaeota under diverse conditions. *Archaea* **1**, 303–309.

Morikawa K., Benedict W. S. and Taylor H. S. (1936) The Activation of Specific Bonds in Complex Molecules at Catalytic Surfaces. I. The Carbon—Hydrogen Bond in Methane and Methane-d4. *J. Am. Chem. Soc.* **58**, 1445–1449.

Murata K., Friedman I. S. and Cremer M. (1972) Geochemistry of diagenetic dolomites in Miocene marine formations of California and Oregon. In *USGS Number Series*

Murata K. J., Friedman I. and Madsen B. M. (1969) *Isotopic Composition of Diagenetic Carbonates in Marine Miocene Formations of California and Oregon*., U.S. Government Printing Office.

Okumura T., Kawagucci S., Saito Y., Matsui Y., Takai K. and Imachi H. (2016) Hydrogen and carbon isotope systematics in hydrogenotrophic methanogenesis under H2-limited and H2-enriched conditions: implications for the origin of methane and its isotopic diagnosis. *Prog. Earth Planet. Sci.* **3**, 14.

O'Neil J. R. (1986) THEORETICAL AND EXPERIMENTAL ASPECTS OF ISOTOPIC FRACTIONATION. *Rev. Mineral.* **16**, 40.

Ono S., Rhim J. H., Gruen D. S., Taubner H., Kölling M. and Wegener G. (2021) Clumped isotopologue fractionation by microbial cultures performing the anaerobic oxidation of methane. *Geochim. Cosmochim. Acta* **293**, 70–85.

Partridge H. and Schwenke D. W. (1997) The determination of an accurate isotope dependent potential energy surface for water from extensive ab initio calculations and experimental data. *J. Chem. Phys.* **106**, 4618–4639.

Penning H., Plugge C. M., Galand P. E. and Conrad R. (2005) Variation of carbon isotope fractionation in hydrogenotrophic methanogenic microbial cultures and environmental samples at different energy status. *Glob. Change Biol.* **11**, 2103–2113.

Peterson K. A. and Dunning T. H. (2002) Accurate correlation consistent basis sets for molecular core–valence correlation effects: The second row atoms Al–Ar, and the first row atoms B–Ne revisited. *J. Chem. Phys.* **117**, 10548–10560.

Postma J. M., Silvester L. F. and Rock P. A. (1988) Thermodynamics of hydrogen-isotope-exchange reactions. 3. An experimental test of the Born-Oppenheimer approximation. *J. Phys. Chem.* **92**, 1308–1312.

Proskurowski G., Lilley M. D., Kelley D. S. and Olson E. J. (2006) Low temperature volatile production at the Lost City Hydrothermal Field, evidence from a hydrogen stable isotope geothermometer. *Chem. Geol.* **229**, 331–343.

Rennow M. (1970) Gleichgewichts-und kinetische Trennfactoren bei der Verdunstung von Wasser. *Staatsexamensarbeit 2 Phys Inst Univ*.

Rhim J. H. (2020) Experimental investigations of isotopologue fractionation during microbial methanogenesis. Ph.D. thesis, Massachusetts Institute of Technology.

Richet P., Bottinga Y. and Javoy M. (1977) A Review of Hydrogen, Carbon, Nitrogen, Oxygen, Sulphur, and Chlorine Stable Isotope Fractionation Among Gaseous Molecules. *Annu. Rev. Earth Planet. Sci.* **5**, 65–110.

Robertson P. J., Scurrell M. S. and Kemball C. (1975) Exchange of alkanes with deuterium over γ -alumina. A Brønsted linear free energy relationship. *J. Chem. Soc. Faraday Trans. 1 Phys. Chem. Condens. Phases* **71**, 903–912.

Rolston J. H., Den Hartog J. and Butler J. P. (1976) The deuterium isotope separation factor between hydrogen and liquid water. *J. Phys. Chem.* **80**, 1064–1067.

Sattler A. (2018) Hydrogen/Deuterium (H/D) Exchange Catalysis in Alkanes. *ACS Catal.* **8**, 2296–2312.

Schoell M. (1980) The hydrogen and carbon isotopic composition of methane from natural gases of various origins. *Geochim. Cosmochim. Acta* **44**, 649–661.

Schweizer K. S., Stratt R. M., Chandler D. and Wolynes P. G. (1981) Convenient and accurate discretized path integral methods for equilibrium quantum mechanical calculations. *J. Chem. Phys.* **75**, 1347–1364.

Smith J. W., Gould K. W. and Rigby D. (1981) The stable isotope geochemistry of Australian coals. *Org. Geochem.* **3**, 111–131.

Smith J. W., Pallasser R. and Pang L. S. K. (1998) Thermal reactions of acetic acid: 13C/12C partitioning between CO2 and CH4. *Org. Geochem.* **29**, 79–82.

Stewart M. K. and Friedman I. (1975) Deuterium fractionation between aqueous salt solutions and water vapor. *J. Geophys. Res. 1896-1977* **80**, 3812–3818.

Stolper D.A., Sessions A. L., Ferreira A. A., Santos Neto E. V., Schimmelmann A., Shusta S. S., Valentine D. L. and Eiler J. M. (2014a) Combined 13C–D and D–D clumping in methane: Methods and preliminary results. *Geochim. Cosmochim. Acta* **126**, 169–191.

Stolper D. A., Lawson M., Davis C. L., Ferreira A. A., Neto E. V. S., Ellis G. S., Lewan M. D., Martini A. M., Tang Y., Schoell M., Sessions A. L. and Eiler J. M. (2014b) Formation temperatures of thermogenic and biogenic methane. *Science* **344**, 1500–1503.

Stolper D. A., Martini A. M., Clog M., Douglas P. M., Shusta S. S., Valentine D. L., Sessions A. L. and Eiler J. M. (2015) Distinguishing and understanding thermogenic and biogenic sources of methane using multiply substituted isotopologues. *Geochim. Cosmochim. Acta* **161**, 219–247.

Stolper D. A., Lawson M., Formolo M. J., Davis C. L., Douglas P. M. J. and Eiler J. M. (2018) The utility of methane clumped isotopes to constrain the origins of methane in natural gas accumulations. *Geol. Soc. Lond. Spec. Publ.* **468**, 23–52.

Suess H. E. (1949) Das Gleichgewicht H2 + H D O ⇌ H D + H2 O und die weiteren Austauschgleichgewichte im System H2 , D2 und H2O. *Z. Für Naturforschung A* **4**, 328–332.

Takai K., Nakamura K., Toki T., Tsunogai U., Miyazaki M., Miyazaki J., Hirayama H., Nakagawa S., Nunoura T. and Horikoshi K. (2008) Cell proliferation at 122 degrees C and isotopically heavy CH4 production by a hyperthermophilic methanogen under high-pressure cultivation. *Proc. Natl. Acad. Sci. U. S. A.* **105**, 10949–10954.

Tang Y., Perry J. K., Jenden P. D. and Schoell M. (2000) Mathematical modeling of stable carbon isotope ratios in natural gases. *Geochim. Cosmochim. Acta* **64**, 2673–2687.

Thauer R. K. (1998) Biochemistry of methanogenesis: a tribute to Marjory Stephenson:1998 Marjory Stephenson Prize Lecture. *Microbiology,* **144**, 2377–2406.

Thiagarajan N., Xie H., Ponton C., Kitchen N., Peterson B., Lawson M., Formolo M., Xiao Y. and Eiler J. (2020) Isotopic evidence for quasi-equilibrium chemistry in thermally mature natural gases. *Proc. Natl. Acad. Sci.* **117**, 3989–3995.

Townsend J., Kirkland J. K. and Vogiatzis K. D. (2019) Chapter 3 - Post-Hartree-Fock methods: configuration interaction, many-body perturbation theory, coupled-cluster theory. In *Mathematical Physics in Theoretical Chemistry* (eds. S. M. Blinder and J. E. House). Developments in Physical & Theoretical Chemistry. Elsevier. pp. 63–117.

Tuckerman M. E., Berne B. J., Martyna G. J. and Klein M. L. (1993) Efficient molecular dynamics and hybrid Monte Carlo algorithms for path integrals. *J. Chem. Phys.* **99**, 2796–2808.

Ulusoy I. S. and Wilson A. K. (2019) Chapter 2 - Slater and Gaussian basis functions and computation of molecular integrals. In *Mathematical Physics in Theoretical Chemistry* (eds. S. M. Blinder and J. E. House). Developments in Physical & Theoretical Chemistry. Elsevier. pp. 31–61.

Urey H. C. (1947) The thermodynamic properties of isotopic substances. *J. Chem. Soc. Resumed*, 562–581.

Valeev E. F. and Sherrill C. D. (2003) The diagonal Born–Oppenheimer correction beyond the Hartree–Fock approximation. *J. Chem. Phys.* **118**, 3921–3927.

Valentine D. L., Chidthaisong A., Rice A., Reeburgh W. S. and Tyler S. C. (2004) Carbon and hydrogen isotope fractionation by moderately thermophilic methanogens 1 1Associate editor: N. E. Ostrom. *Geochim. Cosmochim. Acta* **68**, 1571–1590.

Vinson D. S., Blair N. E., Martini A. M., Larter S., Orem W. H. and McIntosh J. C. (2017) Microbial methane from in situ biodegradation of coal and shale: A review and reevaluation of hydrogen and carbon isotope signatures. *Chem. Geol.* **453**, 128–145.

Vogel J. C., Grootes P. M. and Mook W. G. (1970) Isotopic fractionation between gaseous and dissolved carbon dioxide. *Z. Für Phys. Hadrons Nucl.* **230**, 225–238.

Waldron S., Lansdown J. M., Scott E. M., Fallick A. E. and Hall A. J. (1999) The global influence of the hydrogen isotope composition of water on that of bacteriogenic methane from shallow freshwater environments. *Geochim. Cosmochim. Acta* **63**, 2237–2245.

Wang D. T., Gruen D. S., Lollar B. S., Hinrichs K.-U., Stewart L. C., Holden J. F., Hristov A. N., Pohlman J. W., Morrill P. L., Konneke M., Delwiche K. B., Reeves E. P., Sutcliffe C. N., Ritter D. J., Seewald J. S., McIntosh J. C., Hemond H. F., Kubo M. D., Cardace D., Hoehler T. M. and Ono S. (2015) Nonequilibrium clumped isotope signals in microbial methane. *Science* **348**, 428–431.

Wang D. T., Reeves E. P., McDermott J. M., Seewald J. S. and Ono S. (2018) Clumped isotopologue constraints on the origin of methane at seafloor hot springs. *Geochim. Cosmochim. Acta* **223**, 141–158.

Wang D. T., Sattler A., Paccagnini M. and Chen F. G. (2020) Method for calibrating methane clumped isotope measurements via catalytic equilibration of methane isotopologues on γ-alumina. *Rapid Commun. Mass Spectrom.* **34**, e8555.

Webb M. A. and Miller T. F. (2014) Position-Specific and Clumped Stable Isotope Studies: Comparison of the Urey and Path-Integral Approaches for Carbon Dioxide, Nitrous Oxide, Methane, and Propane. *J. Phys. Chem. A* **118**, 467–474.

Webb M. A., Wang Y., Braams B. J., Bowman J. M. and Miller T. F. (2017) Equilibrium clumped-isotope effects in doubly substituted isotopologues of ethane. *Geochim. Cosmochim. Acta* **197**, 14–26.

Werner H.-J., Knowles P. J., Knizia G., Manby F. R. and Schütz M. (2012) Molpro: a general-purpose quantum chemistry program package. *Wiley Interdiscip. Rev. Comput. Mol. Sci.* **2**, 242–253.

Werner H.-J., Knowles P. J., Knizia G., Manby F. R., Schütz M., Celani P., Györffy W., Kats D., Korona T., Lindh R., Mitrushenkov A., Rauhut G., Shamasundar K. R., Adler T. B., Amos R. D., Bennie S. J., Bernhardsson A., Berning A., Cooper D. L., Deegan M. J. O., Dobbyn A. J., Eckert F., Goll E., Hampel C., Hesselmann A., Hetzer G., Hrenar T., Jansen G., Köppl C., Lee S. J. R., Liu Y., Lloyd A. W., Ma Q., Mata R. A., May A. J., McNicholas S. J., Meyer W., III T. F. M., Mura M. E., Nicklass A., O'Neill D. P., Palmieri P., Peng D., Pflüger K., Pitzer R., Reiher M., Shiozaki T., Stoll H., Stone A. J.,

Tarroni R., Thorsteinsson T., Wang M. and Welborn M. (2019) *MOLPRO, version 2019.2, a package of ab initio programs*., Cardiff, UK.

Whiticar M. J. (1999) Carbon and hydrogen isotope systematics of bacterial formation and oxidation of methane. *Chem. Geol.* **161**, 291–314.

Whiticar M. J., Faber E. and Schoell M. (1986) Biogenic methane formation in marine and freshwater environments: CO2 reduction vs. acetate fermentation—Isotope evidence. *Geochim. Cosmochim. Acta* **50**, 693–709.

Wischert R., Laurent P., Copéret C., Delbecq F. and Sautet P. (2012) γ-Alumina: The Essential and Unexpected Role of Water for the Structure, Stability, and Reactivity of "Defect" Sites. *J. Am. Chem. Soc.* **134**, 14430–14449.

Wolniewicz L. (1983) The X 1Σ+g state vibration-rotational energies of the H2, HD, and D2 molecules. *J. Chem. Phys.* **78**, 6173–6181.

Woon D. E. and Dunning T. H. (1995) Gaussian basis sets for use in correlated molecular calculations. V. Core-valence basis sets for boron through neon. *J. Chem. Phys.* **103**, 4572–4585.

Yarnes C. (2013) δ ^{13}C and δ ^{2}H measurement of methane from ecological and geological sources by gas chromatography/combustion/pyrolysis isotope-ratio mass spectrometry: **δ** ^{13}C and **δ** ^{2}H measurement of methane. *Rapid Commun. Mass Spectrom.* **27**, 1036–1044.

Yoshinaga M. Y., Holler T., Goldhammer T., Wegener G., Pohlman J. W., Brunner B., Kuypers M. M. M., Hinrichs K.-U. and Elvert M. (2014) Carbon isotope equilibration during sulphate-limited anaerobic oxidation of methane. *Nat. Geosci.* **7**, 190–194.

Young E. D., Kohl I. E., Lollar B. S., Etiope G., Rumble D., Li (李姝宁) S., Haghnegahdar M. A., Schauble E. A., McCain K. A., Foustoukos D. I., Sutclife C., Warr O., Ballentine C. J., Onstott T. C., Hosgormez H., Neubeck A., Marques J. M., Pérez-Rodríguez I., Rowe A. R., LaRowe D. E., Magnabosco C., Yeung L. Y., Ash J. L. and Bryndzia L. T. (2017) The relative abundances of resolved l2CH2D2 and 13CH3D and mechanisms controlling isotopic bond ordering in abiotic and biotic methane gases. *Geochim. Cosmochim. Acta* **203**, 235–264.

Zhang Y. and Liu Y. (2018) The theory of equilibrium isotope fractionations for gaseous molecules under super-cold conditions. *Geochim. Cosmochim. Acta* **238**, 123–149.

Zimmermann T. and Vaníček J. (2009) Path integral evaluation of equilibrium isotope effects. *J. Chem. Phys.* **131**, 024111.

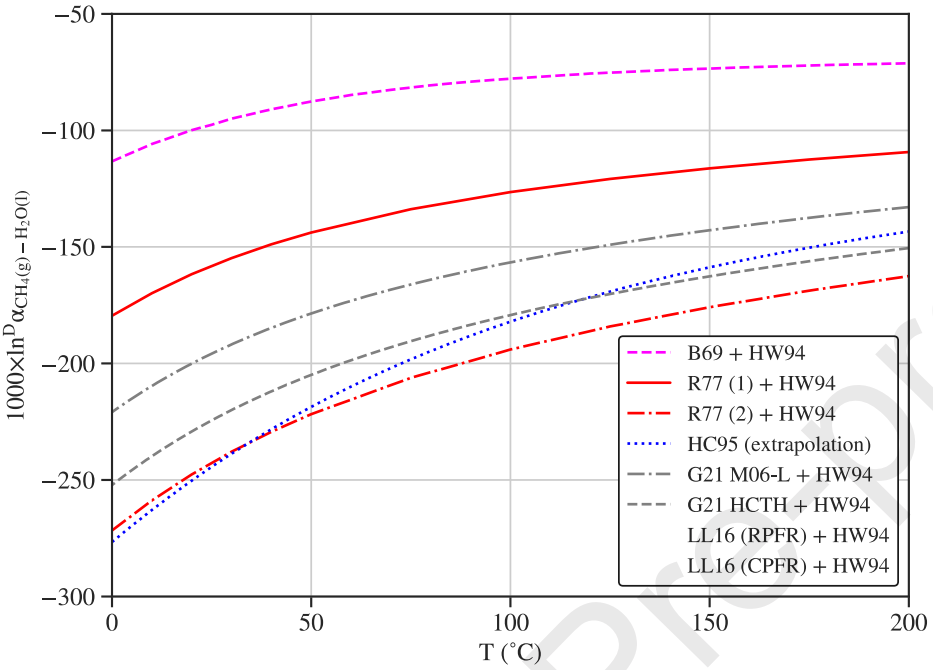

Figure 1: Published theoretical estimates of equilibrium $1000\times\ln^{D}\alpha_{CH4(g)-H2O(l)}$ from 0 to 200°C. Theoretical estimates are based on calculations of $1000\times\ln^{D}\alpha_{CH4(g)-H2O(g)}$ that are converted to $1000\times\ln^{D}\alpha_{CH4(g)-H2O(l)}$ using the experimental calibration of $1000\times\ln^{D}\alpha_{H2O(l)-H2O(g)}$ from Horita and Wesolowski (1994) — this is noted as '+ HW94' when applied. HC95 (extrapolation) is the extrapolation of the equation given in Horibe and Craig (1995) to temperatures below the range of their experiments (200-500°C). B69 is Bottinga (1969). R77 is Richet et al. (1977), where (1) refers to the results where the excess factor $X(CH_4)$ was calculated using a harmonic approximation, while R77 (2) refers to the use of an anharmonic approximation in this calculation. LL16 is Liu and Liu (2016) using their notations where RPFR are calculations performed assuming a harmonic oscillator approximation while "CPFR" (using their terminology) includes higher order corrections for anharmonicity, rotational-vibrational coupling, and other terms. G21 M06-L is the M06-L calculated RPFR as presented in Gropp et al. (2021), while G21 HCTH is the HCTH calculated RPFR from the same work. B69, R77 (1), and R77 (2) are 4th order polynomial fits of $1000\times\ln^{D}\alpha_{CH4(g)-H2(g)}$ vs. 1/T based on calculated values of RPFRs from the given study.

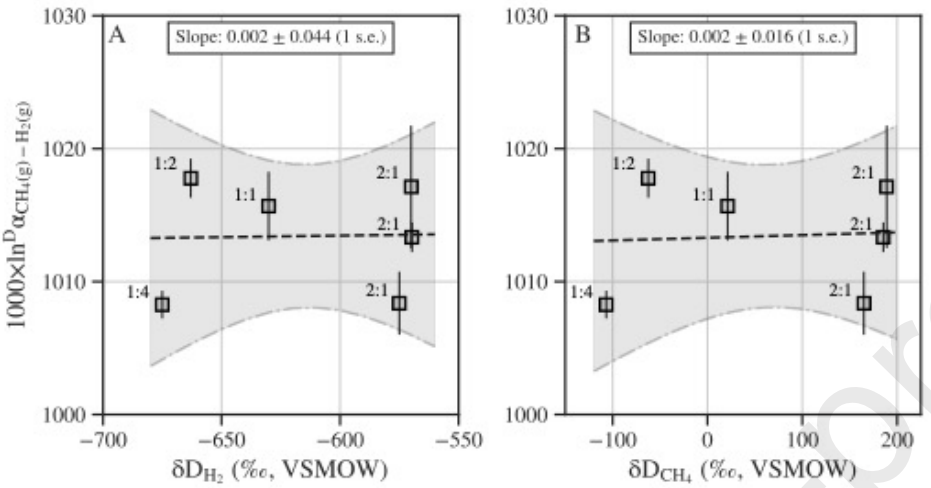

Figure 2: Results from the 50°C equilibration experiments conducted with different H_2:CH_4 stoichiometries (1:4, 1:2, 1:1, and 2:1) to test for dependencies of $1000\times\ln^{D}\alpha_{CH4(g)\text{-}H2(g)}$ on δD: (A) $1000\times\ln^{D}\alpha_{CH4(g)\text{-}H2(g)}$ vs. δD_{H2} of each experiment and (B) $1000\times\ln^{D}\alpha_{CH4(g)\text{-}H2(g)}$ vs. δD_{CH4} of each experiment. Black dotted lines are linear regressions, with slope and standard error given. Grey shading is the 95% confidence interval of the fit. Both slopes are within 1 s.e. of zero indicating there is no measurable dependence of $1000\times\ln^{D}\alpha_{CH4(g)\text{-}H2(g)}$ on the δD value of either H_2 or CH_4. Error bars are ±1 s.e. H_2:CH_4 stoichiometries of experiments are given next to each point.

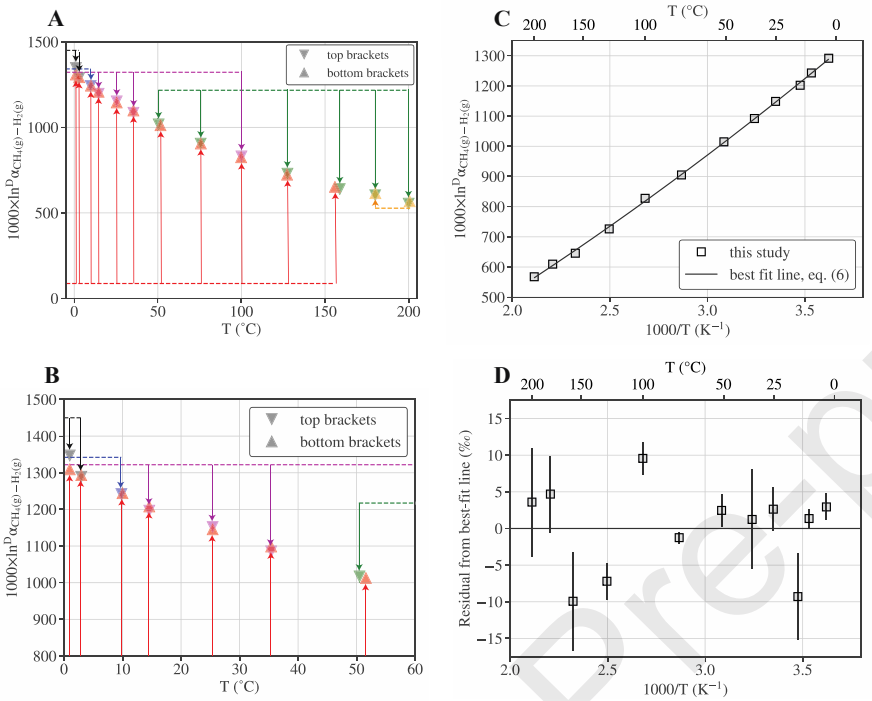

Figure 3: Experimental CH_4-H_2 hydrogen isotopic equilibrium data. (A) Final $1000\times\ln^{D}\alpha_{CH4(g)-H2(g)}$ top-bracket (downward-facing triangles) and bottom-bracket (upward facing triangles) experiments vs. temperature (°C). Arrows indicate the direction $1000\times\ln^{D}\alpha_{CH4(g)-H2(g)}$ values shifted towards in order to equilibrate (i.e., from above or below for top or bottom brackets respectively) and color corresponds to the initial $1000\times\ln^{D}\alpha_{CH4(g)-H2(g)}$ (red is initial gas composition; navy blue is 1°C; purple is 3°C; green is 15°C; black is -9°C; orange is 230°C). (B) Zoomed in plot of A for 0-60°C. (C) Average of bottom- and top-bracket $1000\times\ln^{D}\alpha_{CH4(g)-H2(g)}$ values vs. 1000/T (K^{-1}) and best-fit quadratic line to the data (eq. 6). ±1 s.e. error bars are smaller than the points in all cases. (D) Average of bottom- and top-bracket $1000\times\ln^{D}\alpha_{CH4(g)-H2(g)}$ values vs. temperature (°C) along with our best-fit quadratic line (eq. 6). Error bars are ±1 s.e.

Commented [AT1]: Check the eq. number you give in C

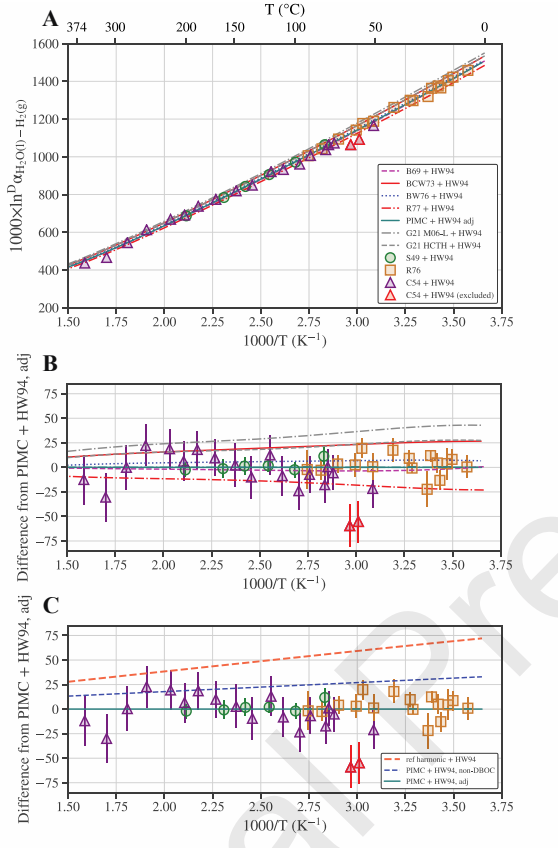

Figure 4: (A) Experimental and theoretical determinations of equilibrium $1000\times\ln^{D}\alpha_{H2O(l)-H2(g)}$ vs. 1000/T (K^{-1}). Theoretical estimates are calculations from Bottinga (1969) (B69); Bron et al. (1973) (BCW73); Bardo and Wolfsberg (1976) (BW76); Richet et al. (1977) (R77); and Gropp et al. (2021) (G21 M06-L; G21 HCTH). Experimental data are given as averages, as discussed in Section 3.4. Experimental data from Suess (1949) (S49) and Cerrai et al. (1954) (C54) were measured as $1000\times\ln^{D}\alpha_{H2O(g)-H2(g)}$ and transformed to $1000\times\ln^{D}\alpha_{H2O(l)-H2(g)}$ using the experimental calibration of $1000\times\ln^{D}\alpha_{H2O(l)-H2O(g)}$ vs. temperature from Horita and Wesolowski (1994) (HW94). Data from Rolston et al. (1976) (R76) are direct experimental determinations of $1000\times\ln^{D}\alpha_{H2O(l)-H2(g)}$. Two data points from Cerrai at al. (1954) are excluded from our fits to the experimental data (red triangles; see discussion in Section 3.5). (B) Differences between theoretical calculations and experimental data vs. our PIMC adjusted ('adj') best-fit line to the experimental data (eq. 8; PIMC + HW94 adjusted). Same legend as (A). This best-fit line was found by offsetting the DBO-corrected PIMC calculation (given as PIMC + HW94) with a constant term of +0.49‰. Errors for data from Suess (1949 and Cerrai et al. (1954) are as reported in the original study. For Rolston et al. (1976), error bars are ±1σ based on replicate measurements, and where not replicated, ±10‰ as estimated within the reference. (C) Differences relative to the DBO-corrected PIMC adj fit for harmonic ('reference harmonic' line; see Section 2.5.1), non-DBO-corrected PIMC, and DBO-corrected PIMC adj (offset by 0.49‰ to fit the experimental data) fits, as well as experimental data.

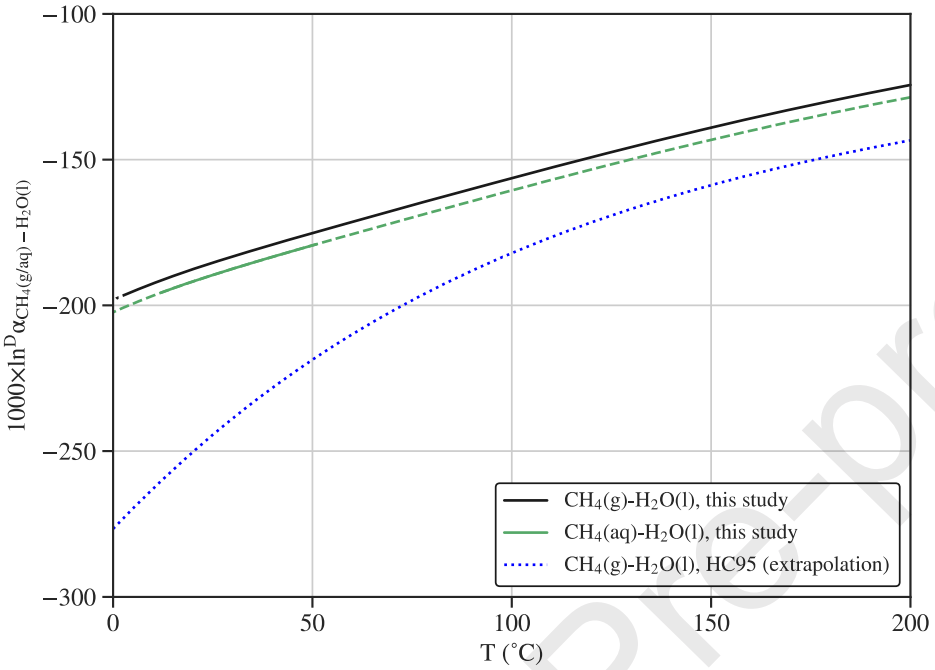

Figure 5: $1000\times\ln{}^{D}\alpha_{CH4(g/aq)-H2O(l)}$ vs. temperature from this study and from Horibe and Craig (1995) [HC95 (extrapolation)]. Dotted and dashed lines indicate extrapolations beyond experimentally calibrated temperatures.

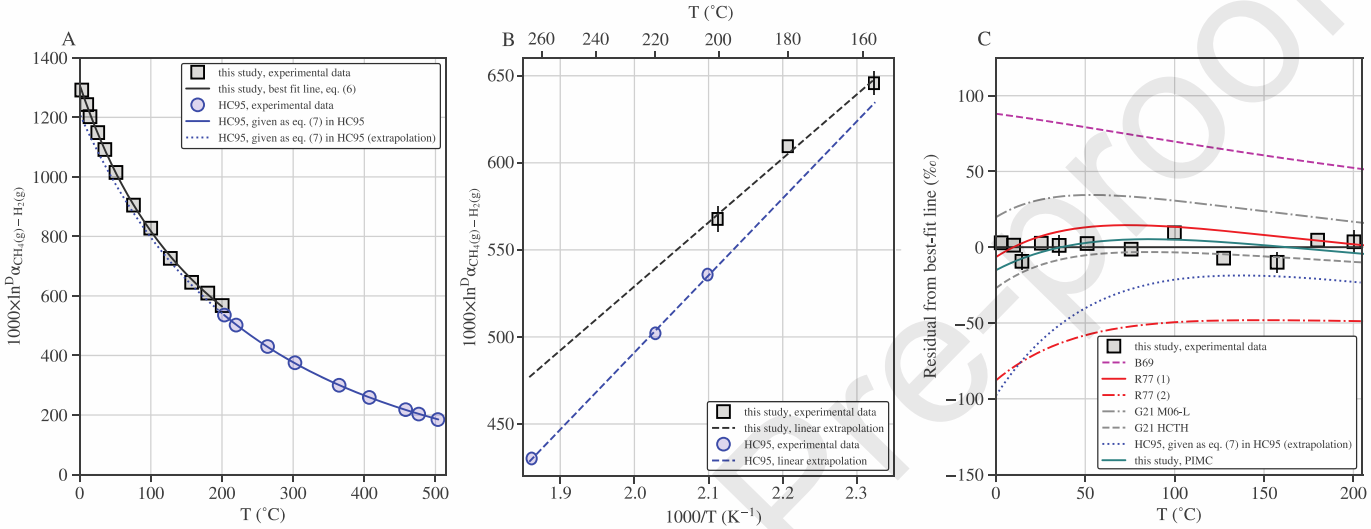

Figure 6: (A) Comparisons of determinations of $1000\times\ln^{D}\alpha_{CH4(g)-H2(g)}$ from this study vs. from Horibe and Craig (1995) (HC95). (B) Experimental determinations of $1000\times\ln^{D}\alpha_{CH4(g)-H2(g)}$ vs. temperature (°C) from this study and Horibe and Craig (1995) (HC95) from 150 to 275°C. Lines are linear extrapolations vs. 1/T (K^{-1}) through the given points and are provided as guidance. The 22.9‰ offset between the two studies at 200°C is also observed at lower and higher temperatures as seen by the extrapolations. (C) Relative differences of $1000\times\ln^{D}\alpha_{CH4(g)-H2(g)}$ between various theoretical calculations and the extrapolation of HC95 vs. the best-fit line to our data (eq. 6). HC95 (extrapolation) is the extrapolation of the equation given in Horibe and Craig (1995; eq. 7 of that study) to temperatures below 200°C; B69 is Bottinga (1969); R77 is Richet et al. (1977), where (1) represents and estimate where the excess factor $X(CH_4)$ is calculated using a harmonic approximation while R77 (2) indicates an anharmonic approximation. G21 M06-L is M06-L calculated RPFR as presented in Gropp et al. (2021), while G21 HCTH is HCTH calculated RPFR from the same work. "this study, PIMC" is the polynomial fit to the DBO-corrected PIMC theoretical calculations presented here. For the theoretical studies, the presented lines are 4th order polynomial fits of $1000\times\ln^{D}\alpha_{CH4(g)-H2(g)}$ vs. 1/T based on calculated values of RPFRs from the given study. Error bars for experimental points shown are ±1 s.e. and are smaller than the symbol when not shown.

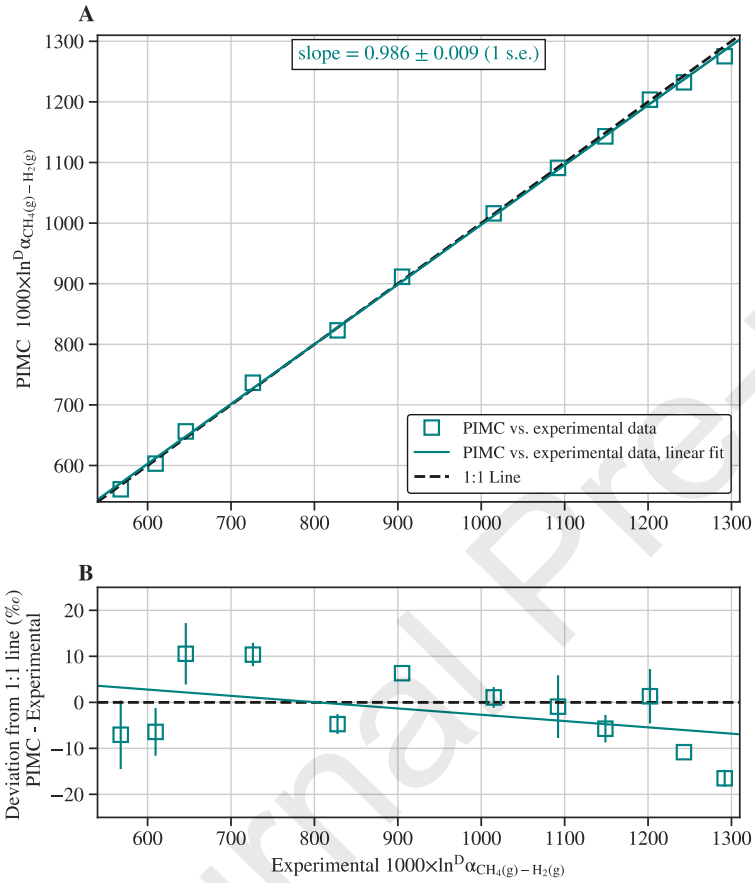

Figure 7: (A) Comparison of DBO-corrected PIMC theoretical calculations of $1000\times\ln^{D}\alpha_{CH4(g)-H2(g)}$ vs. our experimental results. The best-fit line yields a slope of 0.986 ± 0.009 (1 s.e.) and intercept of 10.99 ± 8.81 (1 s.e.). Thus, the two are in 1:1 agreement within 2 s.e. (B) Deviations of theoretical calculations vs. experimental determinations of $1000\times\ln^{D}\alpha_{CH4(g)-H2(g)}$ relative to a 1:1 line. Shading indicates 95% confidence interval for the linear fit. Y-axis error bars are 1 s.e. error for both PIMC and our experimental data propagated in quadrature. 1 s.e. errors smaller than the size of the symbol are omitted (which includes all error in the X-axis directions in addition to several Y-axis error bars).

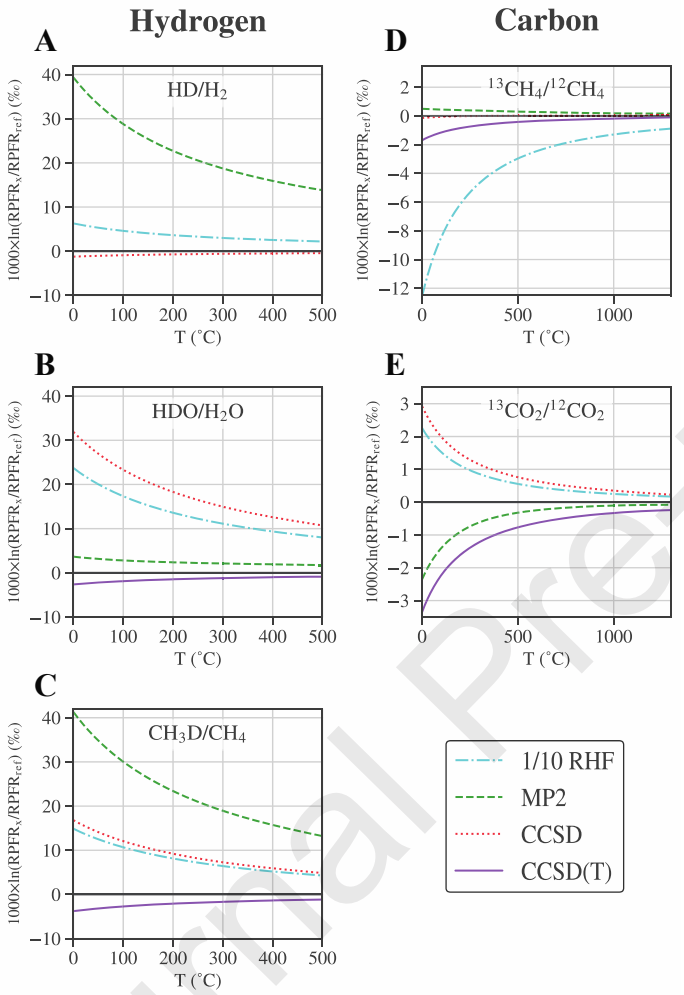

Figure 8: Changes in deuterium (A-C) and ^{13}C (D-E) RPFRs with increasing level of correlation treatment at fixed basis set size (aug-cc-pVQZ) within the harmonic approximation, relative to harmonic calculations using the reference potentials, denoted as 'ref' as described in Section 2.5.1 and given as 0 on the y-axis. As noted in Section 4.5.1, y-axis is $1000\times\ln(RPFR_X/RPFR_{ref})$ in each case, where X is the level of correlation treatment used. Note that the RHF treatment is scaled down by a factor of 1/10. We note that CCSD(T) calculations are not shown in (A) as they are identical to CCSD for H_2.

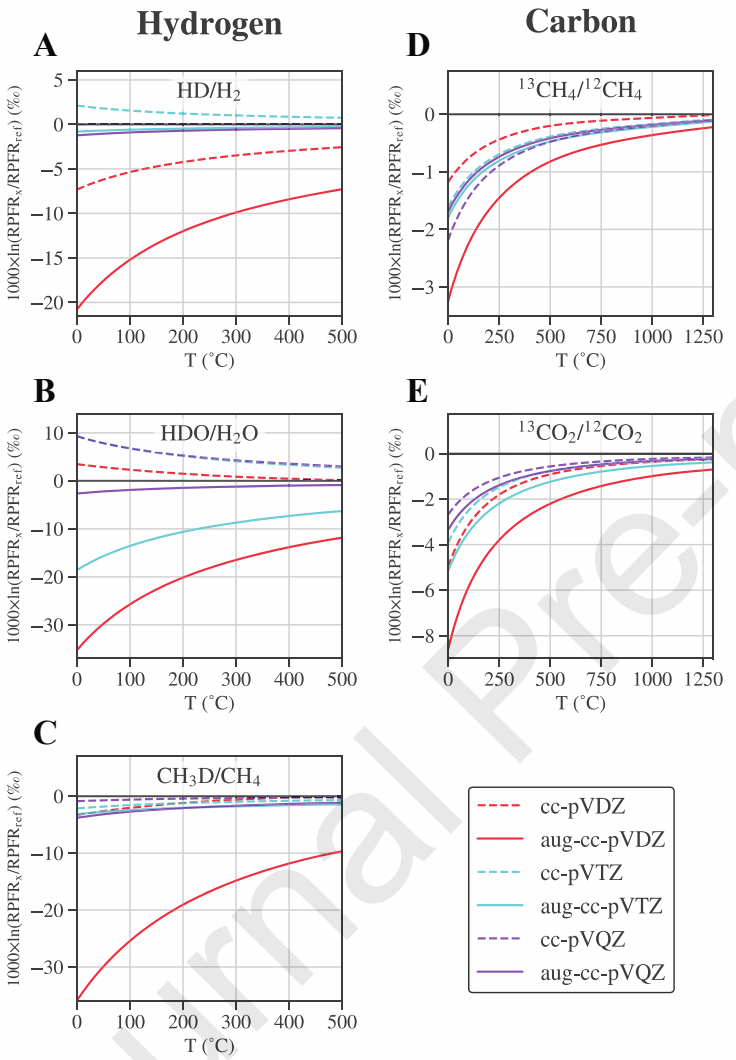

Figure 9: Changes in deuterium (A-C) and ^{13}C (D-E) RPFRs with increasing basis set size at the same level of theory (CCSD(T)) within the harmonic approximation, relative to harmonic calculations using the reference potentials, denoted as 'ref' as described in Section 2.5.1 and given as 0 on the y-axis. As noted in Section 4.5.1, y-axis is $1000\times\ln(RPFR_X/RPFR_{ref})$ in each case, where X is the basis set used.

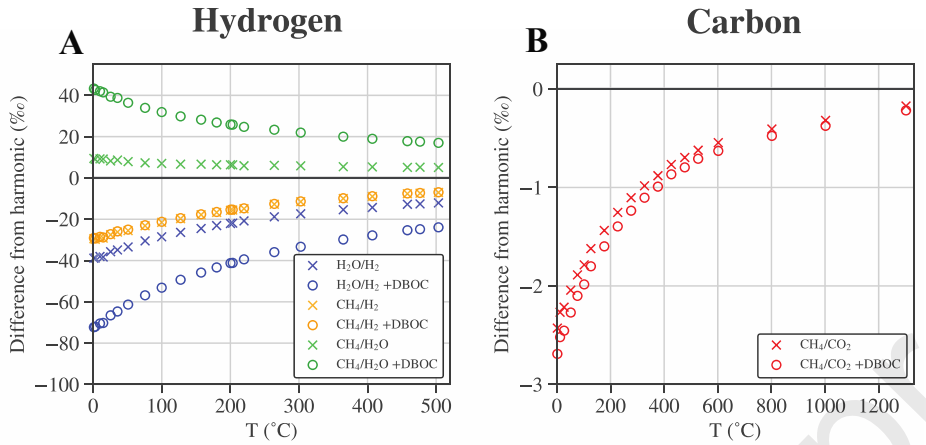

Figure 10: Differences between PIMC calculations for non-DBO-corrected and DBO-corrected cases (given as "+DBOC") vs. harmonic ('reference harmonic') calculations without DBOC. (A) $1000\times\ln^{D}\alpha_{CH4(g)\text{-}H2(g)}$, $1000\times\ln^{D}\alpha_{CH4(g)\text{-}H2O(g)}$, and $1000\times\ln^{D}\alpha_{H2O(g)\text{-}H2(g)}$ (B) for $1000\times\ln^{13}\alpha_{CH4(g)\text{-}CO2(g)}$. In all cases, the same potential energy surface is employed, as described Section 2.5.1.

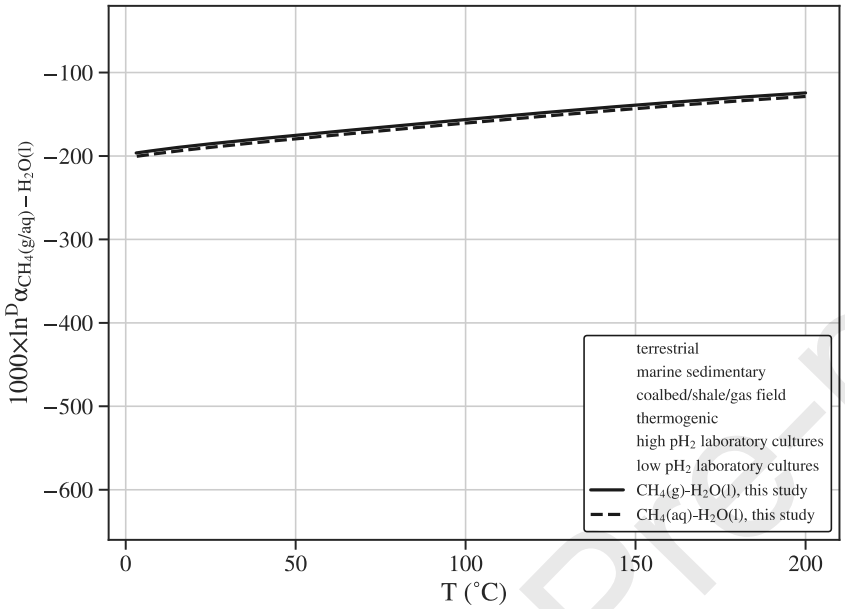

Figure 11: Comparison of $1000\times\ln^{D}\alpha_{CH4(g/aq)-H2O(l)}$ values of environmental and culture samples vs. temperature. For coal/bed/shale/gas field, marine sedimentary, terrestrial, and culture samples, methane is microbial in origin. Their temperatures are the measured or estimated current environmental or experimental temperatures. For thermogenic gases, temperatures are based on measured $^{13}CH_3D$ clumped-isotope abundances (Wang et al., 2015; Giunta et al., 2019). These are compared to our experimental calibrations of $1000\times\ln^{D}\alpha_{CH4(g)-H2O(l)}$ and $1000\times\ln^{D}\alpha_{CH4(aq)-H2O(l)}$ vs. temperature. We provide both as we do not know whether the environmental methane was originally dissolved or in the gas phase; note that the aqueous equation requires extrapolation outside 12 to 51°C.

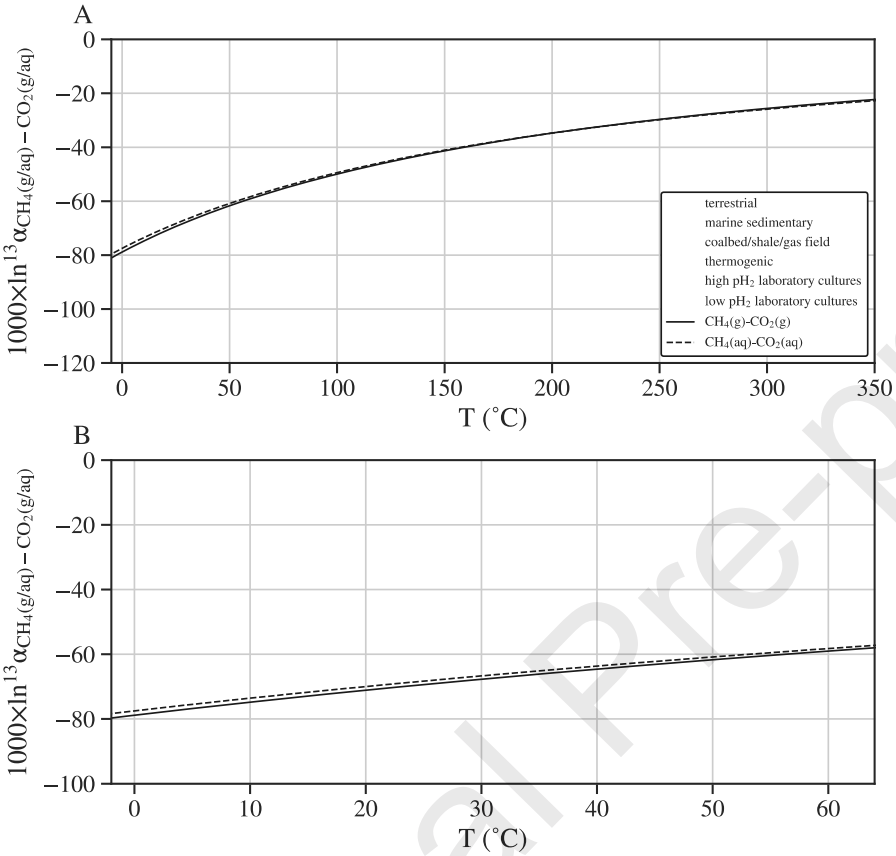

Figure 12: Comparison of $1000\times\ln^{13}\alpha_{CH4(g/aq)\text{-}CO2(g/aq)}$ values vs. temperature. (B) is a zoom in of (A) from 0 to 60°C. For coal/bed/shale/gas field, marine sedimentary, terrestrial, and culture samples, methane is microbial in origin. Their temperatures are the measured or estimated current environmental or experimental temperatures. For thermogenic gases, temperatures are based on measured $^{13}CH_3D$ or combined $^{13}CH_3D$ and $^{12}CH_2D_2$ clumped-isotope abundances (Stolper et al., 2014a). We provide calibrations for both equilibrium values of $1000\times\ln^{13}\alpha_{CH4(g)\text{-}CO2(g)}$ and $1000\times\ln^{13}\alpha_{CH4(aq)\text{-}CO2(aq)}$ vs. temperature. We provide both as we do not know whether the environmental methane and CO_2 was dissolved or in the gas phase; note that the aqueous equation requires extrapolation outside 20 to 60°C.

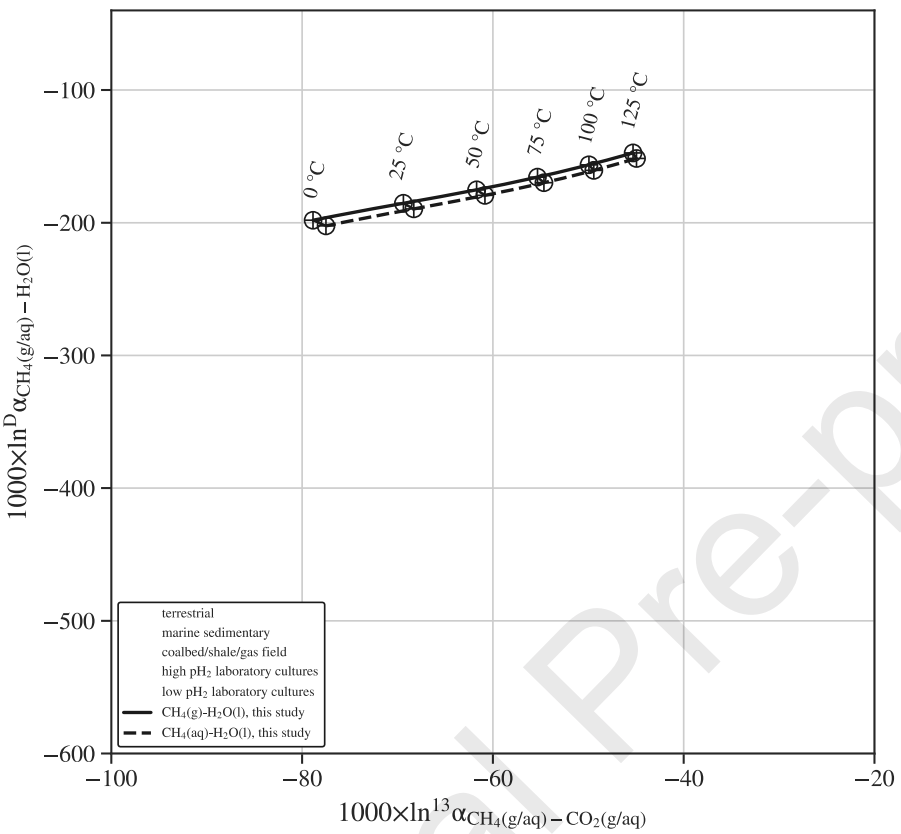

Figure 13: Comparison of $1000\times\ln^{D}\alpha_{CH4(g/aq)\text{-}H2O(l)}$ vs. $1000\times\ln^{13}\alpha_{CH4(g/aq)\text{-}CO2(g/aq)}$ values. All environmental samples are microbial in origin. For equilibrium lines, our various calibrations of $1000\times\ln^{D}\alpha_{CH4(g/aq)\text{-}H2O(l)}$ are compared to our calibrations of $1000\times\ln^{13}\alpha_{CH4(g/aq)\text{-}CO2(g/aq)}$. If the calibration of $1000\times\ln^{D}\alpha_{CH4((g/aq)\text{-}H2O(l)}$ assumes methane to be aqueous, then the calibration for $1000\times\ln^{13}\alpha_{CH4(aq)\text{-}CO2(aq)}$ is used. If the methane is assumed to be gaseous, then the calibration for $1000\times\ln^{13}\alpha_{CH4(g)\text{-}CO2(g)}$ is used. The reticle (crosshair) points are values for equilibrium at temperatures from 0 to 125°C at 25°C increments.

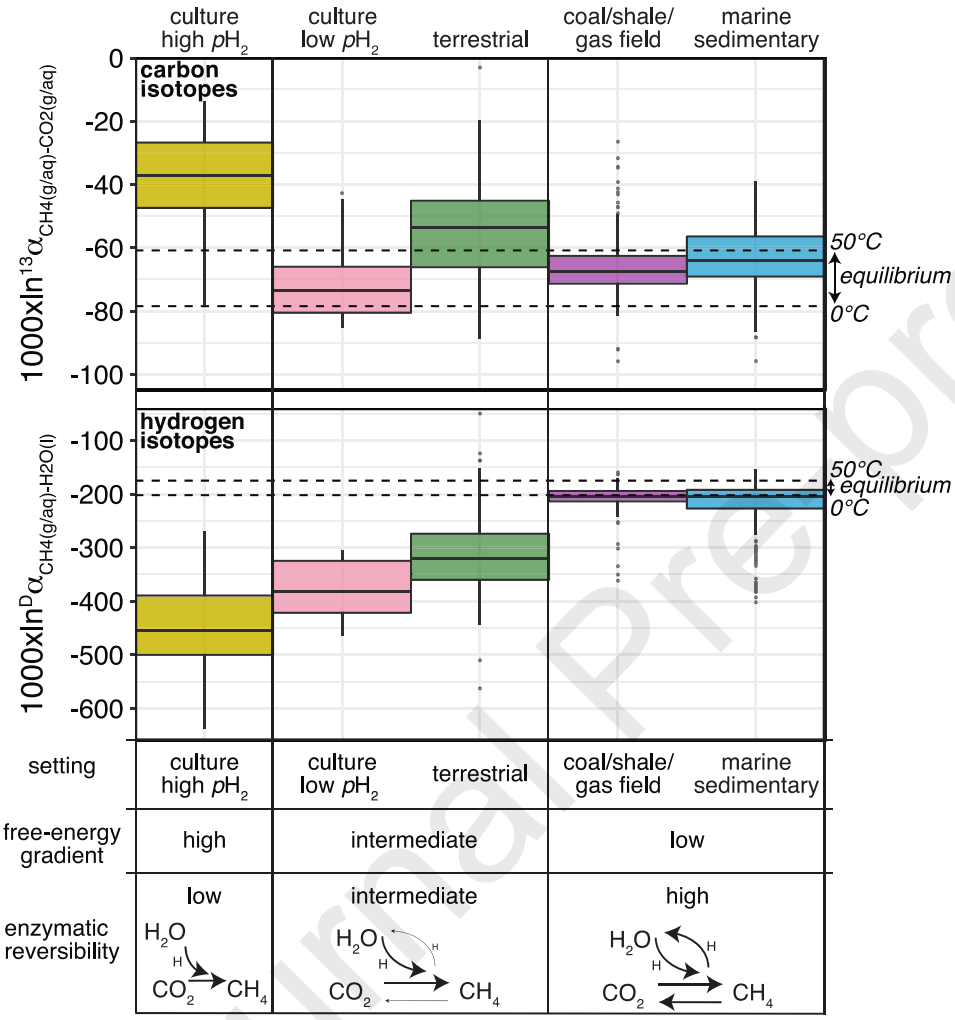

Figure 14: Conceptual illustration of factors controlling relative CH_4-CO_2 carbon and CH_4-H_2O(l) hydrogen isotopic compositions from environmental and pure culture samples. Box-and-whisker plots of data are given in the top two panes along with values expected for equilibrium at 50 and 0°C in the dotted horizontal lines — these represent maximum and minimum values for gaseous or aqueous fractionation factors, whichever provides the larger range at a given temperature. The environmental settings and our interpretations about the free energy available and degree of enzymatically catalyzed isotope-exchange reactions are also given. Light arrows indicate more limited exchange relative to heavier arrows.

Table 1: Initial and final average $1000\times\ln{}^{D}\alpha_{CH4(g)\text{-}H2(g)}$ values from each top- or bottom-bracket experiment

Bracket type	n^a	Starting T (°C)	Starting $1000\times\ln{}^{D}\alpha_{CH4(g)\text{-}H2(g)}$	Final T (°C)	Equilibration time (hr)	Final ${}^{D}\alpha_{CH4(g)\text{-}H2(g)}$	±1σ	±1 s.e.	Final $1000\times\ln{}^{D}\alpha_{CH4(g)\text{-}H2(g)}$	±1σ	±1 s.e.
top	3	-15	1393.2	0.98	33.55	3.8459	0.017	0.010	1347.0	4.5	2.6
bottom	2	*n/a*[e]	88[f]	0.98	335.2	3.7039	0.018	0.013	1309.4	4.9	3.5
top	3	-78	1618.3	2.9	25.12	3.6308	0.020	0.012	1289.4	5.6	3.2
top	3	-9	1376.3	2.9	114.25	3.6348	0.006	0.003	1290.5	1.6	0.9
bottom	2	*n/a*[e]	84.6	2.9	24.00	3.6141	0.026	0.019	1284.9	7.3	5.2
bottom	3	*n/a*[e]	88[f]	2.9	694.65	3.6777	0.013	0.008	1302.3	3.5	2.0
top	2	0.98	1309.2	10	26.10	3.4616	0.011	0.008	1241.7	3.1	2.2
bottom	2	*n/a*[e]	88[f]	9.8	26.08	3.4706	0.012	0.009	1244.3	3.6	2.5
top	2	2.9	1276.8	14.6	26.37	3.3080	0.007	0.005	1196.3	2.1	1.5
bottom	2	*n/a*[e]	85.9	14.6	142.47	3.3474	0.012	0.008	1208.2	3.5	2.5
top	2	2.9	88[f]	25.4	53.18	3.1638	0.009	0.006	1151.8	2.8	2.0
bottom	2	*n/a*[e]	88[f]	25.4	71.82	3.1451	0.002	0.001	1145.9	0.6	0.4
top	2	2.9	1295.6	35.4	53.52	2.9600	0.004	0.003	1085.2	1.3	0.9
bottom	3	*n/a*[e]	88[f]	35.4	24.00	3.0007	0.005	0.003	1098.8	1.6	0.9
top	3	14.6	1183.4	50.5	26.00	2.7653	0.022	0.013	1017.2	8.0	4.6
bottom	2	*n/a*[e]	79.5	50.5	24.00	2.7548	0.004	0.003	1013.3	1.6	1.1
bottom[b]	5	*n/a*[e]	88[f]	51.6	24.00	2.7409	0.006	0.003	1008.3	2.3	1.0
bottom[b]	7	*n/a*[e]	88[f]	51.6	24.00	2.7671	0.011	0.004	1017.8	3.9	1.5
bottom	4	*n/a*[e]	88[f]	51.6	24.00	2.7613	0.014	0.007	1015.7	5.2	2.6
bottom	4	*n/a*[e]	88[f]	51.6	24.00	2.7412	0.013	0.007	1008.4	4.8	2.4
top	2	14.6	1186.2	75.7	25.97	2.4703	0.010	0.007	904.3	3.9	2.7
bottom	3	*n/a*[e]	79.9	75.6	22.6	2.4741	0.012	0.007	905.9	5.0	2.9
top	2	2.9	1292.7	100	53.43	2.2930	0.001	0.000	829.8	0.3	0.2
bottom	2	*n/a*[e]	88[f]	99.8	24.00	2.2831	0.005	0.004	825.5	2.3	1.6
top	2	14.6	1184.4	127.5	25.93	2.0725	0.008	0.005	728.7	3.7	2.6
bottom	2	*n/a*[e]	96.6	127.3	22.57	2.0620	0.007	0.005	723.7	3.2	2.2
top	2	14.6	1190.8	158.8	25.93	1.8946	0.001	0.001	639.0	0.4	0.3
bottom	4	*n/a*[e]	88.6	155.9	22.52	1.9201	0.008	0.004	652.4	4.4	2.2
top	3	18[c]	1165.4	180.0	24.00	1.8217	0.007	0.004	599.8	4.0	2.3
top	2	18[c]	1174.8	180.0	24.00	1.8382	0.006	0.004	608.8	3.3	2.3
bottom	2	200.0	575.2	180.0	50.60	1.8361	0.004	0.003	607.6	2.0	1.4
bottom	3	200.0	610.5	180.0	50.60	1.8624	0.005	0.003	621.8	2.4	1.4
top	2	18[c]	1166.7	200.0	25.07	1.7775	0.001	0.001	575.2	0.6	0.4
top[d]	2	18[c]	1172.9	200.0	25.07	1.8416	0.012	0.009	610.6	6.6	4.7
bottom	2	230.0	544.9	200.6	25.02	1.7648	0.003	0.002	568.1	1.5	1.1
bottom, Ni	3	*n/a*	88[f]	200.1	336.2	1.7374	0.002	0.001	552.4	1.2	0.7

[a] *n* = the number of replicate mass spectrometric measurements of a given experiment

[b] Some injections yielded peak areas outside calibrated range (see Section 2.4 and Section A1)

[c] Temperature estimated from laboratory thermostat; not measured

[d] Excluded from final 200°C average (see Section 3.2.2)

[e] No starting temperature; values correspond to starting gas composition

[f] Not sampled; value assumed

Table 2: Averages of successful top- and bottom-bracket experiments.

T (°C)	$^{D}\alpha_{CH4(g)-H2(g)}$	±1σ	±1 s.e.	$1000\times\ln{}^{D}\alpha_{CH4(g)-H2(g)}$	±1σ	±1 s.e.
2.9	3.6393	0.009	0.007	1291.8	2.6	1.8
9.9	3.4661	0.006	0.004	1243.0	1.8	1.3
14.6	3.3277	0.028	0.020	1202.3	8.3	5.9
25.4	3.1545	0.013	0.009	1148.8	4.2	3.0
35.4	2.9803	0.029	0.020	1092.0	9.6	6.8
50.9	2.7592	0.009	0.006	1014.9	3.1	2.2
75.7	2.4722	0.003	0.002	905.1	1.1	0.8
99.9	2.2880	0.007	0.005	827.7	3.0	2.2
127.4	2.0672	0.007	0.005	726.2	3.6	2.5
157.4	1.9073	0.018	0.013	645.7	9.4	6.7
180.0	1.8396	0.014	0.010	609.5	7.4	5.2
200.2	1.7643	0.019	0.013	567.8	10.5	7.4

Table 3: DBO-corrected PIMC calculations of $1000x\ln^{D}\alpha$ for hydrogen isotopic equilibrium

T (°C)	$1000x\ln^{D}\alpha_{CH4(g)-H2(g)}$	±1 s.e.[a]	$1000x\ln^{D}\alpha_{H2O(g)-H2(g)}$	±1 s.e.[a]	$1000x\ln^{D}\alpha_{CH4(g)-H2O(g)}$	±1 s.e.[a]
0.98	1288.4	0.32	1395.2	0.34	-106.7	0.33
2.94	1275.3	0.37	1382.9	0.41	-107.6	0.25
9.9	1232.2	0.51	1341.2	0.48	-109.0	0.32
14.57	1203.6	0.38	1313.6	0.37	-110.0	0.22
25.4	1143.1	0.25	1256.1	0.27	-113.0	0.22
35.4	1091.1	0.31	1205.3	0.30	-114.3	0.29
50.9	1016.0	0.26	1133.5	0.30	-117.4	0.27
75.65	911.4	0.28	1032.0	0.28	-120.6	0.23
99.9	823.0	0.23	945.7	0.22	-122.7	0.25
127.4	736.6	0.22	860.8	0.19	-124.3	0.19
157.35	656.3	0.19	780.9	0.21	-124.7	0.19
180	603.1	0.18	727.9	0.23	-124.8	0.21
200.2	560.7	0.16	685.1	0.18	-124.4	0.16
203.35	554.4	0.16	678.6	0.16	-124.2	0.14
219.88	522.9	0.15	646.9	0.18	-124.1	0.15
264.07	450.2	0.12	571.8	0.13	-121.6	0.13
302.55	397.0	0.14	516.2	0.16	-119.2	0.13
364.58	327.3	0.10	441.8	0.13	-114.6	0.13
407	288.6	0.11	399.4	0.14	-110.8	0.14
458.1	249.9	0.11	356.0	0.12	-106.1	0.13
476.5	237.4	0.09	341.6	0.10	-104.2	0.10
503.4	220.6	0.08	322.3	0.10	-101.7	0.10

[a] Standard error of the mean for each PIMC calculation is reported here as a measure of statistical uncertainty only.

Table 4: DBO-corrected PIMC calculations of $1000x\ln^{13}\alpha$ for carbon isotopic equilibrium

T (°C)	$1000x\ln^{13}\alpha_{CH4(g)-CO2(g)}$	±1 s.e.[a]
1.85	-77.13	0.06
11.85	-73.09	0.06
26.85	-67.87	0.05
51.85	-60.30	0.05
76.85	-53.92	0.05
101.85	-48.60	0.04
126.85	-44.00	0.04
176.85	-36.59	0.03
226.85	-30.92	0.03
276.85	-26.42	0.01
326.85	-22.82	0.01
376.85	-19.87	0.01
426.85	-17.42	0.01
476.85	-15.39	0.01
526.85	-13.67	0.01
601.85	-11.58	0.01
801.85	-7.83	0.01
1001.85	-5.62	0.01
1301.85	-3.70	0.02

[a] Standard error of the mean for each PIMC calculation is reported here as a measure of statistical uncertainty only.

A. Appendix

A1 Instrument linearity corrections

We determined the dependence of δD measurements with respect to sample injected size (i.e., instrument linearity) by varying the injection volume for both the LBNL internal H_2 and CH_4 standards (i.e., those discussed above, of δD_{CH4} = -165‰ and δD_{H2} = -235‰). For CH_4 measurements, peak areas on the mass 2 ion beam between 40 to 110 volt seconds (Vs; the range over which CH_4 standards were run) showed no statistically resolvable linear dependence of δD_{CH4} as a function of peak area for any analytical session. The slopes for each session are as follows: February 2019: 0.078 ± 0.040 ‰/Vs (1 standard error (s.e.), n = 18); June 2019: -0.018 ± 0.020 ‰/Vs (1 s.e., n = 25); August 2019: 0.019 ± 0.019 ‰/Vs (1 s.e., n = 22); and November 2019: -0.008 ± 0.013 ‰/Vs (1 s.e., n = 8). As all slopes are within 2 s.e. of zero, we do not perform a linearity correction for δD_{CH4} measurements and we generally inject sufficient volumes of CH_4 to yield 40 to 110 Vs on the mass 2 ion beam. Samples of experiments where this was not possible (n = 7) are noted in Table EA2.

For the H_2 standards, we observed a resolvable non-zero linear dependence of measured δD values on sample injection sizes in two of our sessions. Specifically, δD vs. mass 2 peak area from 15 to 110Vs (which is the full range explored for H_2 standards), the slopes for each session are as follows: February 2019: 0.062 ± 0.041 ‰/Vs (1 s.e., n = 11); June 2019: 0.093 ± 0.008 ‰/Vs (1 s.e., n = 18); August 2019: 0.069 ± 0.007 ‰/Vs (1 s.e., n = 20); and November 2019: -0.004 ± 0.057 ‰/Vs (1 s.e., n = 4). The slope for both the June and August 2019 sessions is beyond 2 s.e. of zero. In order to minimize the influence of the dependence of δD_{H2} on injection size, samples were typically injected to produce peak areas within the range of 30 to 80 Vs. Using the June 2019 session as an example (the session with the largest slope in absolute magnitude), over this range in peak areas, δD values are expected to vary by ~4.7‰. Regardless, for the June and August 2019 sessions only, we apply a linearity correction as these sessions yielded slopes beyond 2 s.e. of 0.

We perform linearity corrections by taking the observed dependence of δD vs. injection size (peak area) for the standards from a given measurement session and correcting all measured δD values to the average of standard LBNL peak areas from that session. This correction is performed on all Oztech and methane standards before correction of samples to these standards. As such, choice of the exact peak area value for the correction is unimportant as it will be accounted for during correction based on measured vs. known external standard δD values. This linearity correction assumes that the linearity effect we observed is independent of δD values. We verified this by examining whether δD values of other standards (δD_{H2} range of -762.61 to -124.80‰ and δD_{CH4} range of -159.3‰ to +20.0‰) still exhibited a slope for δD vs. peak area following our linearity correction — differences of up to 90 Vs were examined. Slopes and associated error were calculated using a Monte Carlo error propagation scheme that incorporated the typical precision of the measurements (2.0‰ for δD_{H2} and 2.3‰ for δD_{CH4}) into the error calculation for the slope. In all cases these slopes are within 2σ (based on the Monte Carlo calculations) of 0, justifying our assumption.

A2 Fitting of theoretical fractionation factor estimates to experimental data

Clayton and Kieffer (1991) scaled theoretical calculations of equilibrium fractionation factors as a function of temperature to experimental data using a multiplier in order to ensure fits to high-temperature data yield values of 1000×lnα of 0‰ at infinite temperature. We instead chose to use constant offset terms in our fitting procedure (Sections 3.4 and 3.6). We considered three methods to fit the theoretical fits to experimental determinations of $1000\times\ln^{D}\alpha_{H2O(l)\text{-}H2(g)}$ and $1000\times\ln^{13}\alpha_{CH4(g)\text{-}CO2(g)}$: (1) a constant offset, (2) a multiplicative term, and (3) both a multiplicative and constant offset term. The difference in estimate between the three methods for the calculation of $1000\times\ln^{D}\alpha_{H2O(l)\text{-}H2(g)}$ is between -10‰ and +13‰ (relative to using a constant offset) over the applicable temperature range (6.7 to 357°C). For $1000\times\ln^{13}\alpha_{CH4(g)\text{-}CO2(g)}$, this range is -1 to +3‰. As it is not clear which of these approaches is superior, we elected to use the constant offset approach for two reasons. First it preserves the exact predicted theoretical temperature dependence. Second, the reason Clayton and Kieffer (1991) use a multiplier term is to ensure that theoretical fits of lnα go through 0‰ at infinite temperature. However, because our fits to the theoretical data are based on 4th order polynomials with respect to 1/T, such a requirement (0‰ at infinite T) creates so-called crossovers (O'Neil, 1986) at higher temperatures that are not experimentally or theoretically expected.

A3 Molpro calculations

We used Molpro Version 2019.2 software package (e.g., Werner et al., 2012; Werner et al., 2019; Werner et al., 2020) to calculate harmonic frequencies of all four molecules and the potential energy surface of molecular hydrogen.

A3.1 Potential energy curve of molecular hydrogen

The one-dimensional potential energy surface of the hydrogen molecule is obtained through spline interpolation between a dense set of single point CCSD/cc-pVQZ energy calculations between 0.38 and 1.8 Å with an interval of 0.005 Å. We tighten the energy and orbital convergence thresholds to 10^{-16} and leave the other input parameters on standard settings. We have also confirmed that larger basis sets (up to aug-cc-pV6Z) do not significantly change hydrogen's vibrational frequency (within ±3 cm^{-1}). Energy outside the computed range is approximated by the following fit:

$$E(r) = \begin{cases} E_{eq} + \exp\{-9.56\ (r - r_o)\}, r < 0.38\ \text{Å} \\ 2E_e - \exp\{-1.85\ r\}, r > 1.8\ \text{Å} \end{cases} \quad \text{(A1)}$$

where energy is in units of Hartree, $E_{eq} = -1.17379647$ is the equilibrium (minimum) energy, $E_e = -0.5$ is the energy of electron in a hydrogen atom and $r_o = 0.23$ Å. The high vibrational frequency of hydrogen ensures that the molecule only explores a tight range of molecular configurations around the equilibrium geometry, so we do not expect the accuracy of the fit above to influence computed RPFRs.

A3.2 Calculations of harmonic frequencies

Since the molecules of interest are standard targets of computations, standard input parameters are pre-optimized. Thus, we did not adjust input parameters for the harmonic frequency calculations within Molpro. Nevertheless, we confirmed that tighter convergence criteria for the RHF, MP2, CCSD, and CCSD(T) numerical gradient methods do not change the resultant frequencies (within ±1 cm^{-1}).

Reference harmonic frequencies (Table EA1) are obtained numerically from a known minimum on each of the reference potential energy surfaces (described in Section 2.5.1). We converged the frequencies to 0.1 cm^{-1}.

A4 Environmental and Pure Culture Sample References

Aravena R., Harrison S. M., Barker J. F., Abercrombie H. and Rudolph D. (2003) Origin of methane in the Elk Valley coalfield, southeastern British Columbia, Canada. *Chem. Geol.* **195**, 219–227.

Balabane M., Galimov E., Hermann M. and Létolle R. (1987) Hydrogen and carbon isotope fractionation during experimental production of bacterial methane. *Org. Geochem.* **11**, 115–119.

Bates B. L., McIntosh J. C., Lohse K. A. and Brooks P. D. (2011) Influence of groundwater flowpaths, residence times and nutrients on the extent of microbial methanogenesis in coal beds: Powder River Basin, USA. *Chem. Geol.* **284**, 45–61.

Baublys K. A., Hamilton S. K., Golding S. D., Vink S. and Esterle J. (2015) Microbial controls on the origin and evolution of coal seam gases and production waters of the Walloon Subgroup; Surat Basin, Australia. *Int. J. Coal Geol.* **147–148**, 85–104.

Belyaev S. S., Wolkin R., Kenealy W. R., DeNiro M. J., Epstein S. and Zeikus J. G. (1983) Methanogenic Bacteria from the Bondyuzhskoe Oil Field: General Characterization and Analysis of Stable-Carbon Isotopic Fractionation. *Appl. Environ. Microbiol.* **45**, 691–697.

Berner U., Von Breymann M. T., Faber E. and Bertrand P. (1992) Gas geochemistry of ODP sites 767 and 768, Celebes and Sulu seas. In Bacterial gas. pp. 147–156. Available at: http://pascal-francis.inist.fr/vibad/index.php?action=getRecordDetail&idt=6500833 [Accessed January 14, 2021].

Botz R., Pokojski H.-D., Schmitt M. and Thomm M. (1996) Carbon isotope fractionation during bacterial methanogenesis by CO2 reduction. *Org. Geochem.* **25**, 255–262.

Brosius L. S., Anthony K. M. W., Grosse G., Chanton J. P., Farquharson L. M., Overduin P. P. and Meyer H. (2012) Using the deuterium isotope composition of permafrost meltwater to constrain thermokarst lake contributions to atmospheric CH4 during the last deglaciation. *J. Geophys. Res. Biogeosciences* **117**. Available at: https://agupubs.onlinelibrary.wiley.com/doi/abs/10.1029/2011JG001810 [Accessed January 14, 2021].

Burke R. A. (1993) Possible influence of hydrogen concentration on microbial methane stable hydrogen isotopic composition. *Chemosphere* **26**, 55–67.

Burke R. A., Barber T. R. and Sackett W. M. (1988a) Methane flux and stable hydrogen and carbon isotope composition of sedimentary methane from the Florida Everglades. *Glob. Biogeochem. Cycles* **2**, 329–340.

Burke R. A., Martens C. S. and Sackett W. M. (1988b) Seasonal variations of D/H and 13 C/ 12 C ratios of microbial methane in surface sediments. *Nature* **332**, 829–831.

Burke R. A. and Sackett W. M. (1986) Stable Hydrogen and Carbon Isotopic Compositions of Biogenic Methanes from Several Shallow Aquatic Environments. In Organic marine geochemistry *American Chemical Society Symposium Series* **305**. pp. 297–313.

Chanton J. P., Fields D. and Hines M. E. (2006) Controls on the hydrogen isotopic composition of biogenic methane from high-latitude terrestrial wetlands. *J. Geophys. Res. Biogeosciences* **111**. Available at: https://agupubs.onlinelibrary.wiley.com/doi/abs/10.1029/2005JG000134 [Accessed January 14, 2021].

Douglas P. M. J., Stolper D. A., Smith D. A., Walter Anthony K. M., Paull C. K., Dallimore S., Wik M., Crill P. M., Winterdahl M., Eiler J. M. and Sessions A. L. (2016) Diverse origins of Arctic and Subarctic methane point source emissions identified with multiply-substituted isotopologues. *Geochim. Cosmochim. Acta* **188**, 163–188.

Flores R. M., Rice C. A., Stricker G. D., Warden A. and Ellis M. S. (2008) Methanogenic pathways of coal-bed gas in the Powder River Basin, United States: The geologic factor. *Int. J. Coal Geol.* **76**, 52–75.

Fuchs G., Thauer R., Ziegler H. and Stichler W. (1979) Carbon isotope fractionation by Methanobacterium thermoautotrophicum. *Arch. Microbiol.* **120**, 135–139.

Galimov E. M. and Kvenvolden K. A. (1983) Concentrations and carbon isotopic compositions of CH4 and CO2 in gas from sediments of the Blake Outer Ridge, Deep Sea Drilling Project Leg 76. *Initial Reports of the DSDP* **76**, 403–407.

Games L. M., HayesRobert J. M. and Gunsalus P. (1978) Methane-producing bacteria: natural fractionations of the stable carbon isotopes. *Geochim. Cosmochim. Acta* **42**, 1295–1297.

Giunta T., Young E. D., Warr O., Kohl I., Ash J. L., Martini A., Mundle S. O. C., Rumble D., Pérez-Rodríguez I., Wasley M., LaRowe D. E., Gilbert A. and Sherwood Lollar B. (2019) Methane sources and sinks in continental sedimentary systems: New insights from paired clumped isotopologues 13CH3D and 12CH2D2. *Geochim. Cosmochim. Acta* **245**, 327–351.

Grossman E. L., Coffman B. K., Fritz S. J. and Wada H. (1989) Bacterial production of methane and its influence on ground-water chemistry in east-central Texas aquifers. *Geology* **17**, 495–499.

Gruen D. S., Wang D. T., Könneke M., Topçuoğlu B. D., Stewart L. C., Goldhammer T., Holden J. F., Hinrichs K.-U. and Ono S. (2018) Experimental investigation on the controls of clumped isotopologue and hydrogen isotope ratios in microbial methane. *Geochim. Cosmochim. Acta* **237**, 339–356.

Hattori S., Nashimoto H., Kimura H., Koba K., Yamada K., Shimizu M., Watanabe H., Yoh M. and Yoshida N. (2012) Hydrogen and carbon isotope fractionation by thermophilic hydrogenotrophic methanogens from a deep aquifer under coculture with fermenters. *Geochem. J.* **46**, 193–200.

Hornibrook E. R. C., Longstaffe F. J. and Fyfe W. S. (2000) Factors Influencing Stable Isotope Ratios in CH4 and CO2 Within Subenvironments of Freshwater Wetlands: Implications for δ-Signatures of Emissions. *Isotopes Environ. Health Stud.* **36**, 151–176.

Hornibrook E. R. C., Longstaffe F. J. and Fyfe W. S. (1997) Spatial distribution of microbial methane production pathways in temperate zone wetland soils: Stable carbon and hydrogen isotope evidence. *Geochim. Cosmochim. Acta* **61**, 745–753.

House C. H., Schopf J. W. and Stetter K. O. (2003) Carbon isotopic fractionation by Archaeans and other thermophilic prokaryotes. *Org. Geochem.* **34**, 345–356.

Ijiri A., Inagaki F., Kubo Y., Adhikari R. R., Hattori S., Hoshino T., Imachi H., Kawagucci S., Morono Y., Ohtomo Y., Ono S., Sakai S., Takai K., Toki T., Wang D. T., Yoshinaga M. Y., Arnold G. L., Ashi J., Case D. H., Feseker T., Hinrichs K.-U., Ikegawa Y., Ikehara M., Kallmeyer J., Kumagai H., Lever M. A., Morita S., Nakamura K., Nakamura Y., Nishizawa M., Orphan V. J., Røy H., Schmidt F., Tani A., Tanikawa W., Terada T., Tomaru H., Tsuji T., Tsunogai U., Yamaguchi Y. T. and Yoshida N. (2018) Deep-biosphere methane production stimulated by geofluids in the Nankai accretionary complex. *Sci. Adv.* **4**, eaao4631.

Jenden P. D. and Kaplan I. R. (1986) Comparison of microbial* gases from the Middle America Trench and Scripps Submarine Canyon: implications for the origin of natural gas. *Appl. Geochem.* **1**, 631–646.

Kawagucci S., Kobayashi M., Hattori S., Yamada K., Ueno Y., Takai K. and Yoshida N. (2014) Hydrogen isotope systematics among H2–H2O–CH4 during the growth of the hydrogenotrophic methanogen Methanothermobacter thermautotrophicus strain ΔH. *Geochim. Cosmochim. Acta* **142**, 601–614.

Kimura H., Nashimoto H., Shimizu M., Hattori S., Yamada K., Koba K., Yoshida N. and Kato K. (2010) Microbial methane production in deep aquifer associated with the accretionary prism in Southwest Japan. *ISME J.* **4**, 531–541.

Kirk M. F., Wilson B. H., Marquart K. A., Zeglin L. H., Vinson D. S. and Flynn T. M. (2015) Solute concentrations influence microbial methanogenesis in coal-bearing strata of the Cherokee basin, USA. *Front. Microbiol.* **6**. Available at: https://www.frontiersin.org/articles/10.3389/fmicb.2015.01287/full [Accessed January 14, 2021].

Konn C., Charlou J. l., Holm N. g. and Mousis O. (2015) The Production of Methane, Hydrogen, and Organic Compounds in Ultramafic-Hosted Hydrothermal Vents of the Mid-Atlantic Ridge. *Astrobiology* **15**, 381–399.

Kotarba M. J. and Pluta I. (2009) Origin of natural waters and gases within the Upper Carboniferous coal-bearing and autochthonous Miocene strata in South-Western part of the Upper Silesian Coal Basin, Poland. *Appl. Geochem.* **24**, 876–889.

Krzycki J. A., Kenealy W. R., DeNiro M. J. and Zeikus J. G. (1987) Stable Carbon Isotope Fractionation by Methanosarcina barkeri during Methanogenesis from Acetate, Methanol, or Carbon Dioxide-Hydrogen. *Appl. Environ. Microbiol.* **53**, 2597–2599.

Lansdown J. M., Quay P. D. and King S. L. (1992) CH4 production via CO2 reduction in a temperate bog: A source of 13C-depIeted CH4. *Geochim. Cosmochim. Acta* **56**, 3493–3503.

Londry K. L., Dawson K. G., Grover H. D., Summons R. E. and Bradley A. S. (2008) Stable carbon isotope fractionation between substrates and products of Methanosarcina barkeri. *Org. Geochem.* **39**, 608–621.

Martini A. M., Walter L. M., Budai J. M., Ku T. C. W., Kaiser C. J. and Schoell M. (1998) Genetic and temporal relations between formation waters and biogenic methane: Upper Devonian Antrim Shale, Michigan Basin, USA. *Geochim. Cosmochim. Acta* **62**, 1699–1720.

McIntosh J. C. and Walter L. M. (2005) Volumetrically significant recharge of Pleistocene glacial meltwaters into epicratonic basins: Constraints imposed by solute mass balances. *Chem. Geol.* **222**, 292–309.

McIntosh J. C., Warwick P. D., Martini A. M. and Osborn S. G. (2010) Coupled hydrology and biogeochemistry of Paleocene–Eocene coal beds, northern Gulf of Mexico. *GSA Bull.* **122**, 1248–1264.

McIntosh J., Martini A., Petsch S., Huang R. and Nüsslein K. (2008) Biogeochemistry of the Forest City Basin coalbed methane play. *Int. J. Coal Geol.* **76**, 111–118.

Miller H. M., Chaudhry N., Conrad M. E., Bill M., Kopf S. H. and Templeton A. S. (2018) Large carbon isotope variability during methanogenesis under alkaline conditions. *Geochim. Cosmochim. Acta* **237**, 18–31.

Nakagawa F., Yoshida N., Nojiri Y. and Makarov V. (2002) Production of methane from alasses in eastern Siberia: Implications from its 14C and stable isotopic compositions. *Glob. Biogeochem. Cycles* **16**, 14-1-14–15.

Nguyen T. B., Topçuoğlu B. D., Holden J. F., LaRowe D. E. and Lang S. Q. (2020) Lower hydrogen flux leads to larger carbon isotopic fractionation of methane and biomarkers during hydrogenotrophic methanogenesis. *Geochim. Cosmochim. Acta* **271**, 212–226.

Okumura T., Kawagucci S., Saito Y., Matsui Y., Takai K. and Imachi H. (2016) Hydrogen and carbon isotope systematics in hydrogenotrophic methanogenesis under H2-limited and H2-enriched conditions: implications for the origin of methane and its isotopic diagnosis. *Prog. Earth Planet. Sci.* **3**, 14.

Pantano C. P. (2012) Hydrogeochemical Controls on Microbial Coalbed Methane Accumulations in the Williston Basin, North Dakota. Available at: https://repository.arizona.edu/handle/10150/228441 [Accessed January 14, 2021].

Paull C. K., Lorenson T. D., Borowski W. S., Ussler Iii W., Olsen K. and Rodriguez N. M. (2000) Isotopic composition of CH4, CO2 species, and sedimentary organic matter within samples from the Blake Ridge: Gas source implications. *Proc. ODP, Sci. Results* **164**, 67–78.

Pohlman J. W., Kaneko M., Heuer V. B., Coffin R. B. and Whiticar M. (2009) Methane sources and production in the northern Cascadia margin gas hydrate system. *Earth Planet. Sci. Lett.* **287**, 504–512.

Proskurowski G., Lilley M. D., Kelley D. S. and Olson E. J. (2006) Low temperature volatile production at the Lost City Hydrothermal Field, evidence from a hydrogen stable isotope geothermometer. *Chem. Geol.* **229**, 331–343.

Schlegel M. E., McIntosh J. C., Bates B. L., Kirk M. F. and Martini A. M. (2011) Comparison of fluid geochemistry and microbiology of multiple organic-rich reservoirs in the Illinois Basin, USA: Evidence for controls on methanogenesis and microbial transport. *Geochim. Cosmochim. Acta* **75**, 1903–1919.

Stolper D. A., Martini A. M., Clog M., Douglas P. M., Shusta S. S., Valentine D. L., Sessions A. L. and Eiler J. M. (2015) Distinguishing and understanding thermogenic and biogenic sources of methane using multiply substituted isotopologues. *Geochim. Cosmochim. Acta* **161**, 219–247.

Strąpoć D., Mastalerz M., Schimmelmann A., Drobniak A. and Hedges S. (2008) Variability of geochemical properties in a microbially dominated coalbed gas system from the eastern margin of the Illinois Basin, USA. *Int. J. Coal Geol.* **76**, 98–110.

Sugimoto A. and Wada E. (1995) Hydrogen isotopic composition of bacterial methane: CO2/H2 reduction and acetate fermentation. *Geochim. Cosmochim. Acta* **59**, 1329–1337.

Takai K., Nakamura K., Toki T., Tsunogai U., Miyazaki M., Miyazaki J., Hirayama H., Nakagawa S., Nunoura T. and Horikoshi K. (2008) Cell proliferation at 122°C and isotopically heavy CH4 production by a hyperthermophilic methanogen under high-pressure cultivation. *Proc. Natl. Acad. Sci.* **105**, 10949–10954.

Topçuoğlu B. D., Meydan C., Nguyen T. B., Lang S. Q. and Holden J. F. (2019) Growth Kinetics, Carbon Isotope Fractionation, and Gene Expression in the Hyperthermophile Methanocaldococcus jannaschii during Hydrogen-Limited Growth and Interspecies Hydrogen Transfer. *Appl. Environ. Microbiol.* **85**. Available at: https://aem.asm.org/content/85/9/e00180-19 [Accessed July 2, 2020].

Valentine D. L., Chidthaisong A., Rice A., Reeburgh W. S. and Tyler S. C. (2004) Carbon and hydrogen isotope fractionation by moderately thermophilic methanogens 1 1Associate editor: N. E. Ostrom. *Geochim. Cosmochim. Acta* **68**, 1571–1590.

Waldron S., Hall A. J. and Fallick A. E. (1999) Enigmatic stable isotope dynamics of deep peat methane. *Glob. Biogeochem. Cycles* **13**, 93–100.

Walter K. M., Chanton J. P., Chapin F. S., Schuur E. a. G. and Zimov S. A. (2008) Methane production and bubble emissions from arctic lakes: Isotopic implications for source pathways and ages. *J. Geophys. Res. Biogeosciences* **113**. Available at: https://agupubs.onlinelibrary.wiley.com/doi/abs/10.1029/2007JG000569%4010.1002/%28ISSN%292169-8961.METHANE1 [Accessed January 14, 2021].

Wand U., Samarkin V. A., Nitzsche H.-M. and Hubberten H.-W. (2006) Biogeochemistry of methane in the permanently ice-covered Lake Untersee, central Dronning Maud Land, East Antarctica. *Limnol. Oceanogr.* **51**, 1180–1194.

Wang D. T., Gruen D. S., Lollar B. S., Hinrichs K.-U., Stewart L. C., Holden J. F., Hristov A. N., Pohlman J. W., Morrill P. L., Konneke M., Delwiche K. B., Reeves E. P., Sutcliffe C. N., Ritter D. J., Seewald J. S., McIntosh J. C., Hemond H. F., Kubo M. D., Cardace D., Hoehler T. M. and Ono S. (2015) Nonequilibrium clumped isotope signals in microbial methane. *Science* **348**, 428–431.

Wang D. T., Reeves E. P., McDermott J. M., Seewald J. S. and Ono S. (2018) Clumped isotopologue constraints on the origin of methane at seafloor hot springs. *Geochim. Cosmochim. Acta* **223**, 141–158.

Wassmann R., Thein U. G., Whiticar M. J., Rennenburg H., Seiler W. and Junk W. J. (1992) Methane emissions from the Amazon Floodplain: Characterization of production and transport. *Glob. Biogeochem. Cycles* **6**, 3–13.

Whiticar M. J. and Faber E. (1989) Molecular and stable isotope composition of headspace and total hydrocarbon gases at ODP Leg 104, sites 642, 643, and 644, Vøring Plateau, Norwegian Sea. Proceeding of the Ocean Drilling Program, Scientific Results Leg 1, 327–334

Whiticar M. J., Faber E. and Schoell M. (1986) Biogenic methane formation in marine and freshwater environments: CO2 reduction vs. acetate fermentation—Isotope evidence. *Geochim. Cosmochim. Acta* **50**, 693–709.

Yoshioka H., Sakata S. and Kamagata Y. (2008) Hydrogen isotope fractionation by Methanothermobacter thermoautotrophicus in coculture and pure culture conditions. *Geochim. Cosmochim. Acta* **72**, 2687–2694.

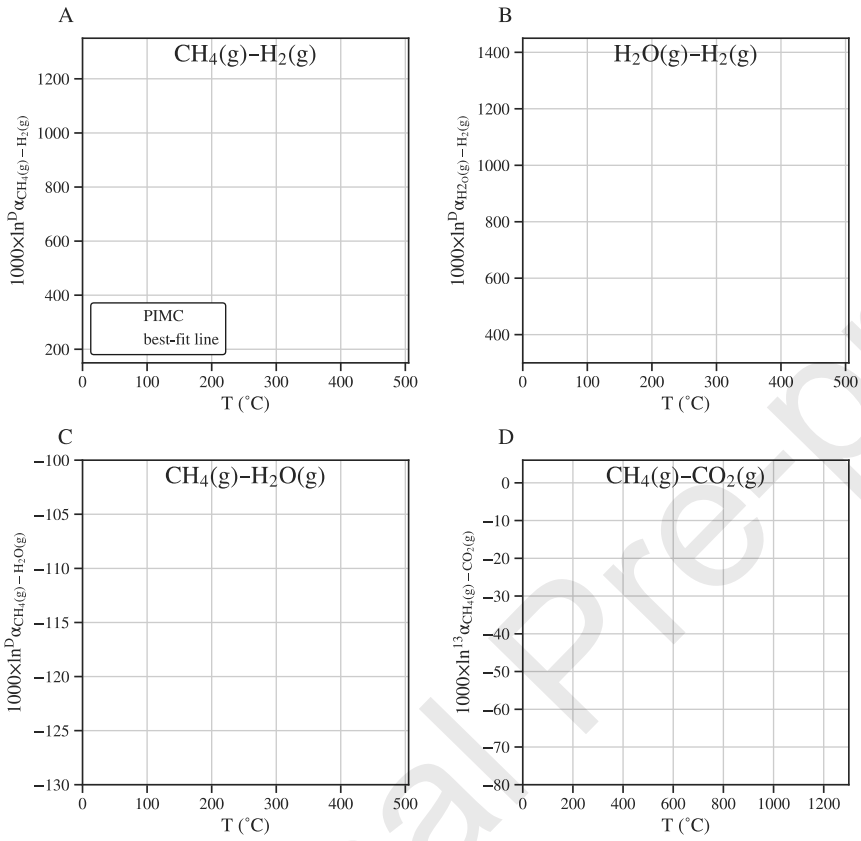

Figure A1: Results from DBO-corrected PIMC calculations for (A) $1000\times\ln^D\alpha_{CH4(g)\text{-}H2(g)}$, (B) $1000\times\ln^D\alpha_{H2O(g)\text{-}H2(g)}$, (C) $1000\times\ln^D\alpha_{CH4(g)\text{-}H2O(g)}$, and (D) $1000\times\ln^{13}\alpha_{CH4(g)\text{-}CO2(g)}$ vs. temperature (°C). Lines are 4th order polynomial fits to the calculated data points vs. 1/T (K^{-1}). Calculated values are given in Tables 3 and 4. The terms for each best-fit line and the associated error is given in Table EA6.

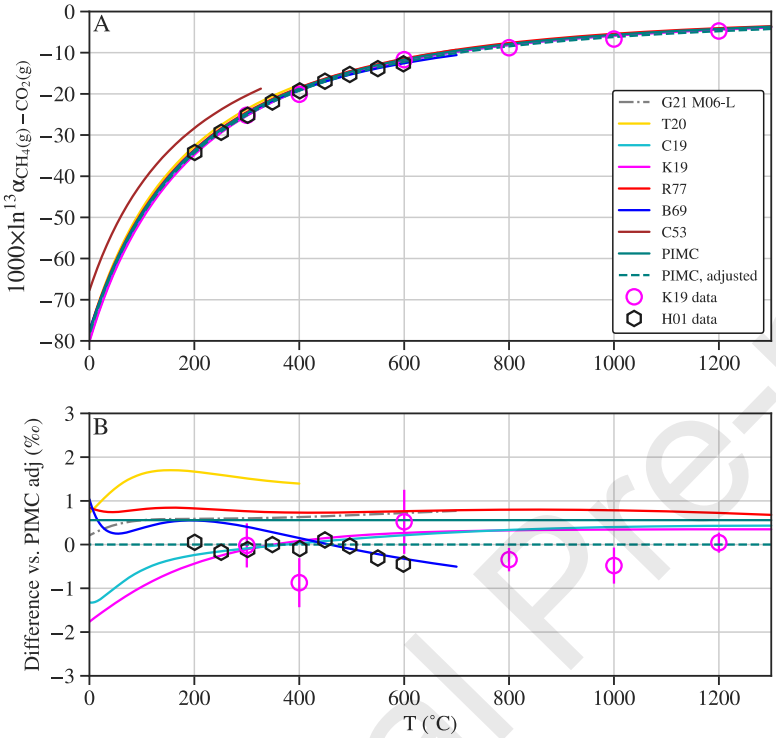

Figure A2: $1000\times\ln{}^{13}\alpha_{CH4(g)\text{-}CO2(g)}$ vs. temperature (°C), showing estimates for $1000\times\ln{}^{13}\alpha_{CH4(g)\text{-}CO2(g)}$ from published experimental fits (Kueter et al., 2019, (K19)), theory (Craig, 1953 (C53); Bottinga, 1969 (B69); Richet et al., 1977 (R77); Chen et al., 2019 (C19); Thiagarajan et al., 2020 (T20); Gropp et al., 2021 (G21 M06-L)), new theoretical calculations done in this study (PIMC (PIMC, adjusted)), and experimental data used to adjust the theoretical fits, as discussed in Section 3.8 (Horita, 2001; Kueter et al., 2019). (B): Difference between $1000\times\ln{}^{13}\alpha_{CH4(g)\text{-}CO2(g)}$ from the various studies vs. our adjusted PIMC line. Craig (1953) is off scale. Error is 1 s.e.; when not shown, error is smaller than symbol.

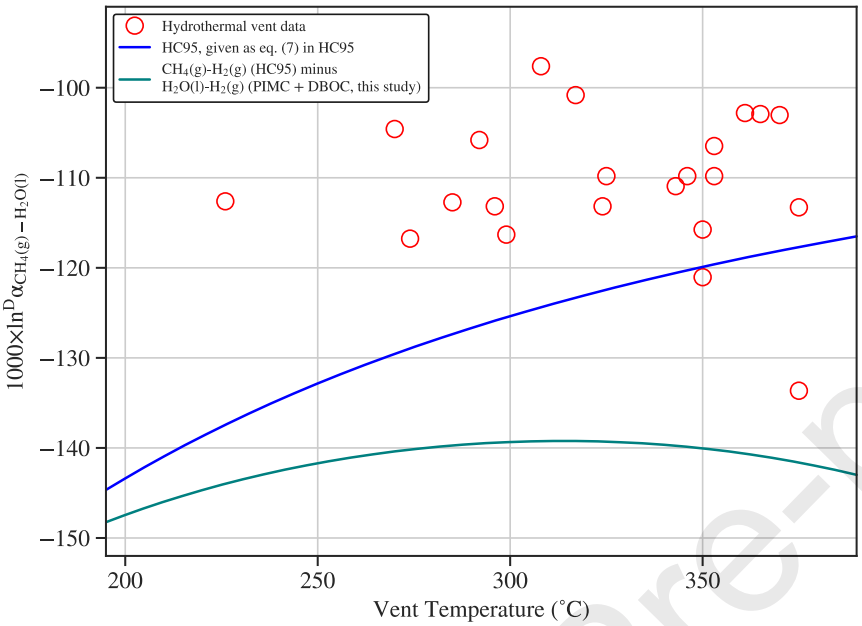

Figure A3: $1000\times\ln^{D}\alpha_{CH4(g)\text{-}H2O(l)}$ vs. temperature (°C) from 200°C to 374°C showing estimate from Horibe and Craig (1995) (HC95) using (1) their given $1000\times\ln^{D}\alpha_{CH4(g)\text{-}H2O(l)}$ equation which uses Suess (1949) in blue, and also using (2) their equation for $1000\times\ln^{D}\alpha_{CH4(g)\text{-}H2(g)}$ combined with the $1000\times\ln^{D}\alpha_{H2O(l)\text{-}H2(g)}$ equation determined in this study in green. Plotted in red are black smoker hydrothermal samples (n = 22) of known vent temperature.

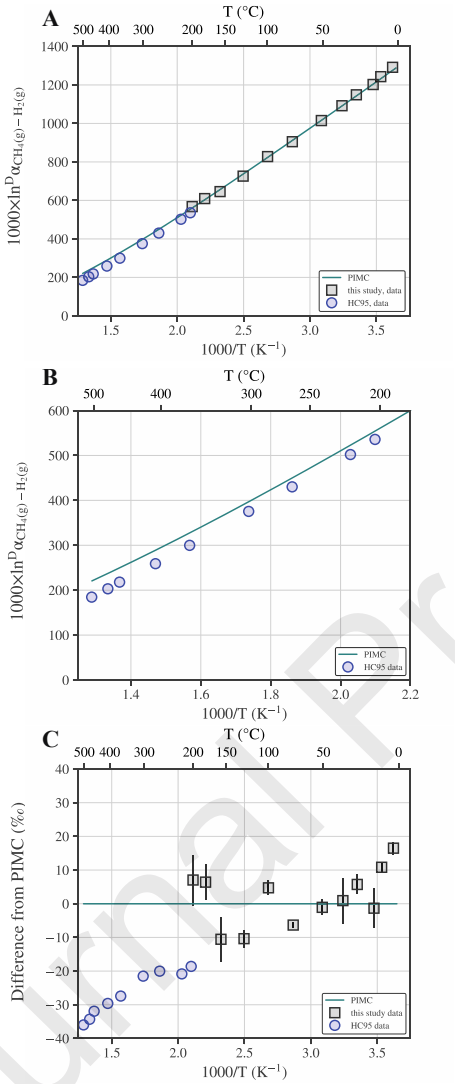

Figure A4: (A) $1000\times\ln^{13}\alpha_{CH4(g)-H2(g)}$ vs. 1000/T (K^{-1}) of the DBO-corrected PIMC polynomial fit from this study, experimental data from this study, and experimental data from Horibe and Craig (1995) (HC95). (B) Zoom-in showing just HC95 data and the PIMC fit from this study. Note the offset between HC95 data and the theoretical line. (C) Difference plot of data from this study and from HC95 relative to PIMC calculations from this study. The PIMC calculations were done at the same experimental temperatures for both our experimental results and those from Horibe and Craig (1995). Error bars are 1 s.e.

Table A1: Diagonal Born-Oppenheimer corrections for the pairs of molecules considered in this study. The corrections are computed by Zhang and Liu (2018) and given here in cm^{-1} units.

Pair of molecules	**H_2O vs H_2 (cm^{-1})**	**CH_4 vs H_2 (cm^{-1})**	**CH_4 vs H_2O (cm^{-1})**	**CH_4 vs CO_2 (cm^{-1})**
ΔC (CCSD/aug-cc-pCVTZ)	6.384[a]	0.066	6.450	0.051

[a] Note that Bardo and Wolfsberg (1976) used 3.8 cm^{-1} as calculated using the RHF method with double-ζ polarized basis set for water and a 54-term wavefunction for hydrogen (Kolos and Wolniewicz, 1964)

Table A2: Average values of 50°C Stoichiometry Experiments

Stoichiometry H_2:CH_4 (vol:vol)	***n*** [a]	**Average δD_{H2}**	**Average δD_{CH4}**	$^{D}\alpha_{CH4(g)-H2(g)}$	±1σ	**$1000 \times \ln {}^{D}\alpha_{CH4(g)-H2(g)}$**	±1σ
1:4[b]	5	-675.0	-106.7	2.7409	0.006	1008.3	2.4
1:2[c]	7	-663.0	-62.4	2.7671	0.011	1017.8	3.9
1:1	4	-630.1	21.3	2.7613	0.015	1015.7	5.3
2:1	4	-575.0	165.0	2.7412	0.012	1008.4	4.5
2:1	3	-570.0	189.0	2.7548	0.022	1017.1	8.0
2:1	2	-569.7	185.4	2.7653	0.004	1013.3	1.6

[a] *n* = the number of replicate mass spectrometric injections

[b] 3 of 5 δD_{H2} and 2 of 5 δD_{CH4} are excluded from the averages presented here on the basis of peak area, see Section 2.4

[c] 3 of 7 δD_{H2} and 4 of 7 δD_{CH4} are excluded from the averages presented here on the basis of peak area, see Section 2.4

Table A3: Calculated PIMC $1000\times\ln^{D}\alpha$ values for hydrogen equilibrium

T (°C)	CH_4/H_2			CH_4/H_2O			H_2O/H_2		
	Without DBO	*With DBO*	*difference*	*Without DBO*	*With DBO*	*difference*	*Without DBO*	*With DBO*	*difference*
0.98	1288.1	1288.4	0.3	-140.6	-106.7	33.9	1428.7	1395.2	-33.5
2.94	1274.9	1275.3	0.4	-141.2	-107.6	33.6	1416.2	1382.9	-33.3
9.9	1231.9	1232.2	0.3	-141.7	-109.0	32.7	1373.6	1341.2	-32.4
14.57	1203.3	1203.6	0.3	-142.3	-110.0	32.3	1345.5	1313.6	-31.9
25.4	1142.8	1143.1	0.3	-144.1	-113.0	31.1	1286.9	1256.1	-30.8
35.4	1090.8	1091.1	0.3	-144.3	-114.3	30.0	1235.1	1205.3	-29.8
50.9	1015.7	1016.0	0.3	-146.1	-117.4	28.7	1161.8	1133.5	-28.3
75.65	911.2	911.4	0.2	-147.2	-120.6	26.6	1058.3	1032.0	-26.3
99.9	822.7	823.0	0.3	-147.6	-122.7	24.9	970.3	945.7	-24.6
127.4	736.3	736.6	0.2	-147.4	-124.3	23.2	883.8	860.8	-23.0
157.35	656.1	656.3	0.2	-146.2	-124.7	21.5	802.3	780.9	-21.4
180	602.9	603.1	0.2	-145.3	-124.8	20.5	748.2	727.9	-20.3
200.2	560.5	560.7	0.2	-144.0	-124.4	19.6	704.5	685.1	-19.4
203.35	554.1	554.4	0.2	-143.7	-124.2	19.5	697.9	678.6	-19.3
219.88	522.7	522.9	0.2	-142.9	-124.1	18.8	665.6	646.9	-18.7
264.07	450.0	450.2	0.2	-138.9	-121.6	17.3	588.8	571.8	-17.1
302.55	396.8	397.0	0.2	-135.3	-119.2	16.1	532.2	516.2	-16.0
364.58	327.1	327.3	0.2	-129.1	-114.6	14.6	456.2	441.8	-14.4
407	288.5	288.6	0.1	-124.4	-110.8	13.6	412.9	399.4	-13.5
458.1	249.7	249.9	0.1	-118.8	-106.1	12.7	368.5	356.0	-12.6
476.5	237.3	237.4	0.1	-116.6	-104.2	12.4	353.9	341.6	-12.3
503.4	220.5	220.6	0.1	-113.6	-101.7	11.9	334.2	322.3	-11.9

Table A4: Calculated PIMC $1000\times\ln^{13}\alpha$ values for carbon equilibrium

T (°C)	CH_4/CO_2		
	Without DBO	*With DBO*	*difference*
1.85	-76.87	-77.13	-0.26
11.85	-72.83	-73.09	-0.25
26.85	-67.62	-67.87	-0.24
51.85	-60.08	-60.30	-0.23
76.85	-53.72	-53.92	-0.21
101.85	-48.41	-48.60	-0.20
126.85	-43.82	-44.00	-0.18
176.85	-36.43	-36.59	-0.16
226.85	-30.78	-30.92	-0.14
276.85	-26.29	-26.42	-0.13
326.85	-22.69	-22.82	-0.12
376.85	-19.75	-19.87	-0.11
426.85	-17.31	-17.42	-0.10
476.85	-15.29	-15.39	-0.10
526.85	-13.57	-13.67	-0.09
601.85	-11.50	-11.58	-0.08
801.85	-7.76	-7.83	-0.07
1001.85	-5.56	-5.62	-0.06
1301.85	-3.65	-3.70	-0.05

Declaration of interests

☒ The authors declare that they have no known competing financial interests or personal relationships that could have appeared to influence the work reported in this paper.

☐The authors declare the following financial interests/personal relationships which may be considered as potential competing interests: